NTNU – Trondheim
Norwegian University of
Science and Technology

Propulsion methods for under water snake robots

Investigation and simulation using foil for propulsion of a snake robot

Simen Strømsøyen

Marine Technology
Submission date: June 2015
Supervisor: Asgeir Johan Sørensen, IMT

Norwegian University of Science and Technology
Department of Marine Technology

NTNU Trondheim
Norwegian University of Science and Technology
Department of Marine Technology

MASTER THESIS IN MARINE CYBERNETICS

Spring 2015

for

Simen Strømsøyen

Propulsion methods for underwater snake robots

Work description

Snake robots seem to have a promising future due to the flexibility and property to maneuver in confined environment. The Norwegian University of Science and Technology (NTNU) and SINTEF started in 2003 a research program on snake robots. They have developed different prototypes to investigate how to control such a robot. It started with ground based snakes, but lately it also underwater snakes has been investigated by NTNU. Maneuvering and transit of snake robots is an important topic in this respect. Underwater robots may be used for mapping and monitoring of the sea bead and inspection and intervention of subsea structures. The aim for this thesis is to investigate propulsion methods for an underwater snake robot. Using the nature as inspiration foil propulsion will be investigated together with the body motion of the snake robot to improve efficiency and speed characteristics.

Scope of work

- Describe the background and motivation for the project.
- Do a literature review of relevant literature and previous work on snake robots and foil propulsion in underwater robotics.
- Formulate a mathematical model of a snake robot (free floating linked structure) and simulate in Matlab.
- Formulate a mathematical model for a “fish tail”.
- Combine the snake robot model and the “fish tai” model and do simulations in Matlab.

The report shall be written in English and edited as a research report including literature survey, description of mathematical models, description of control algorithms, simulation results, model test results, discussion and a conclusion including a proposal for further work. Source code should be provided on a CD with code listing enclosed in appendix. It is supposed that Department of Marine Technology, NTNU, can use the results freely in its research work, unless otherwise agreed upon, by referring to the student’s work. The thesis should be submitted in two copies within June 10th.

Co-supervisor: Professor Kristin Y. Pettersen, Eleni Kelasidi and Pål Liljebäck.

Professor Asgeir J. Sørensen
Supervisor

"I am always doing that which I cannot do, in order that I may learn how to do it."

Pablo Picasso

NORWEGIAN UNIVERSITY OF SCIENCE AND TECHNOLOGY

Abstract

Faculty of Engineering Science and Technology
Department of Marin Technology

Master Thesis

Propulsion methods for underwater snake robots

by Simen Strømsøyen

In this thesis we present a model of a swimming underwater snake robot. How aquatic animals move in water has fascinated people for decades. NTNU started the research on land based snake robots 11 years ago. The last years also underwater snake robots has become a topic. This thesis is based on this research.

In this study an extension of the underwater snake model moving in a 2D plane presented in [1] is derived. The new model makes it possible to include an extra propulsion force in each link. In the new model each link can also have different mass, length and inertia. The new model is implemented in *Matlab R2014b*. The simulations show that the new model gives the same answers as the one proposed in [1].

Further more a quasi-steady model for a oscillating and rotating foil are combined on the new extended underwater snake robot model to simulate a snake with a high aspect ratio caudal fin. Simulation with and without the caudal fin are presented. Results show an increase in speed for both eel and snake like motion. More simulations for the eel-like motion were carried out. This shows a significantly reduction in the work per meter for the underwater snake robot with tail at the same forward velocities. The results also shows that the use of a quasi-steady foil model acceptable. The KC numbers are plotted for 3 different links for the eel motion with caudal fin. This shows a significantly difference in the KC number which motivates for the investigation of using different drag coefficients for the different links.

The effect of a dorsal fin is also investigated. The simulations were done with a caudal fin and a dorsal fin at the fifth link. The results show a decrease of work per meter and an increase of the efficiency for the same simulation parameters. The sideways motion of the center of mass was slightly damp due to the dorsal fin.

The complexity of underwater snake robots makes it challenging to model and there are still a lot of work to be done. Making a maneuvering and transit controller for the underwater snake robot and prove stability is something too continues with. Future control of the tail and angel for attack and optimization of the movements is also necessary. The interaction effects between the snake, caudal fin and dorsal fin could also increase the efficiency for the robot.

Sammendrag

I denne oppgaven har vi prøvd å modellere en sømmende slangerobot. Hvordan fisk, ål, hval og hai beveger seg i vann har fasinert folk i århundrer og ennå er ikke all detaljer om hvordan de beveger seg kjent. NTNU startet sin forskning på land basert slangerobot for 11 år siden og de siste årene har også svømmende slangeroboter vært i fokus. Denne forskningen danner grunnlagte for denne masteroppgaven.

En utvidet modell av den svømmende salngerobot modellen som beveger seg i et 2D plan presentert i [1] er utledet. I den nye modellen kan hver link ha forskjellig masse, treghet og lengde. Det er også mulig å inkludere en ekstra propulsjonskraft som en finne eller truster i hver link. Modellen er implementer I in *Matlab R2014b*. Simuleringen viser samme svar for samme input parametere som den gamle modellen.

Videre har en quasi-steady modell for en oscillerende og roterende foil blitt kombinert med modellen for den svømmende slangen. Foilen skal simulere en hale og resultater med og uten hale har blitt sammenlignet. Resultatene viser en økt hastighet og effektivitet for modellen med hale. Resultatene viser også at en quasi-steady modell kan fr svares for de fleste parameterne som er testet. KC tallet er plottet for 3 forskjellige linker. Resultatene viser en betydelig forskjell i KC talle mellom de forskjellig linkene for en åle bevegelse. Dette motivere for å undersøke muligheten for å bruke forskjellige drag koeffisienter for de forskjellige linkene.

Effekten av en ryggfinne er også testet. En slangerobot med halefinne er simulert med og uten ryggfinne. Simuleringene viser ett reduser energiforbruk og en høyere hastighet for slangen med ryggfinne for de samme input parameterne. Vi så også at sideveisbevegelsen av messesenteret ble dempet noe.

Det å modellere undervanns slanger er veldig komplekst og utfordrende og det er mye som kan undersøkes. Lage en kontroller for manøvrering og transitt og bevise stabilitet er en ting man kan gjøre. Videre er også å lage en kontroller for halen slik at angrepsvinkelen blir optimalisert nødvendig. Interaksjon mellom slange og finer kan også være med på å øke virkningsgraden, så dette er også noe som bør undersøkes, men dette er vanskelig å modellere når man ønsker en forenklet modell.

Acknowledgements

This thesis has been written spring 2015 Norwegian University of Science and Technology (NTNU), Department of Marine Technology. Working with underwater snake robots has been fun and challenging. The modeling of a swimming snake robot is quite complex but I believe that this is the future of underwater robotics.

I want to thank my supervisor Asgeir J. Sørensen for motivation, feedback and guidance through the thesis. I also want to thank my co-supervisors Kristin Y. Pettersen and Pål Liljebäck of always taking the time to answer my questions and their responses to all my emails. I especially want to thank my co-supervisor Eleni Kelasidi for always have time to answering all my questions, helping me with my problems and motivate me. I also want to thank all my classmates for all the fun we have had together during the 5 years. A special thanks goes to my classmate John Martin Godø for all the good discussions about hydrodynamics.

Contents

List of Figures

List of Tables

Abbreviations

UUV	**U**nmanned **U**nderwater **V**ehicles
ROV	**R**emote **O**perated **V**ehicles
AUV	**A**utonomous **U**nderwater **V**ehicles
Rn	**R**eynolds **n**umber
St	**St**rouhals number
KC	**K**eulegan-**C**arpenter number
AR	**A**spect-**r**atio
CM	**C**enter of **M**ass number

Physical Constants

Gravity	g	=	9.81m/s^2
Density of water	ρ	=	1000kg/m^3
Kinematic viscosity	ν	=	$10^{-6}\text{m}^2\text{/s}$

Symbols

a	distance
P	power
W	work
N	Number of links
l_i	Half the length of like number i
m_i	The mass of link i
j_i	The moment of inertia of link i
m_t	The total mass of the snake robot
$\mathbf{L}$	Diagonal matrix with the different link angels
$\mathbf{M}$	Diagonal matrix with the different link masses
$\mathbf{J}$	Diagonal matrix with the different link inertias
θ_i	Angel between joint i and the global x axis
ϕ_i	Angel of joint i
(x_i, y_i)	Global coordinates of the CM of link i
P_x, P_y	Global coordinates of the CM of the snake robot
u_i	Actuator torque extended on link i from link i+1
u_{i-1}	Actuator torque extended on link i from link i-1
$f_{x,i}$	Fluid force in x direction on link i
$f_{y,i}$	Fluid force in y direction on link i
$f_{x,t,i}$	Propulsive force in x direction on link i
$f_{y,t,i}$	Propulsive force in y direction on link i
τ_i	Fluid torque on linke i
$\tau_{t,i}$	Torque from propulsive force on link i

$h_{x,i}$	Joint constraint force in x direction on link i from link i+1
$h_{y,i}$	Joint constraint force in y direction on link i from link i+1
$h_{x,i-1}$	Joint constraint force in x direction on link i from link i-1
$h_{y,i-1}$	Joint constraint force in y direction on link i from link i-1
L_f	Lift from a foil
M_f	Moment from a foil
D_l	Drag on a foil
S	Span of a foil
B	mean cord a foil
ω	angular frequency of the gait pattern
α	amplitude of the gait pattern
δ	phase of the gait pattern
α_l	angel of attack

Chapter 1

Introduction

The aim for this thesis is to investigate propulsion methods for a hyper redundant flexible robot denoted as underwater snake robot. Using the nature as inspiration foil propulsion will be investigated together with the body motion of the snake robot to improve efficiency, speed and maneuvering characteristics. This Thesis is a continuation of the project thesis written autumn 2014 by Simen Strømsøyen.

In this chapter an introduction to fish and snake like propulsion is given together with a litterateur review of previous important work. There is also given an overview of the thesis at the end.

1.1 Background and motivation

Unmanned underwater robots may be used for mapping and monitoring of the sea bead and inspection and intervention of subsea structures. A generic term for these types of robots is Unmanned Underwater Vehicles (UUV). We can distinguish between two types of under UUVs. The Remote Operated Vehicle (ROV) and Autonomous Underwater Vehicle (AUV). The ROVs is remotely operated from a ship or a platform through a cable and are often used for installation, maintenance and inspection of subsea structures. They are often equipped with cameras and manipulator arm(s). AUVs are autonomous and often preprogrammed to follow

a desired path. They are often used for mapping and inspection of the sea bed. The most common propulsion strategy are to day for both AUVs and ROVs to use propeller(s)/thruster(s). For AUVs energy is a limitation and therefore they have a streamlined form to minimize the drag. ROVs do not have this issue and are normally box shaped and have several thrusters, while an AUV normally only have one propeller. There also exist a group of AUVs that uses change in buoyancy together with wings for propulsion. These AUVs are called gliders. They are often used for collecting samples of the water column. They have a low forward velocity but are very efficient and can be out for months.

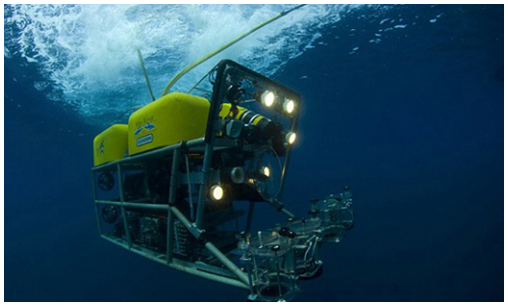

Typical ROV [14]

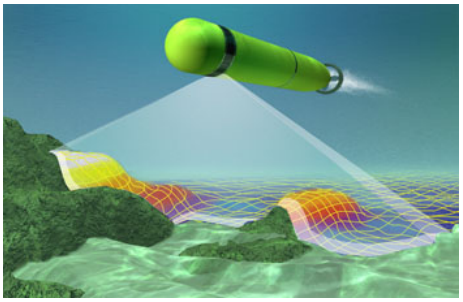

Typical AUV [15]

FIGURE 1.1: Examples of how a ROV and an AUV look like.

We believe that UUVs will be more and more autonomous in the future. Some important properties for an autonomous underwater robot are efficiency and maneuverability. Typical efficiency for an underwater vehicle propeller is typical as low as 0.40 [16]. An efficient propulsion system is important because an AUV do not have an extern power supply like the ROV. The gliders are capable of traveling much longer distance but have poor maneuvering capability due to the slow forward speed and bad steering characteristics. Maneuverability is important for an UUV if you want to maneuver it in confined environment, to avoid collision or if it is following a path. To improve the efficiency and maneuverability, we may look to the nature for inspiration. Snakes, eels and fishes have developed their propulsion method through evolution over a long time. Fish is believed to have high efficiency and at the same time outstanding maneuverability performance. They can change direction in an extremely short distance with a negligible loss in kinetic energy [17]. Their acceleration capabilities are also outstanding.

FIGURE 1.2: Picture of a sailfish, Photo by Alastair Pollock Photography [2]

In 2005 great white shark instrumented with transducers traveled over 20000 km form Africa to Australia and back again in 9 moths [18]. The sailfish (figure 1.2) can swim up to 110 km/t [2]. On the picture in figure 1.3 a killerwhale is jumping approximately 4.5 meters up into the air. A tuna fish can achieve an acceleration that exceeds the gravity 20 times [16].These are examples that show the remarkable properties of bio propulsion. Eels and snakes can theoretically swim both backward and forward and their flexible body is good for swimming in confined spaces. We think this examples alone are motivation enough to study and trying to adapt some of their bio propultion properties.

Another aspect that is important in military applications is that fish propulsion is quite silent. A propeller makes noises that can be heard on a long distance, but it is hard to hear a fish gliding/swimming through the water.

In the nature there are two things that are important. The first on is to survive. The second is to reproduce. It is not necessarily that the most efficient swimmer that survives and gets its genes reproduced. Evolution takes time and it is the on that have a slight advantage that wins. A good example form the book [19] .

Two polar bear researchers was on their way to Svalbard. One of them was bringing a par of spiked shoes. The other one was wondering and asked why he was bringing

FIGURE 1.3: A killer whale jumping approximately 4.5 meters out of the water. Photo by Biosphoto/Christopher Swann [3]

such shoes? Did he think that it would help him running away from the polar bear? The colleague was answering: "I just need to run faster than you".

Some aquatic animals have evolved extreme speed, efficiency and maneuverability performance for hunting. Others have evolved defense mechanisms and camouflage to hide for their enemies. Over a long time they have develop properties of those witch had the spiked shoe. This is something to have in mind when choosing witch aquatic animal to study. Maybe it is possible to take the best part of different aquatic animals and combined in one robot?

1.2 Goals

The goal for this project is to investigate eel and fish propulsion and they mechanism for producing thrust. We will try to combine the maneuverability of the eels and the high causing speeds and efficiency of tunas. A simplified model of an eel like robot that takes the important mechanisms into account will be derived. Then, we will formulate a model for an oscillating foil and combine it with the

eel model. Finally, simulations will be carried out to study and demonstrate the performance of the proposed bio-inspired system.

1.3 Thesis structure

Chapter 1: The chapter explains the motivation for this thesis and an introduction to the thesis topic.

Chapter 2: An overview over the topic is given. Some relevant developed biomimicking concepts are presented. Fundamental hydrodynamic theory is also given in this chapter.

Chapter 3: The chapter derives a general model for an underwater snake robot including both linear, nonlinear drag and added mass effects. A general extra propulsion force is also included for each link.

Chapter 4: A quasi-steady foil model is connected with the model for the underwater snake robot. This is to simulate fines on the snake robot. Especially high aspect ratio fins are relevant to improve the seed and efficiency characteristics.

Chapter 5: Simulations with the derived model are carried out. Simulations with and without foils are done to compar the speed and efficiency.

Chapter 6: Conclusion and future work are presented.

1.4 Contributions

Chapter 1: The propulsion of aquatic animals has fascinated people for centuries. Their remarkable swimming characteristics is the motivation for this thesis.

Chapter 2: A short history is given combine with some relevant theory and developed biomimicking concepts.

Chapter 3: A model of an underwater snake robot swimming in a 2D plane is derived. The model takes into account linear and nonlinear drag and added mass. The links in the model can have different mass effects, inertia and length. An extra propulsion force is also included for each link. This gives the opportunity for adding a tail or thruster force in each link.

Chapter 4: A quasi-steady foil model is combined with the underwater snake robot, which gives the opportunity to add a foil on each link of the snake.

Chapter 5: Simulation shows that the foil improves the efficiency and speed of the underwater snake robot.

Chapter 6: Conclusion and future work are presented.

Chapter 2

Short history, literature survey and important hydrodynamic theory

The purpose of this chapter is to give an overview of the relevant research done in the areas related to snake-like, and underwater biometric robots. This chapter will also present different developed concepts and explain how eels and fish swim and including some important theory about this.

2.1 Short history of fish propulsion and UUVs

Life started in water. Through 10^9 years of evolution in water aquatic animals have developed high speed and low cost propulsion methods [4] [17]. A lot of effort has been put into understanding the physics behind it, but still far form everything is known. Dolphins have been a red line through the study of aquatic animal propulsion. The first known person to study dolphins was Aristotle's. He consider the dolphins as the fastest of all animals [4].

More serious scientific studies were not done before 1900. It was hard to se the movements of the tail due to the high frequency. One mechanical measurement device that where made to investigate this can be seen in figure 2.1

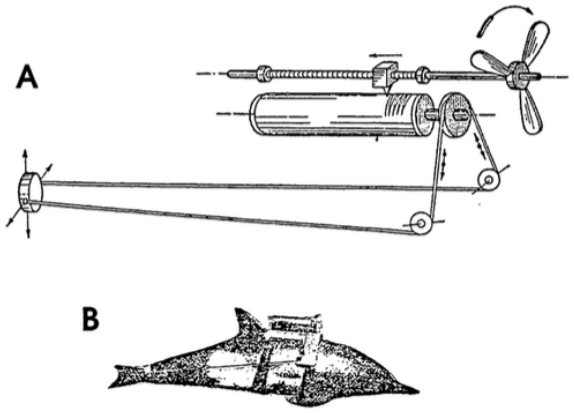

FIGURE 2.1: A: Measurement equipment to measure the moments of the tail on a dolphin. B The divides mounted on a dolphin. [4]

In 1935 Sir James Gray published the article "The propulsive power of the Dolphin" [20]. As one of the first he tried to calculate the resistance of dolphins at reported swimming speeds and their available muscle power. His conclusion was that, assuming turbulent flow over the dolphin's skin, it would need at least 7 times as much muscle power as calculated to attain the reported swimming speeds. Gray proposed two possible explanations to this discrepancy. Either the dolphin must be able to produce seven times as much muscle power per kg of muscle tissue as what is observed in other types of mammalian muscle, or either the skin or the motions of the dolphin must be able to prevent turbulence in the boundary layer close to its body. In this way either his calculations of available power or the calculated resistance must have been wrong, respectively. If assuming laminar flow the available power and calculated resistance agree very well. Given that this is the case the propulsive efficiency of the dolphin must still be very close to 100%. The discrepancy between available power and measured swimming speeds of dolphins has later been termed Gray's paradox, and has been the background of numerous studies on fish swimming. It is clear that the possibilities of discovering

hydrodynamic effects either preventing transition to turbulence in boundary layers or providing highly efficient propulsion makes it interesting to execute detailed studies of the flow around swimming dolphins. Such improved insight could also be used in production of drag reducing ship coating or design of radically different ship and under water propulsion systems. Gray's paradox triggered allot of new studies on bio propultion.

Also the shape of the dolphin has been synonymous with low resistance. The body shape is similar to modern low drag foils as the NACA 66 profiles. In the USA the submarine design since the USS Albacore has been inspered of the dolphin body shape [4].

In the 1970's Sr James Lighthill published articles about aquatic animal propulsion [17]. Lighthill did a huge work trying to analytically describe the hydrodynamics of animal population and it is sill one of most accurate models we have. T. Wu also did a similar work in 1971 [21] [22] [23].

It seems that Gray's paradox is to good to be true. Later it has been discovered different weak spots in Gray's paradox, and it more or less has been prove that the efficiency are not are over one [24]. Some weakness in Grays paradox is that the speed measurements were done by driving a boat and clock the time a dolphin used to pass the boat. The dolphin could have utilized the waves from the boat to get higher speed. He also assumed that the muscular strength is the same as for a human, and this is also wrong. The dolphins micelle are actually 8-10 times stronger than humans [25]. But still the efficiency of aquatic animals is believed to be high. Anyway, still the efficiency is interesting and relevant.

The first ROVs are from 1950s, but it is uncertain who made the very first. The Royal Navy used an ROV to recover practiced torpedoes and mines from the sea bed in the 1950s. ROVs can also be used for rescue operation of submarines. Examples of this are a leaking submarine outside the west cost of Ireland in 1973 and Kursk in 2000. The first commercial ROV was delvered in 1974 as a replacement for the manned submersible. It was not before the 80s that the technology was accepted as replacement for divers. Now ROVs in various sizes are common in the

oil and gas industry for tasks as intervention work on subsea offshore installations and inspection [26]. The development of AUVs started in the 1960s. In the 80s their where a lot of innovations related to computer science and control. This gave the potential for complex guidance and control algorithms [27]. AUVs today are used for tasks that can be preprogrammed. We think that the future will bring more and more intelligence into the UUVs making them more autonomous with ability to plan and re-plan their missions.

Snake robot is something even newer and most research has been on land based snake robots. A swimming snake robot was developed at Tokyo Institute of Technology 2005. Later a few other swimming snakelike robots are developed. Also some fish like robots have been developed the last 15 years. In the next section we will present some relevant examples.

2.2 Relevant biomimic developed concepts

Biomimic robotics has become a hot topic the last years. Biomimetic mean that humans gets inspiration from the nature to create, processes, substances, devices, or systems. There have been done a huge amount of work in this field. In this section we will present some of the most relevant concepts that have been developed.

2.2.1 RoboTuna at Massachusetts Institute of Technology

Massachusetts Institute of Technology (MIT) have done the most extensive work on fish propulsion managed by Professor Michael Triantafyllou. In the 1990's they started developing a RoboTuna. This was the start of making a underwater biometric robot that was mimicking the swimming fish propulsion. In 1995 they built the first prototype RoboTuna I. The aim of this robot was to make a mechanical blue-fin tuna which is one of the fastest fishes [28]. Later the RoboTuna II has been developed with some modifications, see figure 2.2.

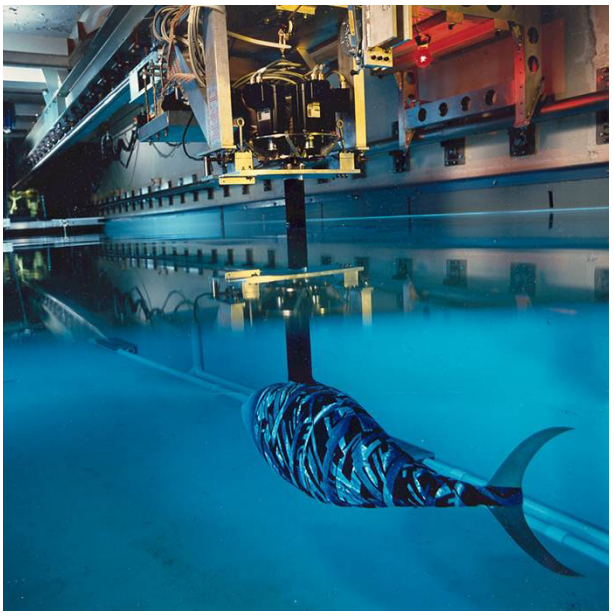

FIGURE 2.2: A picture of the RoboTuna II developed at Massachusetts Institute of Technology (MIT). Photo: Michael Triantafyllou / MIT [5]

A lot of experiments and numerical investigation has been done. Experiments with oscillating foil showed an efficiency up to 87% [29]. They have developed a numerical code and compared the results with Particle Image Velocimetry (PIV) measurements [30]. They have found that the optimal Strouhal number for high efficiency is between 0.25 and 0.35 [31], [32] (The Strouhal number are explained later in this chapter). The fish creates a vortex wake with the tail and body, and can control the votes with the tail to optimize the efficiency [33], [34] . Experiments shows that the total drag for an swimming fish is smaller then for an fish towed in the same speed [35]. Also unsymmetrical oscillations have been investigated [36]. How to calculate the efficiency of a fish is not stright forward. More about this topic can be found in [37].

The Boston Engineering group has now made the RoboTuna to a commercial product. This is the first commercial biomimicing fish robot that is developed to the author's knowledge. They have called it GhostSwimmer and are mainly made for military use, se figure 2.3. The US Navy have also been financial involved in the research at MIT. Forme table 2.1, we can see that the GhostSwimmer has much better speed and efficiency performance compared with the AUV Remus 100.

The acceleration and maneuvering performance are superior. Another important aspect in military is that it is much more silent than an AUV with thruster(s). A silent UUV may also be useful if you want to observe shy aquatic animals. One should notice that the numbers for the GhostSwimmer shown in table 2.1 only are estimates and are still to be verified.

	GhostSwimmer	Remus 100
Max speed	10 knots	5 knots
Endurance: 3 knots	66 hours (assumes same onboard energy)	22 hours
Endurance: 5 knots	14 hours	8 hours

TABLE 2.1: This number are from [13] and shows the speed and efficiency compared with a Remus 100 AUV.

FIGURE 2.3: GhostSwimmer developed of Boston Engineering group and Massachusetts Institute of Technology. Picture from [6]

Also some other concepts have been developed at MIT. A flapping foil under water vehicle [38] and the RoboPike.

2.2.2 G9 fish at the University of Essex

At the University of Essex in United Kingdom they have developed a complete autonomous fish robot.

FIGURE 2.4: The picture shows the G9 fish robot developed at Essex university [7]

Professor Huosheng Hu has managed their work and it started with the G1 fish robot (2003). The G1 fish robot have been followed by a lot of new versions, and in 2005 the G9 version was made, see figure 2.4. They have included an infrared sensor in the mouth of the fish for collision avoidance. There are also different control strategies for turning and swimming. They have focused on adapting the carangiform mode (this are explained later in the chapter), and make it as realistic as possible. The robot is autonomous [39], [40].

2.2.3 FILOSE at the University of Technology in Tallinn

At the Center Biorobotics at the University of Technology in Tallinn (Estonia) they have developed a concept called FILOSE (Fish Locomotion and Sensing). The focus have been to investigate how underwater robots can sense, utilize and adapt to the environmental flow. They have done experiments with the fish robot behind a half cylinder and tried to get the fish to adapt to the vortex shedding. In Tallinn they have installed pressure sensors in the frontal part of the fish to let the robot be all to feel the flow and adapt to it [41], [6]. They have modeled the robot using Lighthills theory, which only take the momentum transferred into the flow into account (added mass). The defectian of the flexible tail is modeled with beam theory [42].

FIGURE 2.5: The picture shows the FILOSE fish robot developed at University of Technology in Tallinn [6].

2.2.4 AmphiBot at Swiss Federal Institute of Technology

The AmphiBot are made to swim like an eel/snake. The AmphiBot has a linked structure an a low aspect ration (aspect ratio is explained later in this chapter) fin at the tail, see figure 2.6. They started in 1999 and have developed AmphiBot I, II and III, and number IV is under planning. They have studied the biology of eels and how they generating their signal that activates the muscles. They have also done a lot of work on how to online generate a reference pattern to follow. The work has not only been on swimming properties. Since it is an AmphiBot they have installed legs so it is able to move both in water and on land. The AmphiBot can walk on the beach and out in the water and start to swim [43], [44], [45], [46], [47].

FIGURE 2.6: Photo of the AmphiBot developed at Swiss Federal Institute of Technology [8].

2.2.5 Snake robots at Tokyo Institute of Technology

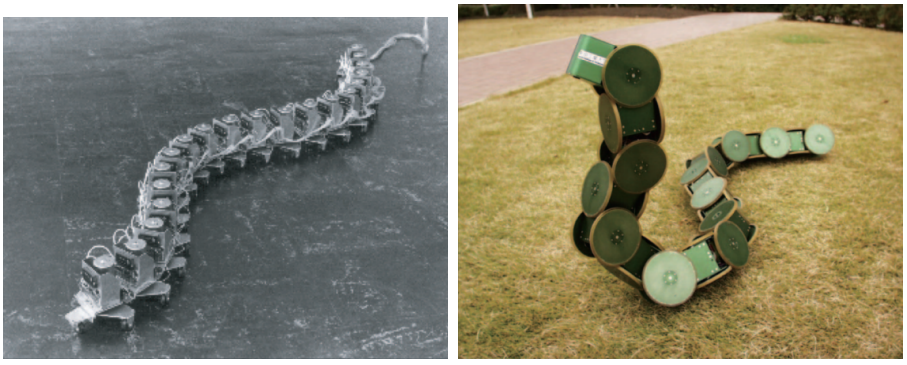

(A) ACM-III snake robot (B) RCM-R3 snake robot

FIGURE 2.7: Snakeroots from University in Tokyo

Shigeo Hirose a professor at Tokyo Institute of Technology in the Department of Mechanical and Aerospace Engineering started to design snake-like robots in 1971. The reason for this was to learn about snakes mechanisms to move and to find future engineering applications. In 1972, he developed the worlds first robot that used the principle of snakes to move. This robot was called ACM-III, it was 2 meters long and had a weight of 28 kg (see picture in figure 2.7a). This snake robot was land based and had wheels to move with. The ACM-III snake-like robot could also wraps around objects and move inside a maze.

In 2001 they developed a new version RCM-R3 (se picture in figure 2.7b). This one was wireless and could move in 3 dimensions, unlike ACM-III that only could move in the floor plane. RCM-R3 also had passive wheels to glide on. The latest snake robot was developed in 2005 and is the ACM-R5 snake like robot (see picture in figure 2.8). The robot is waterproof and can swim in water. It is wireless, 1.6 meters long and has a weight of 6.5 kg. The robot has fins with passive wheels at the tip. This makes it possible to move on the ground and in water. It can achieve 0.4 m/s both in water and ground. The ACM-R5 moves in a helix form when it is swimming. [48]

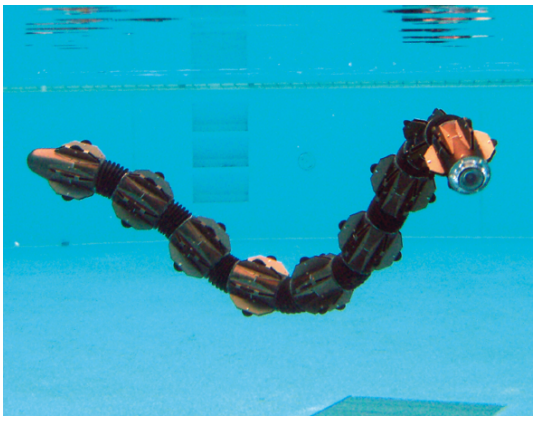

FIGURE 2.8: Picture of the RCM-R5 snake-like robot. Picture from

2.2.6 Snake robot at NTNU

The last 11 years a lot of work have been done on developing snake robots at NTNU. It started from a research project at SINTF in Trondheim and later NTNU. The first snake like robot was called Anna Konda (see figure 2.9).It was a hydraulic firefighter snakelike robot. This was motivated by several major city fires in Trondheim and the idea was to make a self-propelled fire hose. They realized the complexity of snake robots. Later other snake robots have been developed to investigate different aspect of snake robots [9].

FIGURE 2.9: Picture of the Anna Konda snake-like hydraulic firefighter robot [9].

Aiko, Wheekoand and Mamba are the there concepts that have followed after the Anna Konda. The last one, Mamba (see figure 2.10) is also water proof. In each link there is a force transducer. Based on shin guards it measures the forces and

torques in 6 degrees of freedom. Newly the also underwater swimming for the Mamba snake robot have been investigated [9], [49], [1], [50]. The hydrodynamic forces are modeled with a Morrison equation approach including added mass, linear and nonlinear drag. The model is on closed form, which is comprehensive for real time simulations and model based control design. This thesis is an continuation of this work. In addition, we will try to extend the model to handle fins or other exist propulsion forces.

FIGURE 2.10: Picture of the Mamba snake-like robot. Photo by Simen Strømsøyen

2.3 Morphology

Most fishes use fins for proportion and maneuvering in some way. We start by defining the name of the different fins. Figure 2.11 shows the different fins almost all fish, some sharks, whales and eels have. Most fishes have more or less the same arrangement of fins. In this thesis we will only considering the caudal, dorsal and pectoral fins. The caudal fin is the main contributor for trust production. Different aquatic animals have different shapes of the tail. The ones you find on the tuna, some sharks and sailfish (see figure 1.2) are know by their half moon shape an high aspect ratio caudal fin. The aspect ratio is defined as the length or height of the fin divined by the width. These special types of caudal fins are called lunate tails and recognized with a high lift over drag ratio. Eels can also have

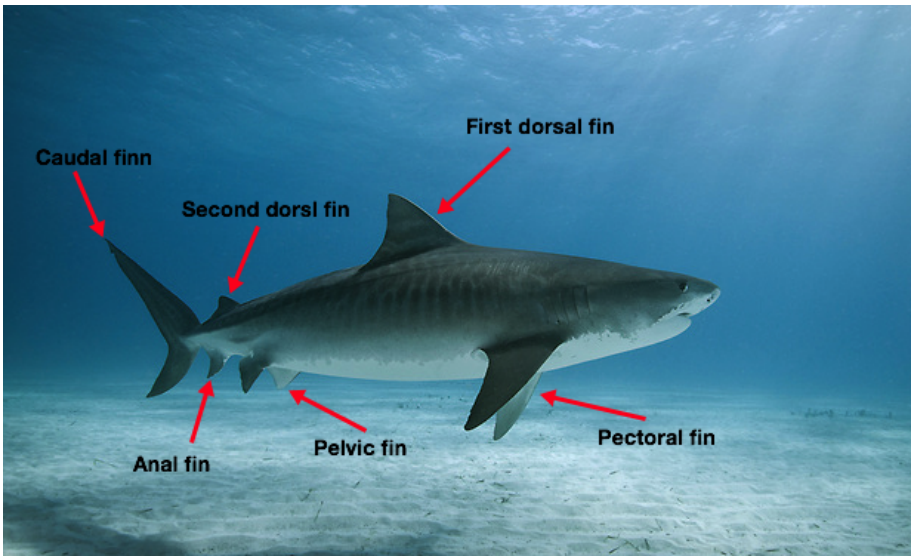

FIGURE 2.11: Picture of a tiger shark showing the different fins we can find on fishes, whales and sharkes. Photo by Alastair Pollock Photography [2]

caudal, dorsal and pectoral fines, but the caudal and dorsal fins can be hard to distinguish because there is no clear distinction between them. Eels have typical low aspect ratio fins.

2.4 Locomotion

Fish locomotion can be classified into two main categories, Periodic (steady) swimming and Transient (unsteady) swimming. Periodic swimming is characterized by cyclic repetition of the propulsive movements. This has been the scientific center for mathematicians and biologists, and will also be the focus of thesis. This is because it is simpler to model. Transient swimming covers rapid stats, mauves and turns. Most fish and eels generate thrust by moving their body in a backward moving propulsive wave (undulation of the body). This is called body or/and caudal fin (BCF) locomotion. It is normal to divide the BFC locomotion into four different categories [10]. They are anguilliform, subcarangiform, carangiform, and the thunniform, (see figure 2.12). The categories is divided by who much of there body that are moving.

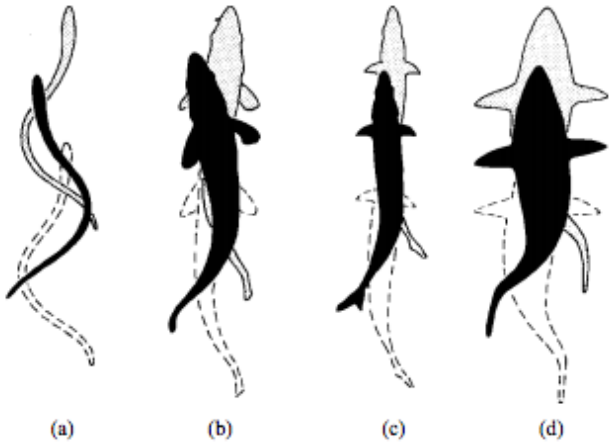

FIGURE 2.12: Figure shows the four different swimming modes. a anguilliform, b subcarangiform, c carangiform and d thunniform mode [10].

In anguilliform mode the entire body are moving in an undulatory movement. The body creates at least on wavelength of the undulatory motion, and the amplitude of the motion is big from head to tail. A lots of anguilliform swimmers are capable of swimming both forward and backward by reversing the direction of the undulation motion. Typical anguilliform swimmers are eels.

The subcarangiform are similar to the anguilliform mode but the undulation motion has less amplitude at the head and incising towards the tail.

Carangiform swimmer has even less motion of the front part of their body. It is almost only the last third of the body that moves. These swimmers are generally faster than subcarangiform and anguilliform swimmers. The compromise for getting the higher speed and efficiency is a reduction in turning/maneuvering and acceleration abilities due to that the body is more rigid.

The thunniform mode is known for being the most efficient mode evolved in the aquatic environment. Almost all the thrust is generated by the lift based method so high cursing speeds over long time are possible. It is almost only the caudal fin that are moving lateral. These bodies are normally streamlined to minimize the pressure drag and the caudal fin is stiff and have a high aspect ratio. The caudal fin often has a half moon shape and is known as lunate tail, see figure 1.2. These animals are optimized for high cursing speeds over a long time in still water,

and have not as god accelerations, turning and slow speed swimming abilities as the anguilliform and subcarangiform swimmers. What is interesting about the thunniform swimmers is that animals form completely different lines have evolved (in biological sense) into the thunniform mode and the lunate tail. Some sharks, marine mammals, teleost fishes and tuna fishes are some of the examples [17], [10].

2.5 Central Pattern Generators (CPG)

Eels of a fish have to move their body in a sinusoidal like motion. For a snake like robot to do this we need a reference signal generator. Different methods have ben proposed for this purpose and we can identify three categories. Motion control based on kinematic or dynamic models of the amphibious snake-like robot, motion equations derived from the Serpenoid Curve or formed by sinusoidal functions, and motions activated by biomimetic neural networks like Central Pattern Generators (CPG) [51], [45]. The Central Pattern Generators have a relative simple mathematical formulation. By using this environment interaction for a CPG controller and complicated calculation of the kinematics and dynamics can be avoided. More information about the CPG can be found here [52].

2.6 Definition motions and forces

There are four main forces that act on a swimming aquatic animal. Vertically, the gravity and the buoyancy. In this thesis, we will only consider swimming in a 2D plane so we assume that the buoyancy and gravity force are equal. Some aquatic animals can regulate their buoyancy others cannot. In the horizontal plane, the thrust and drag forces are acting, see figure 2.13(a). The mechanisms of these forces will be explained in the next section.

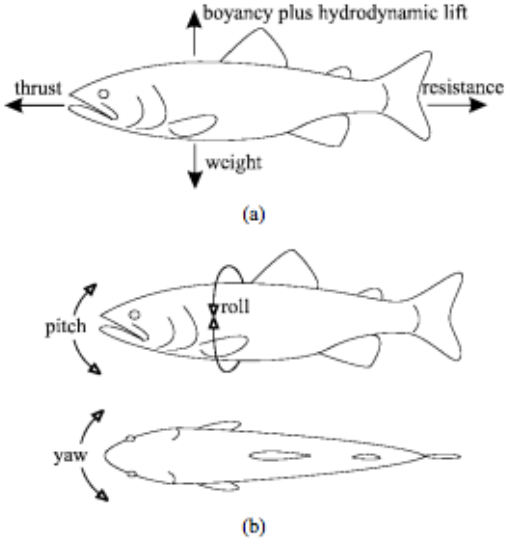

FIGURE 2.13: Figure shows the force balance on a fish (a), and the relevant axis (b) [10].

We use the same definitions on the motions as in ship theory. The yaw, pitch, roll motions ate defined in figure 2.13(b).

2.7 Hydrodynamic definitions and mechanism of swimming propulsion

2.7.1 Thrust

Thrust is a force that generates the forward speed of the aquatic animal or robot. It is usually measured as a mean force generated over one period or cycle. There are different ways for generating thrust. Anguilliform swimmers are mostly using a drag based thrust generation. The forward velocity is created by pressure differences and by moving the body in a backward moving wave similar to paddles. In the other end we have the thunnifom swimmers where the lift from the caudal fin is the dominating thrust force. The added mass effects also contribute to the trust generation and are the most important contribution for sub and carangiform

swimmers. But the lift contributing form the caudal fin should also be included for sub and carangiform swimmers [10].

2.7.2 Added mass

When a fish or an eel are moving their body in water the sounding water mass will start moving, creating a pressure field around the body. The hydrostatic pressure is not included. By integrating this pressure around the body, we find the added mass forces. The added mass should be understood in terms of hydrodynamic pressure and not a physical mass of water moving. We should also note that from the pressure integration it is the force that is proportional to the acceleration that is the added mass. In viscous flow, we will also get a force proportional to the velocity witch will contribute to the drag. Added mass can also be frequency dependent due to the surface boundary condition [53]. In this project, we only look at eels and fish in infinite water and are neglecting the surface boundary condition such that the added mass for 0 frequency can be used.

2.7.3 Drag

The drag contribution has three components. The first is the viscous friction drag as comes from the shear forces between the skin and the water. The second contribution comes form pressure difference and is called form drag. Eel and snake are using this force for propulsion, but tuna fish have a shape and locomotion that minimize this drag force. The last contribution is the energy loss from the vortexes that forms from the caudal and pectoral fines that are generating thrust and lift. This loss has to contributions. One form the tip vortexes that forms on the tip of the fin due to the pressure differences on the to sides of the fin. The other one is the vortexes created behind the fin due to the change in angel of attack. The drag can reduced by controlling the vortex shedding [35].

About the friction drag there is one thing we should note. The fiction drag is not the same for a fish swimming at constant speed and gliding at the same speed.

There is an effect called *boundary layer thinning*. This is due to that the body motion increasing the velocities with respect to the stunning water, causing a thinner and thereby an increased velocity gradient. This gives a higher shear stress with means higher drag. How significant this phenomena is still not known and the estimate wary between 1.12-9 times the gliding fiction drag [10].

2.7.4 Nondimensional parameters

To describe the hydrodynamics some nondimensional number are considered in the literature. Following the relevant parameters is presented.

2.7.4.1 Reynolds number (Re)

The Reynolds number is the ration between the inertia and gravity forces. The Re number is defined as,

$$Re = \frac{UL}{\nu} \tag{2.1}$$

where U is the flow velocity, L is the characteristic length (the diameter for a cylinder, the cord of a foil or length of an UUV), and ν the kinematic viscosity. This is a very important number in hydrodynamics and the magnitude is a guide to determine if the flow is laminar or turbulent. Typical Re number for swimming fish and eels are between 10^3 and $5 * 10^6$ [10].

2.7.4.2 Strouhals number(St)

For a cylinder, the Strouhals number is defined as

$$St = \frac{f_v D}{U}, \tag{2.2}$$

where f_v is the shedding frequency, D is the diameter and U is the inflow velocity.

If we place a fix circular cylinder in a uniform flow the flow will separate form the cylinder surface and form vortexes behind it. This will cause a vortex street that is called a von Karman street. This vortex is creates an oscillating lift (force in cross flow direction) and drag (force in flow direction) force on the cylinder. Strouhals number is normally used for describe this vortex shading phenomena. For a big range of Re numbers (10^3 to $5 * 10^5$) the St number is equal to 0.2 [54].

When a fish is oscillating the body and caudal fin vortexes will form in the wake similar to what we see behind a cylinder. The difference is that the vortexes total in counterclockwise direction witch is opposite of the vortex comes behind a cylinder (see figure 2.19). We say that the fish is making a reveres von Karman street. For a fish the St number is defined as

$$St = \frac{fA}{U}, \tag{2.3}$$

where U is the forward speed, f is the frequency of the tall moment, and A is the peak-to-peak amplitude of the tail. A study done by Triantafyllou at Massachusetts Institute of Technology showed that most fish has a St number in the range of 0.25-0.35. This was calculated from a large number of fish observations of swimming fish in the range for Rn numbers form 10^4 to 10^6 [31]. It is likely to believe that this area of St number give the highest efficiency. We can notice that the optimum St number for fishes are a bit higher than what is the case for a smooth cylinder in approximate same range of Rn numbers.

2.7.4.3 Keulegan-Carpenter number (KC)

The St number was defined for cylinder in uniform flow. We now look at a cylinder in oscillating flow or an eel in steady flow. The KC number reflects the important of the shaded vortices and is the ration between the drag and inertia forces. It is defied as

$$KC = \frac{V_m T}{D}, \tag{2.4}$$

where T is the period flow or of the body motion, V_m is the maximum velocity during on period and D is the diameter of the cylinder or eel [54]. A high KC value means that there will be formed vortexes during period witch gives a higher drag.

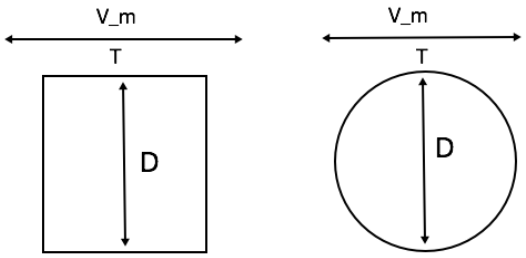

FIGURE 2.14: The figure shows a circular and a squarer cross section in a oscillating flow that has a period of T and a max velocity V_m.

For low KC value the vortexes will be small or not present. Another thing that affects the vortexes is the separation point. Where the separation point occurs is dependent on if the flow is turbulent or laminar and thereby the Rn number [55]. The separation point and KC value will therefore affect the drag coefficient and the thereby the speed and efficiency of the eel or fish.

An eel or a fish are using sideways moments to create a forward speed to a cylinder in oscillating flow. Most fishes and eels have an elliptical or circular cross sections. In figure 2.15, we can se how the flow pattern will look like of different KC number. In [11], a table for the drag and added mass coefficient are given as a function of the Rn number for different KC numbers.

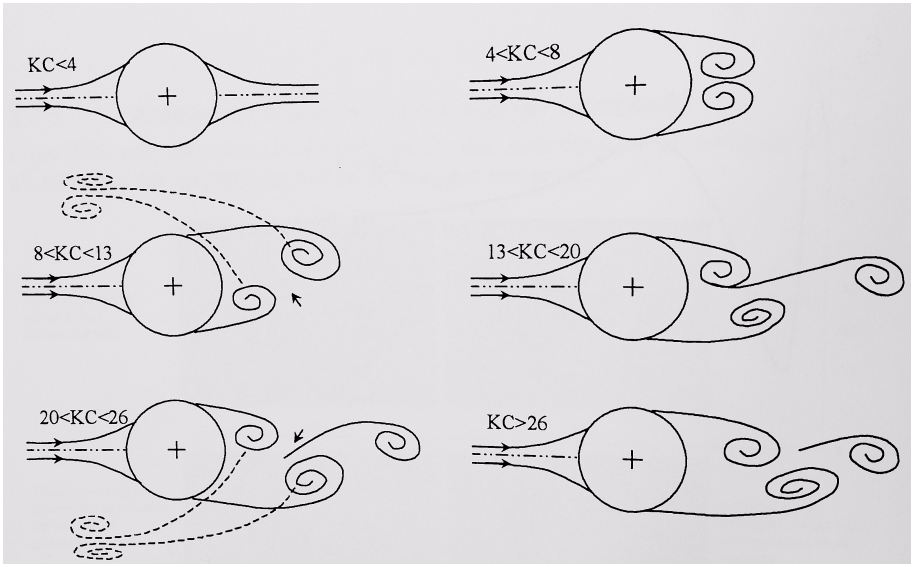

FIGURE 2.15: Flow pattern around a cylinder with different KC numbers [11].

2.7.4.4 Reduced frequency(k)

The reduced frequency is defied as

$$k = \frac{\omega c}{2U}, \tag{2.5}$$

where U is the swimming/forward speed, L is the characteristic length (the cored c of a foil) and ω is the angular oscillation frequency. This is an important parameter in foil theory used to characterize the degree of unsteadiness of the problem. The reduced frequency appears when normalizing the Navier-Stokes equations. For $k = 0$ the flow is steady. If $0 \leq k \leq 0.05$ the flow is considered quasi-steady witch meanest that we can neglect the unsteady effect because they are small. For $0.2 \leq k$ the problem is considered as highly unsteady. [56]

2.7.4.5 Aspect ratio (AR)

Aspect ratio is defined as the span divided by the cord for a rectangular shaped foil. For a foil that are non rectangular the mean cored value are used. Also the

squared of the cored divided by the foil area are used, as given by

$$AR = \frac{s}{c} = \frac{s^2}{A}, \tag{2.6}$$

where A is the area, c is the cord and s is the span of the foil. The aspect ratio are used to compeer different foils. High aspect ratio foils have higher efficiency because the have higher lift to drag ratio. Typical aspect ratio for tunniform swimmers are 4.5-7.2. Tunniform swimmers are known for high efficient cursing speeds.

2.7.4.6 Lift coefficient (C_L)

The lift coefficient is the nondimensional lift define as

$$C_L = \frac{L}{\frac{1}{2}\rho U^2 A} \tag{2.7}$$

where L is the lift force, U is the flow speed and A is the wetted area.

2.7.4.7 Drag coefficient (C_D)

The drag coefficient is the nondimensional drag define as

$$C_D = \frac{D}{\frac{1}{2}\rho U^2 A} \tag{2.8}$$

where D is the drag force, U is the flow speed and A is the wetted area.

2.8 Foil theory

Foil theory have been a huge topic in aerodynamics and the airplane industry. A foil in water, called hydrofoil has the similar characteristics. The only difference is the density of the surrounding fluid. Some fish fins have the same geometry as high aspect ratio foils. Especially the caudal fin on thunniform swimmers has

the same characteristic as a high aspect ratio hydrofoil. This section, will shortly present the relevant theory of foils and how they work. One of the basic theorems in hydrodynamics and foil theory is Kelvins theorem.

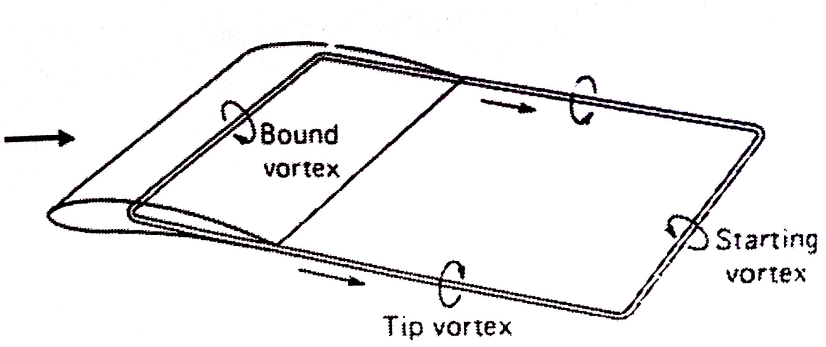

FIGURE 2.16: Vortex system of a foil [12].

Kelvin's theorem of the conservation of circulation states that for an ideal fluid act upon by conservative forces (e.g. gravity) the circulation is constant about any closed material couture moving with the fluid [57].

Ideal fluid is a fluid that is irrotational, incompressible and inviscid. This means that if you integrate the circulation on a contour surrounding the vortex system the circulation is constant. The vortex system of a foil is shown in figure 2.16. There is a starting vortex created because of the change in lift under start up, a tip vortex crated on the tip because of the pressure difference over and under the foil and a bound vortex that is the one that is connected to the lift on the foil.

We also need to define some geometry parameters of the foil. t is the thickness of the foil, s is the tip to tip length of the foil called span and c is the width if the foil called cord length, see figure 2.17. The edge in front of the foil is the leading edge and the edge in the back is called the trailing edge.

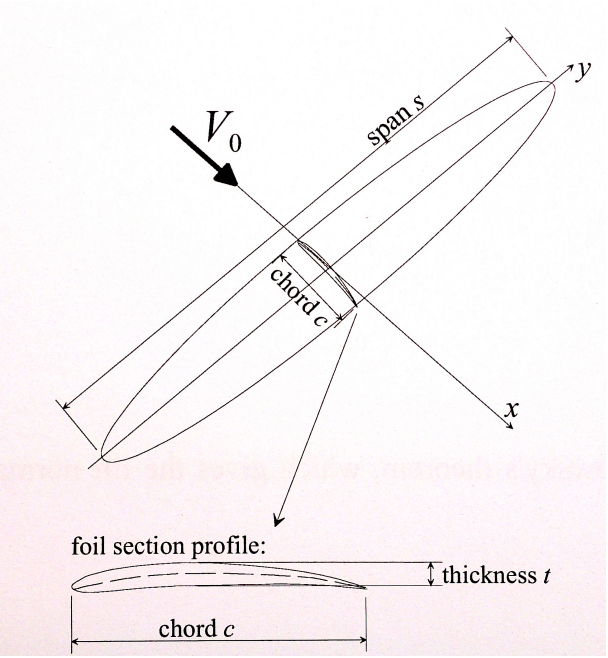

FIGURE 2.17: Geometry of the foil showing the span, cord and thickness of a foil [12]

2.8.1 Lift

For a symmetric foil profile the foil need to be angled to the inflow velocity U to generate lift, se figure 2.18. We call this angel the angel of attack for a steady foil. Then the speed of the fluid will be higher on top of the foil compered with under. This generates a force upwards that we call lift. The lift force acts normal to the inflow velocity. The velocity differs can be modeled as a circulation plus a free stream. A larger angel of attack gives a larger circulation that gives a higher lift. With linear foil theory a flat plate with a unit span the lift coefficient can be expressed as

$$C_L = 2\pi\alpha_l. \tag{2.9}$$

In linear foil theory this assumptions are made:

- Maximum thickness of the foil section is much smaller then the cord length.
- Angel of attack is smal, less then 10^o.

- No flow separation.
- A thin boundary layer.
- linear relation between lift and angel of attack α.

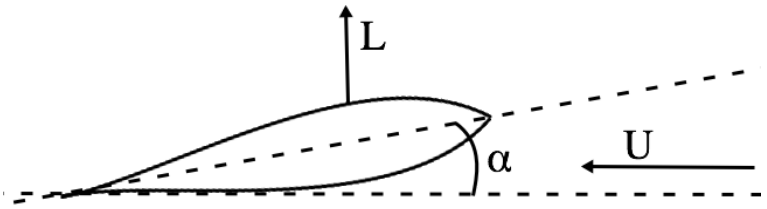

FIGURE 2.18: Angel of attack, α_l. (In the figure α is used as α_l.))

2.8.2 Drag on foils

There at two components that contribute to the drag on a foil as long as the flow do not separate but follows the foil surface form the leading edge to the trailing edge. The components are called friction drag and induced drag. The friction drag is due to shear stresses between the fluid and the foil surface. The induced drag is due to induced velocity which gives a downwash (a fluid velocity downwards on the leading edge) that decrease the angel of attack and thereby the lift. The induced velocity has two components. One is from the tip vortices due to pressure differences. This effect will only be present I 3D. The other one is from the starting vortex or trailing vortex that will induce a velocity downwards on the foil.

2.8.3 Unsteady lift

For an oscillating and rotating foil the angel of attack α_l is always changing, which means that the circulation is always changing. As we now know the circulation is directly coupled to the lift and angel of attack. So an oscillating and rotating foil will have a time dependent lift. From Kelvins theorem, we know that the total circulation of the vortex system is constant. As the angel of attack changes the

lift change and the circulation that crates lift changes. For the total circulation in the system to stay constant a new starting vortex have to be created to balance the total circulation. These vortexes create a revers von Karman Street.

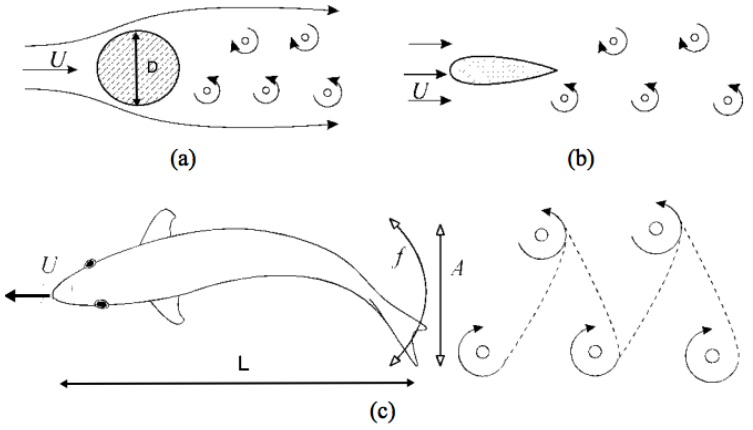

FIGURE 2.19: The figure showes a von Karman Street behind a cylinder (a), an revers von Karman Street behind an oscillating foil (b) and a revers von Karman Street behind a swimming fish (c) [10].

As we can se in figure 2.19, the difference between a von Karman Street and a revers von Karman Street is the direction of the vortex rotation. We can think about it as the vortex that is shed behind a cylinder creates a drag force on the cylinder. While on an oscillating foil crates vortexes that rotates the other way and creates a thrust on the foil. It is this mechanism that also fish uses to generate thrust. And it is especially the tunniform swimmers that utilize this technic.

2.8.4 Stalling

If the foil have a too large angel of attack the foil will stall. This happens when the flow do not manage to stay attached to the foil and separates, typically on the leading edge, see figure 2.20. A steady foil will typical stall between $10^o - 15^o$. When the foil stales the lift force decreases significantly.

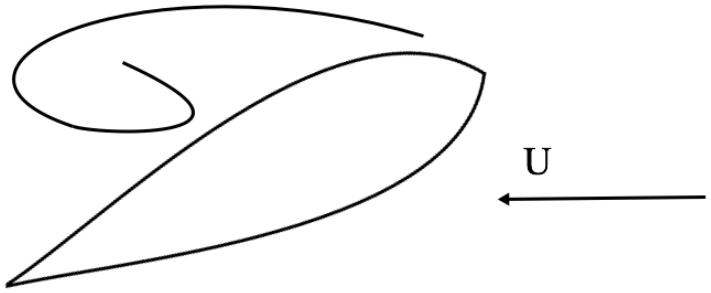

FIGURE 2.20: A stalling foil.

A unsteady foil can achieve a much higher angel of attack than the same foil in steady condition. This is due to a continuously change of the angel of attack and change in circulation [58].

Chapter 3

A 2D complex model of a swimming snake robot

This section will present an extenuation of the model of a snake-like robot moving in a 2D plane presented in [1]. The extension gives the opportunity to include a force and moment from a tail and thruster on the links. It also includes that each link can have different mass, length and inertia since a tail or thruster can effect the inertia, mass and length of the link. The links are still assumed to have the center of mass and buoyancy in the center of the link. The reason for this is that the model would this would complicate the model a lot.

3.1 Parameters of the snake Robot

The snake consist of N links. where each link has a length equal to $2l_i$, where i is the link number. All the links have a equal distributed mass so the center of mass (CM) is always in the mid point. Each link has a mass m_i and a moment of inertia $J_i = \frac{1}{3}m_i l_i^2$. The snakes robot have $N-1$ motorized joints. The total mass of the snake robot we define as the sum of al the link masses (3.1).

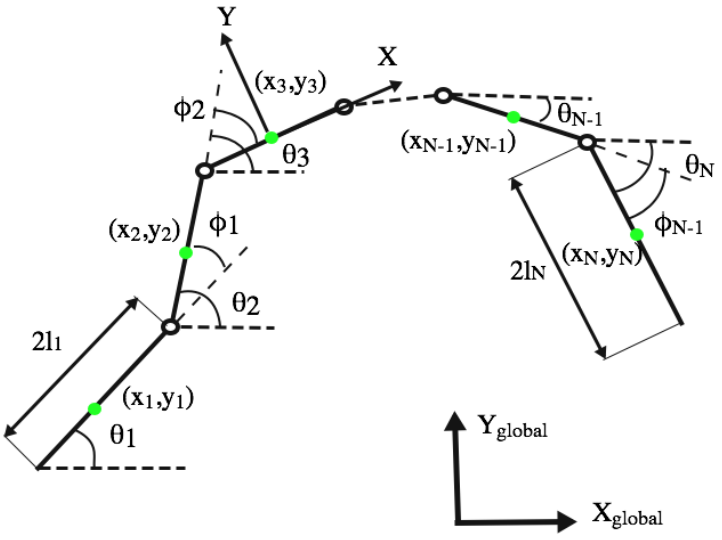

FIGURE 3.1: Forces and moments on a link

$$m_t = \sum_{i=1}^{N} m_i \tag{3.1}$$

Since the links can have a different mass, length and inertia we uses the following diagonal matrices for the mass (M), inertia (J) and length (L):

$$\mathbf{M} = \begin{bmatrix} m_1 & & \\ & \ddots & \\ & & m_N \end{bmatrix} \in \mathbb{R}^{N\times N}, \mathbf{J} = \begin{bmatrix} j_1 & & \\ & \ddots & \\ & & j_N \end{bmatrix} \in \mathbb{R}^{N\times N}$$

$$\mathbf{L} = \begin{bmatrix} l_1 & & \\ & \ddots & \\ & & l_N \end{bmatrix} \in \mathbb{R}^{N\times N}$$

Description of the symbols used in this model can be found in table 3.1. The following sections will describe the kinematic, hydrodynamic and dynamic model of the snake robot. We will also use the following vectors and matrixes:

$$\mathbf{D} = \begin{bmatrix} 1 & -1 & & \\ & \ddots & \ddots & \\ & & 1 & -1 \end{bmatrix} \in \mathbb{R}^{(N-1)\times N}, \mathbf{A} = \begin{bmatrix} 1 & 1 & & \\ & \ddots & \ddots & \\ & & 1 & 1 \end{bmatrix} \in \mathbb{R}^{(N-1)\times N}$$

$$e = [1, 1, \cdots, 1]^T \in \mathbb{R}^N, \mathbf{E} = \begin{bmatrix} e & 0_{N\times 1} \\ 0_{N\times 1} & e \end{bmatrix} \in \mathbb{R}^{2N\times 2}$$

$sin\theta = [sin\theta_1, \cdots, sin\theta_N]^T \in \mathbb{R}^N$

$cos\theta = [cos\theta_1, \cdots, cos\theta_N]^T \in \mathbb{R}^N$

$\dot{\theta}^2 = [\dot{\theta}_1^2, \cdots, \dot{\theta}_N^2]^T \in \mathbb{R}^N$

$X = [x_1, \cdots, x_N]^T \in \mathbb{R}^N$

$Y = [y_1 \cdots, y_N]^T \in \mathbb{R}^N$

$$\mathbf{S}_\theta = \begin{bmatrix} sin\theta_1 & & \\ & \ddots & \\ & & sin\theta_N \end{bmatrix} \in \mathbb{R}^{N\times N}, \mathbf{C}_\theta = \begin{bmatrix} cos\theta_1 & & \\ & \ddots & \\ & & cos\theta_N \end{bmatrix} \in \mathbb{R}^{N\times N}$$

Symbol	Description	Associated vector
N	Number of links	
l_i	Half the length of like number i	
m_i	The mass of link i	
j_i	The moment of inertia of link i	
m_t	The total mass of the snake robot	
$\mathbf{L}$	Diagonal matrix with the different link angels	$\mathbf{L} \in \mathbb{R}^{\mathbf{N}\times\mathbf{N}}$
$\mathbf{M}$	Diagonal matrix with the different link masses	$\mathbf{M} \in \mathbb{R}^{\mathbf{N}\times\mathbf{N}}$
$\mathbf{J}$	Diagonal matrix with the different link inertias	$\mathbf{J} \in \mathbb{R}^{\mathbf{N}\times\mathbf{N}}$
θ_i	Angel between joint i and the global x axis	$\theta \in \mathbb{R}^N$
ϕ_i	Angel of joint i	$\phi \in \mathbb{R}^{N-1}$
(x_i, y_i)	Global coordinates of the CM of link i	$X, Y \in \mathbb{R}^N$
P_x, P_y	Global coordinates of the CM of the snake robot	$P_{CM} \in \mathbb{R}^2$
u_i	Actuator torque extended on link i from link i+1	$u \in \mathbb{R}^{N-1}$
u_{i-1}	Actuator torque extended on link i from link i-1	$u \in \mathbb{R}^{N-1}$
$f_{x,i}$	Fluid force in x direction on link i	$f_x \in \mathbb{R}^N$
$f_{y,i}$	Fluid force in y direction on link i	$f_y \in \mathbb{R}^N$
$f_{x,t,i}$	Propulsive force in x direction on link i	$f_{x,t} \in \mathbb{R}^N$
$f_{y,t,i}$	Propulsive force in y direction on link i	$f_{y,t} \in \mathbb{R}^N$
τ_i	Fluid torque on linke i	$\tau_i \in \mathbb{R}^N$
$\tau_{t,i}$	Torque from propulsive force on linke i	$\tau_{t,i} \in \mathbb{R}^N$
$h_{x,i}$	Joint constraint force in x direction on link i from link i+1	$h_x \in \mathbb{R}^{N-1}$
$h_{y,i}$	Joint constraint force in y direction on link i from link i+1	$h_y \in \mathbb{R}^{N-1}$
$h_{x,i-1}$	Joint constraint force in x direction on link i from link i-1	$h_x \in \mathbb{R}^{N-1}$
$h_{y,i-1}$	Joint constraint force in y direction on link i from link i-1	$h_y \in \mathbb{R}^{N-1}$

TABLE 3.1: Definitions of mathematical terms

3.2 Kinematics

The snake robot have N+2 degrees of freedom an moving in a 2D plane. It is imported to note the distinction between the to angeles θ_i and ϕ_i we are using in the model. The link angeles θ_i where i $\in \{1, \cdots, N\}$ is defined as the angel between the local and the global x axis, see figure 3.1. Positive direction is counterclockwise. The joint angels ϕ_i where $i \in \{1, \cdots, N-1\}$ is the relative angel between two links define as

$$\phi_i = \theta_i - \theta_{i+1}.$$

We assembly the two different angels in the following vectors: $\theta = [\theta_1, \cdots, \theta_N] \in \mathbb{R}^N$, $\phi = [\phi_1, \cdots, \phi_{N-1}] \in \mathbb{R}^N$. The heading or orientation of the snake robot is defined as the average of all the link angels

$$\bar{\theta} = \frac{1}{N} \sum_{i=1}^{N} \theta_i. \tag{3.2}$$

The local frame on each link link is placed in the CM of each link with the y axis normal to the link and the x axis tangential to the link. When the link angel is zero the local coordinate from will be aligned with the global. The rotation matrix from the local frame of link i to the global from is given by:

$$\mathbf{R}_{link,i}^{global} = \begin{bmatrix} cos\theta_i & -sin\theta_i \\ sin\theta_i & cos\theta_i \end{bmatrix}. \tag{3.3}$$

The global position of the mass enter of the snake robot given by P_x and P_y is given by

$$P_{CM} = \begin{bmatrix} P_x \\ P_y \end{bmatrix} = \begin{bmatrix} \frac{\sum_{i=1}^{N} m_i x_i}{m_t} \\ \frac{\sum_{i=1}^{N} m_i y_i}{m_t} \end{bmatrix} = \frac{1}{m_t} \begin{bmatrix} \sum_{i=1}^{N} m_i x_i \\ \sum_{i=1}^{N} m_i y_i \end{bmatrix} = \frac{1}{m_t} \begin{bmatrix} e^T \mathbf{M} X \\ e^T \mathbf{M} Y \end{bmatrix}, \tag{3.4}$$

where e, X, Y and M are defined in section 3.1. Since the link can have different masses we can not do the same abbreviation as in [1].

Link $i+1$ and link i are connected with joint $i \in \{1, \cdots, N-1\}$. We can then define the holonomic constraints (holonomic constraints is a geometric constraint)

$x_{i+1} - x_i = l_i cos\theta_i + l_{i+1} cos\theta_{i+1}$,
$y_{i+1} - x_i = l_i sin\theta_i + l_{i+1} sin\theta_{i+1}$.

We can write this constraints in matrix form using the notation from section 3.1.

$$\mathbf{D}X + \mathbf{AL}cos\theta = 0 \tag{3.5a}$$

$$\mathbf{D}Y + \mathbf{AL}sin\theta = 0 \tag{3.5b}$$

By then combining the holonomic constraints 3.5 with the global CM 3.4 and get an expression for the individual positions of the links:

$$\mathbf{T}X = \begin{bmatrix} -\mathbf{AL}cos\theta \\ P_x \end{bmatrix}, \mathbf{T}Y = \begin{bmatrix} -\mathbf{AL}sin\theta \\ P_y \end{bmatrix} \tag{3.6}$$

where

$$\mathbf{T} = \begin{bmatrix} \mathbf{D} \\ e^T \frac{\mathbf{M}}{m_t} \end{bmatrix} \in \mathbb{R}^{N \times N}. \tag{3.7}$$

It can be shown that

$$\mathbf{T}^{-1} = \begin{bmatrix} \mathbf{M}^{-1}\mathbf{D}^T(\mathbf{D}\mathbf{M}^{-1}\mathbf{D}^T)^{-1} & e^T \end{bmatrix} \in \mathbb{R}^{N \times N}$$

[59]. We can use this to solve (3.6) for X and Y and get

$$X = \mathbf{T}^{-1} \begin{bmatrix} -\mathbf{AL}cos\theta \\ P_x \end{bmatrix}, Y = \mathbf{T}^{-1} \begin{bmatrix} -\mathbf{AL}sin\theta \\ P_y \end{bmatrix} \tag{3.8}$$

which we can write as

$$X = -\mathbf{K}cos\theta + eP_x, \tag{3.9a}$$

$$Y = -\mathbf{K}sin\theta + eP_y, \tag{3.9b}$$

where

$$\mathbf{K} = \mathbf{M}^{-1}\mathbf{D}^T(\mathbf{D}\mathbf{M}^{-1}\mathbf{D}^T)^{-1}\mathbf{A}\mathbf{L}.$$

By differentiating (3.9) ones we get the velocities

$$\dot{X} = \mathbf{K}\mathbf{S}_\theta\dot{\theta} + e\dot{P}_x, \tag{3.10a}$$

$$\dot{Y} = -\mathbf{K}\mathbf{C}_\theta\dot{\theta} + e\dot{P}_y, \tag{3.10b}$$

and by differentiating the velocities we get the accelerations of the links

$$\ddot{X} = \mathbf{K}\mathbf{C}_\theta\dot{\theta}^2 + \mathbf{K}\mathbf{S}_\theta\ddot{\theta} + e\ddot{P}_x, \tag{3.11a}$$

$$\ddot{Y} = \mathbf{K}\mathbf{S}_\theta\dot{\theta}^2 - \mathbf{K}\mathbf{C}_\theta\ddot{\theta} + e\ddot{P}_y. \tag{3.11b}$$

3.3 Hydrodynamics

The hydrodynamics of a swimming fish or eel are really complex and as mentioned before still not completely understood. An exact model is therefore not possible to make. The most accurate way to calculate the fluid forces are CFD (Computational Fluid Dynamics) which means to solve the Navies Stokes equation numerically. The computational cost of such a method is extremely high and not suitable for real time control. In this thesis we will use the same modeling approach as in [49]. We will follow the same steps, but extend the fluid model to fit the extended kinematic equation. in particular use the Morrison equation including both the added mass and drag considering that the snake robot is a

slender body. Each link is considered as an isolated segment, and the snake robot is approximated to have an elliptical cross section. The fluid forces are only dependent on the transverse link motion witch means that we neglect the coupled effect of the sideways and forward velocity. The assumptions we do:

Assumption 1. The fluid is irrotational, incompressible and viscid.

Assumption 2. The robot is natural buoyant.

Assumption 3. The current in inertial frame, $v_c = [V_{x,i} V_{y,i}]^T$ is irrotational.

The fluid forces are a function of the current. In ship control it is common to assume that the current is constant in the body frame witch means that $\dot{v}_c = 0$. This assumption is not correct when turning and the current should instead be assumed constant in inertia frame as in assumption 3 [49].

The fluid forces on link i are expressed with the relative velocity witch is defined as $v_{r,i}^{link,i} = \dot{p}_i^{link,i} - v_{c,i}^{link,i}$ where $v_{c,i}^{link,i}$ is given as $v_{c,i}^{link,i} = (\boldsymbol{R}_{link,i}^{global})^T v_c = [v_{x,i}, v_{y,i}]^T$. $v_{c,i}^{link,i}$ is the current velocity in body frame and $v_c = [V_{x,i} V_{y,i}]^T$ is the current velocity in inertia frame. Due to assumption 3 we can the write

$$\dot{v}_{c,i}^{link,i} = \frac{d}{dt}\left((\boldsymbol{R}_{link,i}^{global})^T v_c\right) = \begin{bmatrix} -sin\theta_i\dot{\theta}_i & cos\theta_i\dot{\theta}_i \\ -cos\theta_i\dot{\theta}_i & -sin\theta_i\dot{\theta}_i \end{bmatrix} \begin{bmatrix} V_{x,i} \\ V_{y,i} \end{bmatrix}. \tag{3.12}$$

Each link is subjected to a fluid torque and force acting on the center of mass of the link. As mention before the fluid force consist of both an added mass and a drag term. The drag model that we are using taks into account the generalized case of anisotropic friction acting on each link. This means that the drag coefficient are different in x and y direction. c_t is the drag coefficient in x direction (tangential to the link) and c_n is the drag coefficient in y direction (normal to the link).

$$f_i^{link,i} = -\hat{\boldsymbol{C}}_{A,\dot{v}_{r,i}}^{link,i} - \hat{\boldsymbol{C}}_{D,\dot{v}_{r,i}}^{link,i} - \hat{\boldsymbol{C}}_{D,sgn}\left(v_{r,i}^{link,i}\right)\left(v_{r,i}^{link,i}\right)^2, \tag{3.13}$$

where $\hat{\boldsymbol{C}}_{\boldsymbol{D}}$ and $\hat{\boldsymbol{C}}_{\boldsymbol{A}}$ is constant (2×2) matrices depending on the fluid characteristics and body shape and $\dot{v}_{r,i}^{link,i} = \ddot{p}_i^{link,i} - \dot{v}_{c,i}^{link,i}$ are the relative acceleration on link i.

Note that the fluid force is a function of the x coordinate on the link. To get the total force $f_i^{link,i}$ we have to integrate $df_i^{link,i}(x)$ over the link. We now make a new assumption.

Assumption 4. The relative velocity at each section of link i in body frame is the same as the relative velocity in the center of mass of each link.

This assumption is valid because the link length is small compered with the total length of the robot. The assumption is valuable because we then avoid numerical calculation du to the nonlinear terms.

The cross section of the robot is assumed to be elliptical with the major diameter given as 2a and the minor diameter given as 2b. The links have the length $2l_i$. The matrixes $\hat{\boldsymbol{C}}_{\boldsymbol{D}}$ and $\hat{\boldsymbol{C}}_{\boldsymbol{A}}$ can then be expressed as

$$\hat{\boldsymbol{C}}_{\boldsymbol{D}} = \begin{bmatrix} \boldsymbol{c_t} & 0_{N\times 1} \\ 0_{N\times 1} & \boldsymbol{c_n} \end{bmatrix} = \begin{bmatrix} \frac{1}{2}\rho\pi C_f \frac{a+b}{2} 2\boldsymbol{L} & 0_{N\times 1} \\ 0_{N\times 1} & \frac{1}{2}\rho C_D 2a 2\boldsymbol{L} \end{bmatrix}, \tag{3.14}$$

$$\hat{\boldsymbol{C}}_{\boldsymbol{A}} = \begin{bmatrix} \boldsymbol{\mu_t} & 0_{N\times 1} \\ 0_{N\times 1} & \boldsymbol{\mu_n} \end{bmatrix} = \begin{bmatrix} 0_{N\times 1} & 0_{N\times 1} \\ 0_{N\times 1} & \frac{1}{2}\rho C_A a^2 2\boldsymbol{L} \end{bmatrix}, \tag{3.15}$$

where ρ is the density and

$\boldsymbol{c_t} = diag([c_{t,1}, \cdots, c_{t,N}])$,
$\boldsymbol{c_n} = diag([c_{n,1}, \cdots, c_{n,N}])$,
$\boldsymbol{\mu_n} = diag([\mu_{n,1}, \cdots, \mu_{n,N}])$.

Note that $\boldsymbol{\mu_t} = 0$. This is the added mass in x direction and for a slender body this can be neglected because it is so small compered with the body mass. Also note that the C_f and C_D here are constant because we assume that all links have the same fluid characteristics and cross section. If this is not the case the constants C_f and C_D can be replaced with diagonal matrixes $\boldsymbol{C_f}$ and $\boldsymbol{C_D}$. Fore future information look at the end of this section.

We now need to find the fluid torques acting τ_i in links. The fluid torques are often neglected since it is assumed they have little effects on the motion of the robot. The fluid torques is included in this model because it gives a more accurate model and they are directly coupled to the power consumption. Since demand of improving the efficiency to allow longer missions and the fluid torques are significantly contributions to the actuator torques, we will take them into consideration [49].

The fluid torques are a result of fluid forces acting normal to the link when the link rotates. The links are similar to a flat plate oscillating in an irrotational flow. It can be shown that the fluid torque can be modeled as

$$\tau = -\mathbf{\Lambda_1}\ddot{\theta} - \mathbf{\Lambda_2}\dot{\theta} - \mathbf{\Lambda_3}\dot{\theta} \mid \dot{\theta} \mid \tag{3.16}$$

, similarly to approach presented in [49], where

$\mathbf{\Lambda_1} = diag([\Lambda_{1,1}, \cdots, c_{1,N}])$,
$\mathbf{\Lambda_2} = diag([\Lambda_{2,1}, \cdots, c_{2,N}])$,
$\mathbf{\Lambda_3} = diag([\Lambda_{3,1}, \cdots, c_{3,N}])$.

$\Lambda_{1,i}$, $\Lambda_{2,i}$ and $\Lambda_{3,i}$ are parameters depending on the shape of the body and the fluid characteristics. $\Lambda_{1,i}$ is the added mass parameter and for a cylinder with elliptical cross section added mass has an analytical form. In this thesis we will only consider equal elliptical cross sections. The links have an total length of $2\boldsymbol{L}$ then $\Lambda_{1,i}$ becomes

$$\boldsymbol{\lambda_1} = \frac{1}{12}\rho\pi C_M(a^2 - b^2)\boldsymbol{L}^3, \tag{3.17}$$

where C_M is the added inertia coefficient. To fined $\Lambda_{2,i}$ and $\Lambda_{3,i}$ we need to integrate the moment around the CM created by the drag force on link i due to that the link is rotating.The torque form an infinitesimal length on link i can be

written as

$$d\tau_{drag} = sdf_{drag} = -sC_{Ld_x}s\dot{\theta}_i ds - sC_{Ld_x}sgn(s\dot{\theta}_i)(s\dot{\theta}_i)^2 ds \tag{3.18}$$

where s is the distance from the CM to the element ds on link i and $C_{Ld_x} = (1/2)\rho\pi C_f(a+b)/2$. By integtating this over the link from $-l_i$ to l_i we get the total torque caused by the drag, as given by

$$\tau_{drag} = -\int_{-l_i}^{l_i}(sC_{Ld_x}s\dot{\theta}_i ds + sC_{Ld_x}sgn(s\dot{\theta}_i)(s\dot{\theta}_i)^2)ds = -\Lambda_{2,i}\dot{\theta}_i - \Lambda_{3,i}\dot{\theta}_i \mid \dot{\theta}_i \mid \tag{3.19}$$

where $\Lambda_{2,i}$ and $\Lambda_{3,i}$ are given by

$$\Lambda_{2,i} = \frac{1}{6}\rho\pi C_f(a+b)l_i^3 \quad \text{and} \quad \Lambda_{3,i} = \frac{1}{8}\rho\pi C_f(a+b)l_i^4 \tag{3.20}$$

on matrix form $\mathbf{\Lambda_2}$ and $\mathbf{\Lambda_3}$ becomes

$$\mathbf{\Lambda_2} = \frac{1}{6}\rho\pi C_f(a+b)\boldsymbol{L}^3 \quad \text{and} \quad \mathbf{\Lambda_3} = \frac{1}{8}\rho\pi C_f(a+b)\boldsymbol{L}^4 \tag{3.21}$$

To sum up the $\hat{\boldsymbol{C}}_{\boldsymbol{A}}$ and $\mathbf{\Lambda_1}$ represent the added mass from the fluid on the links. The $\hat{\boldsymbol{C}}_{\boldsymbol{D}}$, $\mathbf{\Lambda_2}$ and $\mathbf{\Lambda_3}$ represent the drag forces parameters. The fluid force in global frame are given by

$$\begin{aligned} f_i^{global} &= \boldsymbol{R}_{link,i}^{global} f_i^{link,i} = \begin{bmatrix} cos\theta_i & -sin\theta_i \\ sin\theta_i & cos\theta_i \end{bmatrix} \begin{bmatrix} f_{x,i}^{link,i} \\ f_{y,i}^{link,i} \end{bmatrix} \\ = -\boldsymbol{R}_{link,i}^{global}\hat{\boldsymbol{C}}_{\boldsymbol{A}} &\left((\boldsymbol{R}_{link,i}^{global})^T \begin{bmatrix} \ddot{x}_i \\ \ddot{y}_i \end{bmatrix} - \begin{bmatrix} -sin\theta_i\dot{\theta}_i & cos\theta_i\dot{\theta}_i \\ -cos\theta_i\dot{\theta}_i & -sin\theta_i\dot{\theta}_i \end{bmatrix} \begin{bmatrix} V_{x,i} \\ V_{y,i} \end{bmatrix} \right) \\ &-\boldsymbol{R}_{link,i}^{global}\hat{\boldsymbol{C}}_{\boldsymbol{D}} \begin{bmatrix} V_{r_x,i} \\ V_{r_y,i} \end{bmatrix} - \boldsymbol{R}_{link,i}^{global}\hat{\boldsymbol{C}}_{\boldsymbol{D}} sgn\left(\begin{bmatrix} V_{r_x,i} \\ V_{r_y,i} \end{bmatrix} \right) \begin{bmatrix} V_{r_x,i}^2 \\ V_{r_y,i}^2 \end{bmatrix}, \end{aligned} \tag{3.22}$$

where

$$\begin{bmatrix} V_{r_x,i} \\ V_{r_y,i} \end{bmatrix} = (\boldsymbol{R}_{link,i}^{global})^T \begin{bmatrix} \dot{x}_i - V_{x,i} \\ \dot{y}_i - V_{y,i} \end{bmatrix}. \tag{3.23}$$

If we the do the multiplications, we can write the fluid forces on the links on vector form in the global coordinate frame as

$$f = \begin{bmatrix} f_x \\ f_y \end{bmatrix} = \begin{bmatrix} f_{Ax} \\ f_{Ay} \end{bmatrix} + \begin{bmatrix} f^I_{Dx} \\ f^I_{Dy} \end{bmatrix} + \begin{bmatrix} f^{II}_{Dx} \\ f^{II}_{Dy} \end{bmatrix} \tag{3.24}$$

where f_{Ax} and f_{Ay} is the added mass forces and expressed as

$$\begin{aligned} \begin{bmatrix} f_{Ax} \\ f_{Ay} \end{bmatrix} = &- \begin{bmatrix} \boldsymbol{\mu_n}\mathbf{S}^2_\theta & -\boldsymbol{\mu_n}\mathbf{S}_\theta\mathbf{C}_\theta \\ -\boldsymbol{\mu_n}\mathbf{S}_\theta\mathbf{C}_\theta & \boldsymbol{\mu_n}\mathbf{C}^2_\theta \end{bmatrix} \begin{bmatrix} \ddot{X} \\ \ddot{Y} \end{bmatrix} \\ &- \begin{bmatrix} -\boldsymbol{\mu_n}\boldsymbol{S}_\theta\mathbf{C}_\theta & -\boldsymbol{\mu_n}\mathbf{S}^2_\theta \\ \boldsymbol{\mu_n}\mathbf{C}^2_\theta & \boldsymbol{\mu_n}\mathbf{S}_\theta\mathbf{C}_\theta \end{bmatrix} \begin{bmatrix} V^a_x \\ V^a_y \end{bmatrix} \dot{\theta} \end{aligned} \tag{3.25}$$

where $V^a_x = diag(V_{x,1} \cdots V_{x,n}) \in \mathbb{R}^{N\times N}$ and $V^a_y = diag(V_{y,1} \cdots V_{y,n}) \in \mathbb{R}^{N\times N}$. $f^I_{Dx}, f^I_{Dy}, f^{iI}_{Dx}$ and f^I_{Dy} is the linear and non linear drag forces in x and y direction and are expressed as

$$\begin{bmatrix} f^I_{Dx} \\ f^I_{Dy} \end{bmatrix} = - \begin{bmatrix} \boldsymbol{c_t}\boldsymbol{C}^2_\theta + \boldsymbol{c_n}\boldsymbol{S}^2_\theta & (\boldsymbol{c_t} - \boldsymbol{c_n})\boldsymbol{S}_\theta\boldsymbol{C}_\theta \\ (\boldsymbol{c_t} - \boldsymbol{c_n})\boldsymbol{S}_\theta\boldsymbol{C}_\theta & \boldsymbol{c_t}\boldsymbol{S}^2_\theta + \boldsymbol{c_n}\boldsymbol{C}^2_\theta \end{bmatrix} \begin{bmatrix} \dot{X} - V_x \\ \dot{Y} - V_y \end{bmatrix} \tag{3.26}$$

$$\begin{bmatrix} f^{II}_{Dx} \\ f^{II}_{Dy} \end{bmatrix} = - \begin{bmatrix} \boldsymbol{c_t}\boldsymbol{C}_\theta & -\boldsymbol{c_n}\boldsymbol{S}_\theta \\ \boldsymbol{c_t}\boldsymbol{S}_\theta & \boldsymbol{c_n}\boldsymbol{C}_\theta \end{bmatrix} sgn(\begin{bmatrix} V_{rx} \\ V_{ry} \end{bmatrix}) \begin{bmatrix} V^2_{rx} \\ V^2_{ry} \end{bmatrix} \tag{3.27}$$

where the relative velocity $V_r = [V_{rx}, V_{ry}]^T$ is

$$V_r = \begin{bmatrix} V_{rx} \\ V_{ry} \end{bmatrix} = \begin{bmatrix} \boldsymbol{C}_\theta & \boldsymbol{S}_\theta \\ -\boldsymbol{S}_\theta & \boldsymbol{C}_\theta \end{bmatrix} \begin{bmatrix} \dot{X} - V_x \\ \dot{X} - V_y \end{bmatrix}). \tag{3.28}$$

We have now determined the fluid forces and torques in the inertia frame.

Remark on the drag coefficients:
We should note that as a fish or eel are oscillating the tail and body also have a forward speed. So if the first link of the snake robot sheds a vortex ant the robot has a forward velocity this may affect the link number 2 or 3 or 4 depending on how large the forward velocity is.

This means that the inflow velocity affect the cross flow. For high forward velocity U the cross flow velocity times the period ($V_m T$) have to be bigger compared with a low U velocity to get vortex shading from the cross section. For slow swimming this will have less effect, but as the U velocity increases it gets more and more important. This motivate for introducing a new number that takes this effect into account. We have called it Strømsøyen-Godø number (SG).

SG (Strømsøyen-Godø) number: There is actually to ways to define the KC number. If we uses the forward velocity U and the length L, instead of the maximum velocity of the cross section during on period V_m and D is the diameter we get

$$KC_U = \frac{UT}{L}, \tag{3.29}$$

The KC_U number says how many lengths L the fish is moving during one period T of the tail. A high KC_U number means the fish or eel are moving a long distance during one tail period. A high KC_U number means you have big sways moments and big vortices can form. By multiplying the KC_{V_m} number with the inverse of KC_U we get

$$SG = \frac{KC_V}{KC_U} = \frac{V_m TL}{DUT} = \frac{VL}{UD}, \tag{3.30}$$

which we have defined as the SG number. Normally, we get vortex shedding for large KC_{V_m} numbers but if we also have a large U velocity the KC_U number get large and the SG number gets smaller. In that sense, we are taking the forward velocity into account. We have a large V_m velocity and a low inflow velocity U velocity the SG number becomes large and there will be vortexes. We can see that the SG number is proportional to the angel of attack V/U. Similar problem are discussed on maneuvering theory for ships by Faltinsen in [55].

3.4 Dynamics

We will now present the equation of motion of the swimming snake robot. We uses $\ddot{\theta}$ and $\ddot{P}_{CM}$ to express the dynamics. By looking at a single link, we can draw a free body diagram, see figure 3.2.

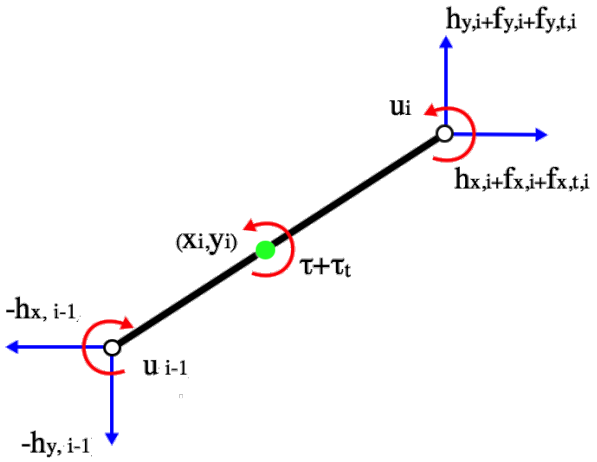

FIGURE 3.2: Parameters of the robot

We start with the translatory motion and uses Newtons second law:

$$\sum F = ma.$$

Using figure 3.2 the force balance i x and y direction for one link can be expressed as follow

$$m_i\ddot{x}_i = h_{x,i} - h_{x,i-1} + f_{x,i} + f_{x,t,i} \tag{3.31a}$$

$$m_i\ddot{y}_i = h_{y,i} - h_{y,i-1} + f_{y,i} + f_{y,t,i}. \tag{3.31b}$$

Each link have a mass m_i where the center of mass for each link are pleased in the center of the link. $h_{x,i}, h_{y,i}, h_{x,i-1}$ and $h_{y,i-1}$ are the joint constraint forces, τ and

τ_t are respectively the fluid moment on the link and the moment from a tail.The forces $f_{x,i}, f_{y,i}, f_{x,t,i}$ and $f_{y,t,i}$ are the forces from the fluid respectively for the link and tail in x and y direction. u_i and $u_{(-1}$ is the actuator torques on link i from link $i-1$ and $i+1$. We can the write the force expression in x and y direction for a the links on matrix form as

$$\boldsymbol{M}\ddot{X} = \boldsymbol{D}^T h_x + f_x + f_{x,t} \tag{3.32a}$$

$$\boldsymbol{M}\ddot{Y} = \boldsymbol{D}^T h_y + f_y + f_{y,t} \tag{3.32b}$$

where $h_x = [h_{x,1}, \cdots, h_{x,N}]^T \in \mathbb{R}^N$, $h_y = [h_{y,1}, \cdots, h_{y,N}]^T \in \mathbb{R}^N$, $f_{x,t} = [f_{x,t,1}, \cdots, f_{x,t,N}]^T \in \mathbb{R}^N$, $f_{y,t} = [f_{y,t,1}, \cdots, f_{y,t,N}]^T \in \mathbb{R}^N$ and $\mathbf{M}$ is the mass matrix and $\mathbf{D}$ the subtraction matrix both given in section 2.1. By differentiating (3.4) twice with respect to time and replacing $M\ddot{X}$ and $M\ddot{Y}$ with the equations in (3.32) we get

$$\ddot{P}_{CM} = \begin{bmatrix} \ddot{P}_x \\ \ddot{P}_y \end{bmatrix} = \frac{1}{m_t} \begin{bmatrix} e^T \boldsymbol{M}\ddot{X} \\ e^T \boldsymbol{M}\ddot{Y} \end{bmatrix} = \frac{1}{m_t} \begin{bmatrix} e^T(\boldsymbol{D}^T h_x + f_x + f_{x,t}) \\ e^T(\boldsymbol{D}^T h_y + f_y + f_{y,t}) \end{bmatrix}. \tag{3.33}$$

By noting that $e^T D^T h_X = 0$ we can write (3.33) as

$$\ddot{P}_{CM} = \frac{1}{m_t} \begin{bmatrix} e^T & 0_{1\times N} \\ 0_{1\times N} & e^T \end{bmatrix} (f + f_t) = \frac{1}{m_t} \boldsymbol{E}^T (f + f_t). \tag{3.34}$$

where $f = [f_x \quad f_y]^T$ and $f_t = [f_{x,t} \quad f_{y,t}]^T$. We then insert equation (3.11), (3.25) and (3.24) inn (3.34) for the fluid force f and get

$$\ddot{P}_{CM} = \frac{1}{m_t}\begin{bmatrix} e^T & 0_{1\times N} \\ 0_{1\times N} & e^T \end{bmatrix}\Big(\begin{bmatrix} \boldsymbol{\mu_n S_\theta^2} & -\boldsymbol{\mu_n S_\theta C_\theta} \\ -\boldsymbol{\mu_n S_\theta C_\theta} & \boldsymbol{\mu_n C_\theta^2} \end{bmatrix}\begin{bmatrix} \boldsymbol{K C_\theta}\dot{\theta}^2 + \boldsymbol{K S_\theta}\ddot{\theta} + e\ddot{P}_x \\ \boldsymbol{K S_\theta}\dot{\theta}^2 - \boldsymbol{K C_\theta}\ddot{\theta} + e\ddot{P}_y \end{bmatrix} - \begin{bmatrix} -\boldsymbol{\mu_n S_\theta C_\theta} & -\boldsymbol{\mu_n S_\theta^2} \\ \boldsymbol{\mu_n C_\theta^2} & \boldsymbol{\mu_n S_\theta C_\theta} \end{bmatrix}\begin{bmatrix} V_x^a \\ V_y^a \end{bmatrix}\dot{\theta}\Big) + \frac{1}{m_t}\begin{bmatrix} e^T & 0_{1\times N} \\ 0_{1\times N} & e^T \end{bmatrix}(f_D^I + f_D^{II} + f_t) \tag{3.35}$$

where $f = f_D^I + f_D^{II}$. f_D^I and f^{II} are the linear (3.26) and nonlinear (3.27) fluid force. Notices that the acceleration of the center of mass $\ddot{P}_x$ and $\ddot{P}_y$ now appears at both sides of the equal sign. By solving for the equation for $\ddot{P}_x$ and $\ddot{P}_y$ we get the final equation

$$\begin{aligned}\ddot{P}_{CM} = \begin{bmatrix} \ddot{P}_x \\ \ddot{P}_y \end{bmatrix} &= -\boldsymbol{M_P}\begin{bmatrix} e^T\boldsymbol{\mu_n S_\theta^2} & -e^T\boldsymbol{\mu_n S_\theta C_\theta} \\ -e^T\boldsymbol{\mu_n S_\theta C_\theta} & e^T\boldsymbol{\mu_n C_\theta^2} \end{bmatrix}\begin{bmatrix} \boldsymbol{K}(\boldsymbol{C_\theta}\dot{\theta}^2 + \boldsymbol{S_\theta}\ddot{\theta}) \\ \boldsymbol{K}(\boldsymbol{S_\theta}\dot{\theta}^2 - \boldsymbol{C_\theta}\ddot{\theta}) \end{bmatrix} \\ -\boldsymbol{M_p}&\begin{bmatrix} -e^T\boldsymbol{\mu_n S_\theta C_\theta} & -e^T\boldsymbol{\mu_n S_\theta^2} \\ e^T\boldsymbol{\mu_n C_\theta^2} & e^T\boldsymbol{\mu_n S_\theta C_\theta} \end{bmatrix}\begin{bmatrix} V_x^a \\ V_y^a \end{bmatrix}\dot{\theta} + \boldsymbol{M_p}\begin{bmatrix} e^T(f_{Dx}^I + f_{Dx}^{II} + f_{tx}) \\ e^T(f_{Dy}^I + f_{Dy}^{II} + f_{ty}) \end{bmatrix}\end{aligned} \tag{3.36}$$

where

$$\boldsymbol{M_p} = \begin{bmatrix} m_{11} & m_{12} \\ m_{21} & m_{22} \end{bmatrix} = \begin{bmatrix} m_t + e^T\boldsymbol{\mu_n S_\theta^2}e & -e^T\boldsymbol{\mu_n S_\theta C_\theta}e \\ -e^T\boldsymbol{\mu_n S_\theta C_\theta}e & m_t + e^T\boldsymbol{\mu_n C_\theta^2}e \end{bmatrix}^{-1}.$$

Note that the determinant, $m_t^2 + m_t\mu_n + \mu_n^2\sum_{i=1}^{N-1}\sum_{j=1+1}^{N}(sin(\theta_i - \theta_j))^2$ of M_p is non zero for $m \neq 0$ and $N \neq 0$ and therefor invertible. If f_{xt}, f_{yt} is dependent on the acceleration the equation (3.36) have to be modified.

The torque balance is given by Newtons second law

$$\sum Moments = J\ddot{\theta}$$

and by looking at figure 3.2 the balance for one link becomes

$$J\ddot{\theta}_i = u_i - u_{i-1} - l_i sin\theta_i(h_{x,i} + h_{x,i-1}) + l_i cos\theta_i(h_{y,i} + h_{y,i-1}) + \tau_i + \tau_{i,t}. \quad (3.37)$$

where u_i and u_{i-1} are the actuator sources extended on link i from link $i+1$ and link $i-1$ respectively. τ_i is the fluid moment on the link given by equation (3.16) and $\tau_{i,t}$ is the fluid moment from the tail or thruster on the link. On matrix form, we can write the torque balance as

$$J\ddot{\theta} = \boldsymbol{D^T}u - \boldsymbol{LS_\theta A^T}h_x + \boldsymbol{LC_\theta A^T}h_y + \tau + \tau_t. \quad (3.38)$$

The the joint constraint forces are unknown so we replace them by solving equation (3.32) for the h_x and h_y. This is done by multiplying by $\mathbf{D}$ on both sides. $(\mathbf{DD^T})^{-1}$ is nonsingular. h_x and h_y can then be expressed as

$$h_x = (\boldsymbol{DD^T})^{-1}\boldsymbol{D}(\boldsymbol{M}\ddot{X} - f_x - f_{x,t}) \quad (3.39a)$$

$$h_y = (\boldsymbol{DD^T})^{-1}\boldsymbol{D}(\boldsymbol{M}\ddot{Y} - f_y - f_{y,t}). \quad (3.39b)$$

The fluid forces (3.24) and (3.25) are inserted for f_x and f_y and the accelerations form (3.11) are inserted for $\ddot{X}$ and $\ddot{Y}$ in (3.39). The joint joint constraint forces

are the given as

$$h_x = (\boldsymbol{DD^T})^{-1}\boldsymbol{D}(\boldsymbol{M}(\boldsymbol{KC_\theta}\dot{\theta}^2 + \boldsymbol{KS_\theta}\ddot{\theta} + e\ddot{P}_x) + \boldsymbol{\mu_n S_\theta^2}(\boldsymbol{KC_\theta}\dot{\theta}^2 + \boldsymbol{KS_\theta}\ddot{\theta} + e\ddot{P}_x) - \boldsymbol{\mu_n S_\theta C_\theta}(\boldsymbol{KS_\theta}\dot{\theta}^2 - \boldsymbol{KC_\theta}\ddot{\theta} + e\ddot{P}_y) - \boldsymbol{\mu_n S_\theta C_\theta} V_x^a\dot{\theta} - \boldsymbol{\mu_n S_\theta^2} V_y^a\dot{\theta} - f_{Dx} - f_{x,t}) \tag{3.40a}$$

$$h_y = (\boldsymbol{DD^T})^{-1}\boldsymbol{D}(\boldsymbol{M}(\boldsymbol{KS_\theta}\dot{\theta}^2 - \boldsymbol{KC_\theta}\ddot{\theta} + e\ddot{P}_y) - \boldsymbol{\mu_n S_\theta C_\theta}(\boldsymbol{KC_\theta}\dot{\theta}^2 + \boldsymbol{KS_\theta}\ddot{\theta} + e\ddot{P}_x) + \boldsymbol{\mu_n C_\theta^2}(\boldsymbol{KS_\theta}\dot{\theta}^2 - \boldsymbol{KC_\theta}\ddot{\theta} + e\ddot{P}_y) + \boldsymbol{\mu_n C_\theta^2} V_x^a\dot{\theta} + \boldsymbol{\mu_n S_\theta C_\theta} V_y^a\dot{\theta} - f_{Dy} - f_{y,t}). \tag{3.40b}$$

By the inserting the joint constraint forces (3.40) in the torque balance equation (3.38) we get

$$\begin{aligned} J\ddot{\theta} = {} & \boldsymbol{D^T}u - \boldsymbol{LS_\theta A^T}[(\boldsymbol{DD^T})^{-1}\boldsymbol{D}(\boldsymbol{M}(\boldsymbol{KC_\theta}\dot{\theta}^2 + \boldsymbol{KS_\theta}\ddot{\theta} + e\ddot{P}_x) \\ & + \boldsymbol{\mu_n S_\theta^2}(\boldsymbol{KC_\theta}\dot{\theta}^2 + \boldsymbol{KS_\theta}\ddot{\theta} + e\ddot{P}_x) \\ & - \boldsymbol{\mu_n S_\theta C_\theta}(\boldsymbol{KS_\theta}\dot{\theta}^2 - \boldsymbol{KC_\theta}\ddot{\theta} + e\ddot{P}_y) - \boldsymbol{\mu_n S_\theta C_\theta} V_x^a\dot{\theta} - \boldsymbol{\mu_n S_\theta^2} V_y^a\dot{\theta} - f_{Dx} - f_{x,t})] \\ & + \boldsymbol{LC_\theta A^T}[(\boldsymbol{DD^T})^{-1}\boldsymbol{D}(\boldsymbol{M}(\boldsymbol{KS_\theta}\dot{\theta}^2 - \boldsymbol{KC_\theta}\ddot{\theta} + e\ddot{P}_y) \\ & - \boldsymbol{\mu_n S_\theta C_\theta}(\boldsymbol{KC_\theta}\dot{\theta}^2 + \boldsymbol{KS_\theta}\ddot{\theta} + e\ddot{P}_x) \\ & + \boldsymbol{\mu_n C_\theta^2}(\boldsymbol{KS_\theta}\dot{\theta}^2 - \boldsymbol{KC_\theta}\ddot{\theta} + e\ddot{P}_y) \\ & + \boldsymbol{\mu_n C_\theta^2} V_x^a\dot{\theta} + \boldsymbol{\mu_n S_\theta C_\theta} V_y^a\dot{\theta} - f_{Dy} - f_{y,t})] - \boldsymbol{\Lambda_1}\ddot{\theta} - \boldsymbol{\Lambda_2}\dot{\theta} - \boldsymbol{\Lambda_3}\dot{\theta} \mid \dot{\theta} \mid + \tau_t. \end{aligned} \tag{3.41}$$

Notice that the torque equation (4.29) still consist of the accelerations of the mass senter $\ddot{P}_x$ and $\ddot{P}_y$. To get the final expression for $\ddot{\theta}$ we then have to replace the accelerations with (3.36). We the get

$$\boldsymbol{M_\theta}\ddot{\theta} + \boldsymbol{W_\theta}\dot{\theta}^2 + \boldsymbol{V_\theta}\dot{\theta} + \boldsymbol{\Lambda_3}\dot{\theta} \mid \dot{\theta} \mid + K_y(f_{Dy} + f_{y,t}) + K_x(f_{Dx} + f_{x,t})) - \tau_t = \boldsymbol{D^T}u \tag{3.42}$$

where the constants $M_\theta, W_\theta, V_\theta, K_x$ and K_y are given as

$$\begin{aligned}
M_\theta = {} & \boldsymbol{J} + \boldsymbol{L}\boldsymbol{S}_{\boldsymbol{\theta}}\boldsymbol{V}\boldsymbol{S}_{\boldsymbol{\theta}} + \boldsymbol{L}\boldsymbol{C}_{\boldsymbol{\theta}}\boldsymbol{V}\boldsymbol{C}_{\boldsymbol{\theta}} + \boldsymbol{\Lambda_1} + \boldsymbol{S}_{\boldsymbol{\theta}}A_1(\boldsymbol{S}_{\boldsymbol{\theta}}^{\boldsymbol{2}}\boldsymbol{K}\boldsymbol{S}_{\boldsymbol{\theta}} + \boldsymbol{S}_{\boldsymbol{\theta}}\boldsymbol{C}_{\boldsymbol{\theta}}\boldsymbol{K}\boldsymbol{C}_{\boldsymbol{\theta}}) \\
& - \boldsymbol{C}_{\boldsymbol{\theta}}A_1(-\boldsymbol{S}_{\boldsymbol{\theta}}\boldsymbol{C}_{\boldsymbol{\theta}}\boldsymbol{K}\boldsymbol{S}_{\boldsymbol{\theta}} - \boldsymbol{C}_{\boldsymbol{\theta}}^{\boldsymbol{2}}\boldsymbol{K}\boldsymbol{C}_{\boldsymbol{\theta}}) \\
& + (K_{S_\theta x} + K_{C_\theta x})(-m_{11}e^T\boldsymbol{\mu_n}(\boldsymbol{S}_{\boldsymbol{\theta}}^{\boldsymbol{2}}\boldsymbol{K}\boldsymbol{S}_{\boldsymbol{\theta}} + \boldsymbol{S}_{\boldsymbol{\theta}}\boldsymbol{C}_{\boldsymbol{\theta}}\boldsymbol{K}\boldsymbol{C}_{\boldsymbol{\theta}}) \\
& - m_{12}e^T\boldsymbol{\mu_n}(-\boldsymbol{S}_{\boldsymbol{\theta}}\boldsymbol{C}_{\boldsymbol{\theta}}\boldsymbol{K}\boldsymbol{S}_{\boldsymbol{\theta}} + \boldsymbol{C}_{\boldsymbol{\theta}}^{\boldsymbol{2}}\boldsymbol{K}\boldsymbol{C}_{\boldsymbol{\theta}})) \\
& + (K_{S_\theta y} + K_{C_\theta y})(-m_{21}e^T\boldsymbol{\mu_n}(\boldsymbol{S}_{\boldsymbol{\theta}}^{\boldsymbol{2}}\boldsymbol{K}\boldsymbol{S}_{\boldsymbol{\theta}} + \boldsymbol{S}_{\boldsymbol{\theta}}\boldsymbol{C}_{\boldsymbol{\theta}}\boldsymbol{K}\boldsymbol{C}_{\boldsymbol{\theta}}) \\
& - m_{22}e^T\boldsymbol{\mu_n}(-\boldsymbol{S}_{\boldsymbol{\theta}}\boldsymbol{C}_{\boldsymbol{\theta}}\boldsymbol{K}\boldsymbol{S}_{\boldsymbol{\theta}} + \boldsymbol{C}_{\boldsymbol{\theta}}^{\boldsymbol{2}}\boldsymbol{K}\boldsymbol{C}_{\boldsymbol{\theta}})) \qquad (3.43a)
\end{aligned}$$

$$\begin{aligned}
W_\theta = {} & \boldsymbol{L}\boldsymbol{S}_{\boldsymbol{\theta}}\boldsymbol{V}\boldsymbol{C}_{\boldsymbol{\theta}} - \boldsymbol{L}\boldsymbol{C}_{\boldsymbol{\theta}}\boldsymbol{V}\boldsymbol{S}_{\boldsymbol{\theta}} + \boldsymbol{S}_{\boldsymbol{\theta}}A_1(\boldsymbol{S}_{\boldsymbol{\theta}}^{\boldsymbol{2}}\boldsymbol{K}\boldsymbol{C}_{\boldsymbol{\theta}} - \boldsymbol{S}_{\boldsymbol{\theta}}\boldsymbol{C}_{\boldsymbol{\theta}}\boldsymbol{K}\boldsymbol{S}_{\boldsymbol{\theta}}) \\
& - \boldsymbol{C}_{\boldsymbol{\theta}}A_1(\boldsymbol{C}_{\boldsymbol{\theta}}^{\boldsymbol{2}}\boldsymbol{K}\boldsymbol{S}_{\boldsymbol{\theta}} - \boldsymbol{S}_{\boldsymbol{\theta}}\boldsymbol{C}_{\boldsymbol{\theta}}\boldsymbol{K}\boldsymbol{C}_{\boldsymbol{\theta}}) \\
& + (K_{S_\theta x} + K_{C_\theta x})(-m_{11}e^T\boldsymbol{\mu_n}(\boldsymbol{S}_{\boldsymbol{\theta}}^{\boldsymbol{2}}\boldsymbol{K}\boldsymbol{C}_{\boldsymbol{\theta}} - \boldsymbol{S}_{\boldsymbol{\theta}}\boldsymbol{C}_{\boldsymbol{\theta}}\boldsymbol{K}\boldsymbol{S}_{\boldsymbol{\theta}}) \\
& - m_{12}e^T\boldsymbol{\mu_n}(-\boldsymbol{S}_{\boldsymbol{\theta}}\boldsymbol{C}_{\boldsymbol{\theta}}\boldsymbol{K}\boldsymbol{C}_{\boldsymbol{\theta}} + \boldsymbol{C}_{\boldsymbol{\theta}}^{\boldsymbol{2}}\boldsymbol{K}\boldsymbol{S}_{\boldsymbol{\theta}})) \\
& + (K_{S_\theta y} + K_{C_\theta y})(-m_{21}e^T\boldsymbol{\mu_n}(\boldsymbol{S}_{\boldsymbol{\theta}}^{\boldsymbol{2}}\boldsymbol{K}\boldsymbol{C}_{\boldsymbol{\theta}} - \boldsymbol{S}_{\boldsymbol{\theta}}\boldsymbol{C}_{\boldsymbol{\theta}}\boldsymbol{K}\boldsymbol{S}_{\boldsymbol{\theta}}) \\
& - m_{22}e^T\boldsymbol{\mu_n}(-\boldsymbol{S}_{\boldsymbol{\theta}}\boldsymbol{C}_{\boldsymbol{\theta}}\boldsymbol{K}\boldsymbol{C}_{\boldsymbol{\theta}} + \boldsymbol{C}_{\boldsymbol{\theta}}^{\boldsymbol{2}}\boldsymbol{K}\boldsymbol{S}_{\boldsymbol{\theta}})) \qquad (3.43b)
\end{aligned}$$

$$\begin{aligned}
V_\theta = {} & \boldsymbol{\Lambda_2} - \boldsymbol{S}_{\boldsymbol{\theta}}\boldsymbol{A_1}(\boldsymbol{S}_{\boldsymbol{\theta}}\boldsymbol{C}_{\boldsymbol{\theta}}V_x^a + \boldsymbol{S}_{\boldsymbol{\theta}}^{\boldsymbol{2}}V_y^a) - \boldsymbol{C}_{\boldsymbol{\theta}}\boldsymbol{A_1}(\boldsymbol{C}_{\boldsymbol{\theta}}^{\boldsymbol{2}}V_x^a + \boldsymbol{S}_{\boldsymbol{\theta}}\boldsymbol{C}_{\boldsymbol{\theta}}V_y^a) \\
& + (K_{S_\theta x} + K_{C_\theta x})(-m_{11}e^T\boldsymbol{\mu_n}(-\boldsymbol{S}_{\boldsymbol{\theta}}\boldsymbol{C}_{\boldsymbol{\theta}}V_x^a - \boldsymbol{S}_{\boldsymbol{\theta}}^{\boldsymbol{2}}V_y^a) - m_{12}e^T\boldsymbol{\mu_n}(\boldsymbol{C}_{\boldsymbol{\theta}}^{\boldsymbol{2}}V_x^a + \boldsymbol{S}_{\boldsymbol{\theta}}\boldsymbol{C}_{\boldsymbol{\theta}}V_y^a)) \\
& + (K_{S_\theta y} + K_{C_\theta y})(-m_{21}e^T\boldsymbol{\mu_n}(-\boldsymbol{S}_{\boldsymbol{\theta}}\boldsymbol{C}_{\boldsymbol{\theta}}V_x^a - \boldsymbol{S}_{\boldsymbol{\theta}}^{\boldsymbol{2}}V_y^a) - m_{22}e^T\boldsymbol{\mu_n}(\boldsymbol{C}_{\boldsymbol{\theta}}^{\boldsymbol{2}}V_x^a + \boldsymbol{S}_{\boldsymbol{\theta}}\boldsymbol{C}_{\boldsymbol{\theta}}V_y^a)) \\
& \qquad (3.43c)
\end{aligned}$$

$$K_x = -\boldsymbol{L}\boldsymbol{S}_{\boldsymbol{\theta}}\boldsymbol{A}^{\boldsymbol{T}}(\boldsymbol{D}\boldsymbol{D}^{\boldsymbol{T}})^{-1}\boldsymbol{D} + (K_{S_\theta x} + K_{C_\theta x})m_{11}e^T + (K_{S_\theta y} + K_{C_\theta y})m_{21}e^T \qquad (3.43d)$$

$$K_y = \boldsymbol{L}\boldsymbol{C}_{\boldsymbol{\theta}}\boldsymbol{A}^{\boldsymbol{T}}(\boldsymbol{D}\boldsymbol{D}^{\boldsymbol{T}})^{-1}\boldsymbol{D} + (K_{S_\theta x} + K_{C_\theta x})m_{12}e^T + (K_{S_\theta y} + K_{C_\theta y})m_{22}e^T \qquad (3.43e)$$

where

$$K_{S_\theta x} = \boldsymbol{L}\boldsymbol{S}_{\boldsymbol{\theta}}\boldsymbol{A}^{\boldsymbol{T}}(\boldsymbol{D}\boldsymbol{D}^{\boldsymbol{T}})^{-\mathbf{1}}\boldsymbol{D}(\boldsymbol{M} + \boldsymbol{\mu}_{\boldsymbol{n}}\boldsymbol{S}_{\boldsymbol{\theta}}{}^{2})e \tag{3.44a}$$

$$K_{S_\theta y} = \boldsymbol{L}\boldsymbol{S}_{\boldsymbol{\theta}}\boldsymbol{A}^{\boldsymbol{T}}(\boldsymbol{D}\boldsymbol{D}^{\boldsymbol{T}})^{-\mathbf{1}}\boldsymbol{D}(-\boldsymbol{\mu}_{\boldsymbol{n}}\boldsymbol{S}_{\boldsymbol{\theta}}\boldsymbol{C}_{\boldsymbol{\theta}})e \tag{3.44b}$$

$$K_{C_\theta y} = \boldsymbol{L}\boldsymbol{C}_{\boldsymbol{\theta}}\boldsymbol{A}^{\boldsymbol{T}}(\boldsymbol{D}\boldsymbol{D}^{\boldsymbol{T}})^{-\mathbf{1}}\boldsymbol{D}(-\boldsymbol{M} - \boldsymbol{\mu}_{\boldsymbol{n}}\boldsymbol{C}_{\boldsymbol{\theta}}{}^{2})e \tag{3.44c}$$

$$K_{C_\theta x} = \boldsymbol{L}\boldsymbol{C}_{\boldsymbol{\theta}}\boldsymbol{A}^{\boldsymbol{T}}(\boldsymbol{D}\boldsymbol{D}^{\boldsymbol{T}})^{-\mathbf{1}}\boldsymbol{D}(\boldsymbol{\mu}_{\boldsymbol{n}}\boldsymbol{S}_{\boldsymbol{\theta}}\boldsymbol{C}_{\boldsymbol{\theta}})e \tag{3.44d}$$

$$V = \boldsymbol{A}^{\boldsymbol{T}}(\boldsymbol{D}\boldsymbol{D}^{\boldsymbol{T}})^{-\mathbf{1}}\boldsymbol{D}\boldsymbol{M}\boldsymbol{K} \tag{3.44e}$$

$$A_1 = \boldsymbol{L}\boldsymbol{A}^{\boldsymbol{T}}(\boldsymbol{D}\boldsymbol{D}^{\boldsymbol{T}})^{-\mathbf{1}}\boldsymbol{D}\boldsymbol{\mu}_{\boldsymbol{n}} \tag{3.44f}$$

The equation of motion of the snake robot are now given with equation (3.36) and (3.42). By introducing the state variable $x = [\theta^T, P_{CM}^T, \dot{\theta}^T, \dot{P}_{CM}^T]^T \in \mathbb{R}^{2N+4}$ we can write the model of the snake robot in state space form as

$$\dot{x} = \begin{bmatrix} \dot{\theta} \\ \dot{P}_{CM} \\ \ddot{\theta} \\ \ddot{P}_{CM} \end{bmatrix} = F(x, u) \in \mathbb{R}^{2N+4}. \tag{3.45}$$

Chapter 4

Tail modeling and merging of the swimming snake robot model and the tail model

The scope of this chapter is to model the caudal fin of a swimming aquatic animal and combine it with the underwater snake robot model presented. in the previous chapter. The aim is to make the snake robot more efficient and faster. As we saw from the literature chapter, the tunniform swimmers are known for their high efficient cursing speeds. Most of the work that has been done in underwater biomimicking robotics has ether tried to make fish like or a snake/eel/amphibian like robot. We want to investigate if it is possible to combine the maneuvering capabilities and the flexible body of anguilliform swimmers like eels and the high efficiency and speed characteristics of tunniform swimmers like tunas into one underwater robot. As we have seen in previously chapters the theory stats that the main mechanisms for thrust generation for the tunniform and carangiform mode is added mass and lift. In this chapter, we will first propose a model for a tunniform like caudal fin and then combine it with the underwater snake robot model derived in the previous chapter.

4.1 Tail modeling

Studies on aquatic animals have stated that the BCF swimmers have stated that there are three mechanisms that are used for propulsion. This are drag, added mass and lift. Which for the three forces that are dominant depends on the swimming mode. From the anguilliform mode where the drag force is dominating to the tunniform mode where the lift force is dominating. In between the added mass is dominating. In the modeling of biomimicking robots that are suppose to mimic eel and fish one of the most common used method is Lighthill's elongated-body theory, see [17] for the method. This method only considers the added mass effect as important. Later work have shown that also the lift force is important, also for carangiform and subcarangiform swimmers [10]. We will therefore try to model a lunate tail including both the added mass and lift force and try to make the snake robot faster and more efficient.

We start by defining some important parameters for a foil. As we have seen the cord c is the width of the foil. We then define b as

$$b = c/2.$$

The lift force acting normal to the inflow velocity U acts in the lift center and is places at $c/4$ or $b/2$ from the leading edge (red dot in figure 4.1). The mid cord point is $c/2$ or b from the leading edge (green dot in figure 4.1, and the blue dot is places 3c/4 from the leading edge (blue dot in figure 4.1).

There are three analytical methods for modeling lift on a foil. It is steady lift, quasi-steady lift and unsteady lift. The lift forces on a BCF swimmer is definitely not steady and mostly likely unsteady [56]. There are two methods for calculating lift on an unsteady flat plate. It is the Theodorsen's method and Wagner's method. Theodorsen's methods include the Theodorsen function multiplied with the quasi-steady lift for a foil. This method is in frequency domain and the rotation motion and the oscillation motion are given as complex functions. Wagner's method is on the other hand in the time domain. Wagner considered a flat plat that had

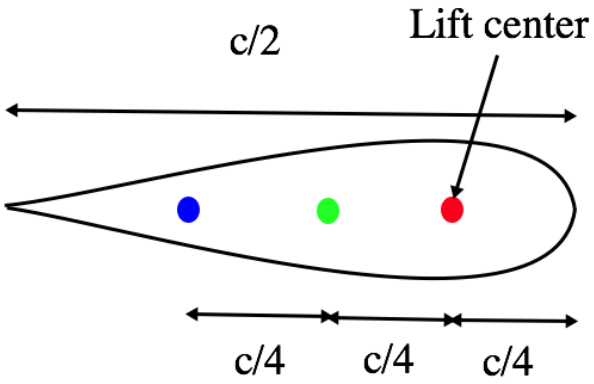

FIGURE 4.1: Lift center on a foil

a step change in angel of attack. The Wagner method includes the Dirac delta function and the Wagner function and is not easy to solve analytically. We will therefore use a quasi-steady foil model in this thesis to model the lift and added mass on a foil. A quasi-steady model can easier be combined with the derived underwater snake model, avoiding numerical algorithms to calculate the lift and keep the model on closed form.

Remark: By neglecting the unsteady part of the lift we neglect the fluid memory effect. When a foil chance angel of attack vortices are shed from the trailing adage. This vortices will create a downwash that decreases the angel of attack and thereby the efficiency. As the foil move forward the effect becomes smaller but there will continuously form new vortices. Both the Theodorsen and Wagner function accounts for this but they assume that the vortices are aligned on a straight line behind the foil. This is not realistic, especially not for big amplitude motions. More over it gives a good approximation and is the most used analytical methods for calculating lift on an unsteady form. The Theodorsen and Wagner function are related through the Laplace transform [58].

4.1.1 2D tail model

The quasi-steady lift on a flat plate with an unit span can be modeled as

$$L_f = \pi\rho b^2\left(\ddot{h} + U\dot{\delta} - ba\ddot{\delta}\right) + 2\pi\rho U^2 b\left(\delta + \frac{\dot{h}}{U} + \frac{b\dot{\delta}}{U}\left(\frac{1}{2} - a\right)\right) \tag{4.1}$$

and the corresponding moment

$$\begin{aligned} M_f = &-\pi\rho b^2\left(\left(\frac{1}{2} - a\right)Ub\dot{\delta} + b^2\left(\frac{1}{8} + a^2\right)\ddot{\delta} - ab\ddot{h}\right) \\ &+ 2\pi\rho U^2 b^2\left(a + \frac{1}{2}\right)\left(\delta + \frac{\dot{h}}{U} + \frac{b\dot{\delta}}{U}\left(\frac{1}{2} - a\right)\right) \end{aligned} \tag{4.2}$$

[56]. The first term is the added mass force and moment and the second is the lifting force and moment.The first term is the added mass force and moment and the second is the lifting force and moment. h is the oscillation motion and δ is the rotation motion, U is the forward velocity or inflow velocity to the foil, ρ is the density and a is the distance between the rotation axis and the mid cord given in semi cords (c/2). If the rotation axis are placed in the lift center a is $-1/2$. The added mass is modeled as a flat plate with a constant length c. So the effect that the plate is rotating and the projected length changes are neglected. If we look at the second term (the angel of attack contribution to the lift and moment) it consists of three parts. The first one δ is the angel the foil is rotate relative to the inflow velocity U. The angel of attack, α_l in steady foil theory. The two other terms is the quasi-steady terms. The second one is the contribution from the translator oscillation and the third is form the rotation motion. The rotation term is similar to the Weissinger approximation. This means that we satisfy the body boundary condition only in 3c/4 from the leading edge [55]. This two motions will affect the inflow velocity (angel of attack α_l) and thereby the lift and moment.

The lift in (4.1) and the moment in (4.2) are the linearized lift and moment. The non linearized lift and moment are given as

$$L_f = \pi\rho b^2\left(\ddot{h} + U\dot{\delta} - ba\ddot{\delta}\right) + 2\pi\rho U^2 b\left(\delta + atan\left(\frac{\dot{h}}{U}\right) + atan\left(\frac{b\dot{\delta}}{U}\left(\frac{1}{2} - a\right)\right)\right) \tag{4.3}$$

$$\begin{aligned} M_f = &-\pi\rho b^2\left(\left(\frac{1}{2} - a\right)Ub\dot{\delta} + b^2\left(\frac{1}{8} + a^2\right)\ddot{\delta} - ab\ddot{h}\right) \\ &+ 2\pi\rho U^2 b^2\left(a + \frac{1}{2}\right)\left(\delta + atan\left(\frac{\dot{h}}{U}\right) + atan\left(\frac{b\dot{\delta}}{U}\left(\frac{1}{2} - a\right)\right)\right) \end{aligned} \tag{4.4}$$

.

4.1.2 3D extension of the tail model

We are now going to extend the foil to 3D. This is done by a 2D+t approached. If we look at the lunate tail the cord length is decreasing from the mid to the tip of the foil. By dividing the tail into m sections with constant cord lengths we can approximate the tail shape. If all the sections have the same span (ΔS) the total lift can be calculated using the mean cord length of all the sections and then multiply the lift and moment with total span S. We will now show the lift a moment formulas for a foil with finite span. We will prepare the equations for merging with the underwater snake robot model so we will write it on matrix form. This means that you can calculate the lift for N foil at the same time.

First, we define the span matrix. This is a diagonal matrix with the total span of foil i on the diagonal i in the matrix.

$$\boldsymbol{S} = diag(S_1, \cdots, S_N). \tag{4.5}$$

The half cord (b) matrix is given by the mean cord of the foil i, on the diagonal i in the matrix.

$$\boldsymbol{B} = diag(b_{mean,1}, \cdots, b_{mean,N}) \tag{4.6}$$

The mean half cord is the calculated form as the average half cord (b) of the foil divided int m sections with equal spans.

$$b_{mean,i} = \frac{1}{m}\sum_{i=1}^{m} b_i \tag{4.7}$$

$\boldsymbol{B^2}, \boldsymbol{B^3}, \boldsymbol{B^4}$ are given as

$$\boldsymbol{B}^2 = diag(b^2_{mean,1}, \cdots, b^2_{mean,N}), \tag{4.8a}$$

$$\boldsymbol{B}^3 = diag(b^3_{mean,1}, \cdots, b^3_{mean,N}), \tag{4.8b}$$

$$\boldsymbol{B}^4 = diag(b^4_{mean,1}, \cdots, b^4_{mean,N}). \tag{4.8c}$$

We can then write the lift and drag on matrix form as

$$\begin{aligned} L_f = {} & \boldsymbol{S}\pi\rho\left(\boldsymbol{B}^2\ddot{h} + \boldsymbol{B}^2 U\dot{\delta} - \boldsymbol{B}^3 a\ddot{\delta}\right) \\ & + \boldsymbol{S}2\pi\rho U^2\boldsymbol{B}\left(\delta + atan\left(\frac{\dot{h}}{U}\right) + atan\left(\boldsymbol{B}\frac{\dot{\delta}}{U}\left(\frac{1}{2} - a\right)\right)\right) \end{aligned} \tag{4.9}$$

$$\begin{aligned} M_f = {} & \boldsymbol{S}(-\pi\rho\left(\boldsymbol{B}^3\left(\frac{1}{2} - a\right)U\dot{\delta} + \boldsymbol{B}^4\left(\frac{1}{8} + a^2\right)\ddot{\delta} - \boldsymbol{B}^3 a\ddot{h}\right) \\ & + \boldsymbol{S}2\pi\rho U^2\left(a + \frac{1}{2}\right)\boldsymbol{B}^2\left(\delta + atan\left(\frac{\dot{h}}{U}\right) + atan\left(\boldsymbol{B}\frac{\dot{\delta}}{U}\left(\frac{1}{2} - a\right)\right)\right). \end{aligned} \tag{4.10}$$

Note that h and δ and their time derivatives are given as a $n \times 1$ vector.

4.1.3 Drag on 3D foil

We have neglected the shed vortices form the change in angel of attack. Det drag will therefor only consist of two parts

$$D_l = D_i + D_f \tag{4.11}$$

where D_i is the induced drag from the tip vortices and D_f if the friction drag. If we assume that the flow is turbulent the friction drag can be calculated as

$$D_f = 2\left(1 + 2\frac{t_{max}}{c}\right) C_F \tag{4.12}$$

where

$$C_F = \frac{0.0075}{(logR_n - 2)^2} \tag{4.13}$$

and Rn is the Reynolds number [12]. If we assume that the codes are elliptical distributed the induced drag can be written as

$$D_i = \frac{C_L^2}{\pi Asp} \tag{4.14}$$

where C_L is the lift coefficient and Asp is the aspect ratio. This also a good approximation for the cord distributions then elliptical [12].

4.2 Merging the under water snake robot model and the tail model

We will now combine the tail model with the lift and moment equations in (4.9) and (4.10). First, we need to define the forward velocity U of the robot. We have chosen to use the velocity of the CM of the snake robot as U corrected for the current velocity. U is the given by

$$U = \sqrt{(\dot{P}_x - V_x^a)^2 + (\dot{P}_y - V_y^a)^2}. \tag{4.15}$$

The heading is also needed. This is not trivial for a snake robot and in the previous chapter we defined it as the average of all the θ angels, see (3.3).Sins we have already used the CM to define the velocity U we have chosen to define the heading ψ as

$$\psi = arctan(\frac{\dot{P}_y - V_y^a}{\dot{P}_x - V_x^a}) \tag{4.16}$$

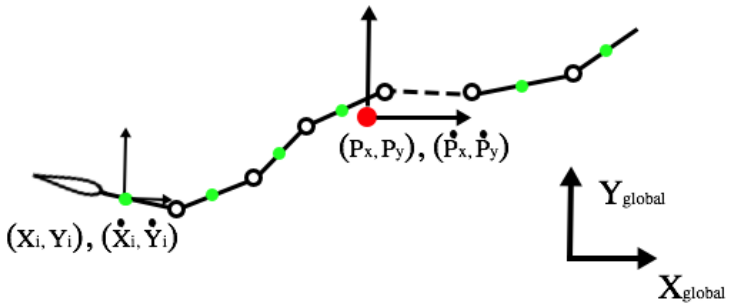

FIGURE 4.2: The under water snake robot with tail

Figure 4.2 shows the total center of mass and the foil placed on the underwater snake robot. Also the δ and h and the time derivatives form (4.9) and (4.10) need to be defined as parameters of the robot. δ is the yaw angel of the foil relative to the U velocity, see figure 4.3. In this thesis we will only consider straight-line swimming so we assume that the heading is constant. This assumption will simplify the equations slightly. By this assumption we can write

$$\delta = \theta - \psi \tag{4.17a}$$

$$\dot{\delta} = \dot{\theta} \tag{4.17b}$$

$$\ddot{\delta} = \ddot{\theta}. \tag{4.17c}$$

The β angel is the angel between the velocity U and the inflow velocity to the foil, see figure 4.3. β is defined as

$$\beta = atan\left(\frac{\dot{h}}{U}\right). \tag{4.18}$$

We then define a rotation matrix between the global coordinate system and the coordinate system with respect to U, as given by

$$\boldsymbol{R}_{global}^{heading} = \begin{bmatrix} \boldsymbol{C}_{\psi} & -\boldsymbol{S}_{\psi} \\ \boldsymbol{S}_{\psi} & \boldsymbol{C}_{\psi} \end{bmatrix}, \tag{4.19}$$

where

$\boldsymbol{C}_{\psi} = cos\psi I$

$\boldsymbol{S_\psi} = sin\psi I$

I is the identity matrix $\in \mathbb{R}^{N\times N}$.

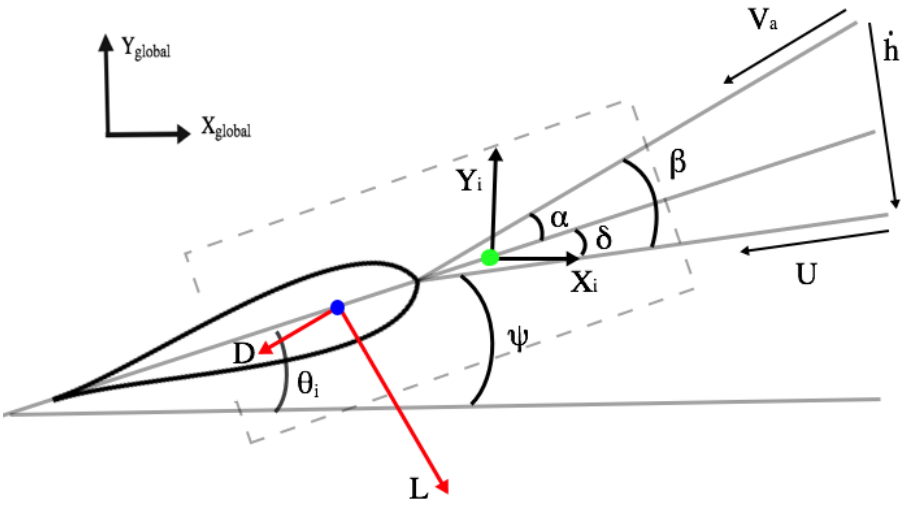

FIGURE 4.3: Definitions of angels, velocities and forces on the foil.

Now we can define the position, velocity and acceleration as z, $\dot{z}$, $\ddot{z}$ respectively in the new coordinate system, as

$$z = \boldsymbol{R}^{heading}_{global} \begin{bmatrix} X \\ Y \end{bmatrix} \tag{4.20}$$

,

$$\dot{z} = \boldsymbol{R}^{heading}_{global} \begin{bmatrix} \dot{X} - V^a_x \\ \dot{Y} - V^a_y \end{bmatrix} \tag{4.21}$$

,

$$\ddot{z} = \boldsymbol{R}^{heading}_{global} \begin{bmatrix} \ddot{X} \\ \ddot{Y} \end{bmatrix} = \boldsymbol{R}^{heading}_{global} \begin{bmatrix} \mathbf{KC}_\theta \dot{\theta}^2 + \mathbf{KS}_\theta \ddot{\theta} + e\ddot{P}_x \\ \mathbf{KS}_\theta \dot{\theta}^2 - \mathbf{KC}_\theta \ddot{\theta} + e\ddot{P}_y \end{bmatrix}. \tag{4.22}$$

Looking at figure 4.3 the h, $\dot{h}$ and $\ddot{h}$ from (4.9) and (4.10) are the y component of the position, velocity and acceleration of the link of the snake robot in the new

coordinate system. They become

$$h = -(\boldsymbol{S}_{\boldsymbol{\psi}} X + \boldsymbol{C}_{\boldsymbol{\psi}} Y), \tag{4.23a}$$

$$\dot{h} = -(\boldsymbol{S}_{\boldsymbol{\psi}} (\dot{X} - V_x^a) + \boldsymbol{C}_{\boldsymbol{\psi}} (\dot{Y} - V_y^a)), \tag{4.23b}$$

$$\ddot{h} = -(\boldsymbol{S}_{\boldsymbol{\psi}} (\mathbf{K}\mathbf{C}_\theta \dot{\theta}^2 + \mathbf{K}\mathbf{S}_\theta \ddot{\theta} + e\ddot{P}_x) + \boldsymbol{C}_{\boldsymbol{\psi}} (\mathbf{K}\mathbf{S}_\theta \dot{\theta}^2 - \mathbf{K}\mathbf{C}_\theta \ddot{\theta} + e\ddot{P}_y)). \tag{4.23c}$$

The forces from the foil are to be given in the global x and y frame. By decompose the lift and drag force in x and y direction we get the following expressions for the for the tail force in x and y direction.

$$f_{x,t} = \boldsymbol{S}_{\boldsymbol{\beta}+\boldsymbol{\psi}} L_f - \boldsymbol{C}_{\boldsymbol{\beta}+\boldsymbol{\psi}} D_l, \tag{4.24a}$$

$$f_{y,t} = \boldsymbol{C}_{\boldsymbol{\beta}+\boldsymbol{\psi}} L_f + \boldsymbol{S}_{\boldsymbol{\beta}+\boldsymbol{\psi}} D_l, \tag{4.24b}$$

$$\tau_t = M_f, \tag{4.24c}$$

where

$\boldsymbol{C}_{\boldsymbol{\psi}+\boldsymbol{\beta}} = diag(cos(\psi + \beta_1) \cdots cos(\psi + \beta_N))$,

$\boldsymbol{S}_{\boldsymbol{\psi}+\boldsymbol{\beta}} = diag(sin(\psi + \beta_1) \cdots sin(\psi + \beta_N))$.

Looking at equation (4.9), (4.10) and 4.24, we see that the tail moment an force are dependent on the accelerations. We therefore separate the terms that are dependent on acceleration and the other ones as follow

$$f_{x,t} = f_{x,t}^A + f_{x,t}^R, \tag{4.25a}$$

$$f_{y,t} = f_{y,t}^A + f_{y,t}^R, \tag{4.25b}$$

$$\tau_t = \tau_t^A + \tau_t^R, \tag{4.25c}$$

where

$$f_{x,t}^{A} = \boldsymbol{S}_{\boldsymbol{\beta+\psi}}\pi\rho\boldsymbol{S}\left(\boldsymbol{B}^2\ddot{h} - \boldsymbol{B}^3 a\ddot{\delta}\right) \tag{4.26a}$$

$$f_{y,t}^{A} = \boldsymbol{C}_{\boldsymbol{\beta+\psi}}\pi\rho\boldsymbol{S}\left(\boldsymbol{B}^2\ddot{h} - \boldsymbol{B}^3 a\ddot{\delta}\right) \tag{4.26b}$$

$$\tau_t^{A} = -\boldsymbol{S}\pi\rho\left(\boldsymbol{B}^4\left(\frac{1}{8} + a^2\right)\ddot{\delta} - \boldsymbol{B}^3 a\ddot{h}\right) \tag{4.26c}$$

$$\tag{4.26d}$$

and

$$f_{x,t}^{R} = \boldsymbol{S}_{\boldsymbol{\beta+\psi}}\left(\pi\rho\boldsymbol{S}\left(aU\dot{\delta}\right) + \boldsymbol{S}2\pi\rho U^2\boldsymbol{B}\left(\delta + atan\left(\frac{\dot{h}}{U}\right) + atan\left(\boldsymbol{B}\frac{\dot{\delta}}{U}\left(\frac{1}{2} - a\right)\right)\right)\right) \tag{4.27a}$$

$$f_{y,t}^{R} = \boldsymbol{C}_{\boldsymbol{\beta+\psi}}\left(\pi\rho\boldsymbol{S}\left(aU\dot{\delta}\right) + \boldsymbol{S}2\pi\rho U^2\boldsymbol{B}\left(\delta + atan\left(\frac{\dot{h}}{U}\right) + atan\left(\boldsymbol{B}\frac{\dot{\delta}}{U}\left(\frac{1}{2} - a\right)\right)\right)\right) \tag{4.27b}$$

$$\begin{aligned}\tau_t^{R} = &-\boldsymbol{S}\pi\rho\boldsymbol{B}^3\left(\frac{1}{2} - a\right)U\dot{\delta} \\ &+ \boldsymbol{S}2\pi\rho U^2\left(a + \frac{1}{2}\right)\boldsymbol{B}^2\left(\delta + atan\left(\frac{\dot{h}}{U}\right) + atan\left(\boldsymbol{B}\frac{\dot{\delta}}{U}\left(\frac{1}{2} - a\right)\right)\right).\end{aligned} \tag{4.27c}$$

By then inserting (4.26), (4.25), (4.23), (4.17) and (3.11) in (3.36) and solving for $\ddot{P}_x, \ddot{P}_y$ we get

$$
\begin{aligned}
\begin{bmatrix} \ddot{P}_x \\ \ddot{P}_y \end{bmatrix} &= -\boldsymbol{M_p^t} \begin{bmatrix} e^T\boldsymbol{\mu_n S_\theta^2} & -e^T\boldsymbol{\mu_n S_\theta C_\theta} \\ -e^T\boldsymbol{\mu_n S_\theta C_\theta} & e^T\boldsymbol{\mu_n C_\theta^2} \end{bmatrix} \begin{bmatrix} \boldsymbol{K(C_\theta}\dot{\theta}^2 + \boldsymbol{S_\theta}\ddot{\theta}) \\ \boldsymbol{K(S_\theta}\dot{\theta}^2 - \boldsymbol{C_\theta}\ddot{\theta}) \end{bmatrix} \\
&-\boldsymbol{M_p^t} \begin{bmatrix} -e^T\boldsymbol{\mu_n S_\theta C_\theta} & -e^T\boldsymbol{\mu_n S_\theta^2} \\ e^T\boldsymbol{\mu_n C_\theta^2} & e^T\boldsymbol{\mu_n S_\theta C_\theta} \end{bmatrix} \begin{bmatrix} V_x^a \\ V_y^a \end{bmatrix} \dot{\theta} + \boldsymbol{M_p^t} \begin{bmatrix} e^T(f_{Dx}^I + f_{Dx}^{II} + f_{x,t}^R) \\ e^T(f_{Dy}^I + f_{Dy}^{II} + f_{y,t}^R) \end{bmatrix} \\
&+\boldsymbol{M_p^t} \begin{bmatrix} -e^T\boldsymbol{S_{\beta+\psi}}\pi\rho\boldsymbol{SB^2S_\psi} & -e^T\boldsymbol{S_{\beta+\psi}}\pi\rho\boldsymbol{SB^2C_\psi} \\ -e^T\boldsymbol{C_{\beta+\psi}}\pi\rho\boldsymbol{SB^2S_\psi} & -e^T\boldsymbol{C_{\beta+\psi}}\pi\rho\boldsymbol{SB^2C_\psi} \end{bmatrix} \begin{bmatrix} \mathbf{KC}_\theta\dot{\theta}^2 + \mathbf{KS}_\theta\ddot{\theta} \\ \mathbf{KS}_\theta\dot{\theta}^2 - \mathbf{KC}_\theta\ddot{\theta} \end{bmatrix} \\
&-\boldsymbol{M_p^t} \begin{bmatrix} e^T\boldsymbol{S_{\beta+\psi}}\boldsymbol{S}\rho\pi\boldsymbol{B}^3a \\ e^T\boldsymbol{C_{\beta+\psi}}\boldsymbol{S}\rho\pi\boldsymbol{B}^3a \end{bmatrix} \ddot{\theta}
\end{aligned} \tag{4.28}
$$

, where

$$
\begin{aligned}
\boldsymbol{M_p^t} &= \begin{bmatrix} m_{11} & m_{12} \\ m_{21} & m_{22} \end{bmatrix} \\
&= \begin{bmatrix} m_t + e^T\boldsymbol{\mu_n S_\theta^2}e + e^T\boldsymbol{S_{\psi+\beta}}\pi\rho\boldsymbol{SB^2S_\psi}e & -e^T\boldsymbol{\mu_n S_\theta C_\theta}e + e^T\boldsymbol{S_{\psi+\beta}}\pi\rho\boldsymbol{SB^2C_\psi}e \\ -e^T\boldsymbol{\mu_n S_\theta C_\theta}e + e^T\boldsymbol{C_{\psi+\beta}}\pi\rho\boldsymbol{SB^2S_\psi}e & m_t + e^T\boldsymbol{\mu_n C_\theta^2}e + e^T\boldsymbol{C_{\psi+\beta}}\pi\rho\boldsymbol{SB^2C_\psi}e \end{bmatrix}^{-1}.
\end{aligned}
$$

, and the forces $f_{x,t}^R$ and $f_{y,t}^R$are given in (4.27). We also have to modify the moment equation (3.42). By inserting (4.25) in (4.29), we get

$$
\begin{aligned}
J\ddot{\theta} = \;& \boldsymbol{D^T}u - \boldsymbol{LS_\theta A^T}[(\boldsymbol{DD^T})^{-1}\boldsymbol{D}(\boldsymbol{M}(\boldsymbol{KC_\theta}\dot{\theta}^2 + \boldsymbol{KS_\theta}\ddot{\theta} + e\ddot{P}_x) \\
&+ \boldsymbol{\mu_n S_\theta^2}(\boldsymbol{KC_\theta}\dot{\theta}^2 + \boldsymbol{KS_\theta}\ddot{\theta} + e\ddot{P}_x) \\
&- \boldsymbol{\mu_n S_\theta C_\theta}(\boldsymbol{KS_\theta}\dot{\theta}^2 - \boldsymbol{KC_\theta}\ddot{\theta} + e\ddot{P}_y) - \boldsymbol{\mu_n S_\theta C_\theta}V_x^a\dot{\theta} - \boldsymbol{\mu_n S_\theta^2}V_y^a\dot{\theta} \\
&- f_{Dx} - f_{Dx} - f_{x,t}^R - f_{x,t}^A)] \\
&+ \boldsymbol{LC_\theta A^T}[(\boldsymbol{DD^T})^{-1}\boldsymbol{D}(\boldsymbol{M}(\boldsymbol{KS_\theta}\dot{\theta}^2 - \boldsymbol{KC_\theta}\ddot{\theta} + e\ddot{P}_y) \\
&- \boldsymbol{\mu_n S_\theta C_\theta}(\boldsymbol{KC_\theta}\dot{\theta}^2 + \boldsymbol{KS_\theta}\ddot{\theta} + e\ddot{P}_x) \\
&+ \boldsymbol{\mu_n C_\theta^2}(\boldsymbol{KS_\theta}\dot{\theta}^2 - \boldsymbol{KC_\theta}\ddot{\theta} + e\ddot{P}_y) \\
&+ \boldsymbol{\mu_n C_\theta^2}V_x^a\dot{\theta} + \boldsymbol{\mu_n S_\theta C_\theta}V_y^a\dot{\theta} - f_{Dy} - f_{y,t}^A - f_{y,t}^R)] \\
&- \boldsymbol{\Lambda_1}\ddot{\theta} - \boldsymbol{\Lambda_2}\dot{\theta} - \boldsymbol{\Lambda_3}\dot{\theta} \mid \dot{\theta} \mid + \tau_t^A + \tau_t^R.
\end{aligned} \tag{4.29}
$$

If we then insert (4.26), (4.23), (4.17), (3.11) and solving for $\ddot{\theta}$ we get

$$\begin{aligned} M_\theta\ddot{\theta}+W_\theta\dot{\theta}^2 + V_\theta\dot{\theta} + \Lambda_3\dot{\theta} \mid \dot{\theta} \mid + K_y(f_{Dy} + f^R_{y,t}) \\ + K_x(f_{Dx} + f^R_{x,t}) - \tau^A_t = D^T u, \end{aligned} \tag{4.30}$$

where the constants $M_\theta, W_\theta, V_\theta, K_x$ and K_y are given in appendix A and and $f^R_{x,t}$, $f^R_{y,t}$ and $\tau^R_t$are given in (4.27). We have now combined the a quasi-steady foil model for the tail including both added mass and lift forces with the under water snake robot model derived in chapter 3 and the same state space model as in chapter 3 is achieved.

Chapter 5

Simulation results

5.1 Validation of extended snake like model

In this section, the extended model presented in chapter 3 are implemented in *Matlab R2014b* and compared with the already existing model given in [1]. The reason for this is to validate the new kinematic and dynamic equations and the implementation. All the extra propulsive forces in the extended model are zero. All links have the same length, mass and inertia. The simulation is don with 10 links. Both models are simulated on the same computer and same Matlab version. To solve the dynamic equation the *ode23tb* solver in Matlab was used with a relative and absolute error tolerance of 10^{-4}. All parameters are the same in both models. Both added mass, linear and nonlinear drag is included. In the following the mathematical excretion for an eel like motion are presented. All the parameters that are used are presented and finally all the simulation results for both models are presented and discussed.

5.1.1 Locomotion

In the validation of the extended model an eel like motion is used. The locomotion of the snake robot is achieved by controlling the joints to follow a desired angel.

The reference angels are given by

$$\phi_i^* = \alpha * \left(\frac{n-1}{n+1}\right) sin(\omega t + (i-1)\beta) + \gamma \qquad i = 1, \cdots, n-1 \tag{5.1}$$

where $\alpha(n-1)/(n+1)$ is the increasing amplitude from head to tail, ω is the frequency of the motion, β is the phase between the joints and γ is an offset angel that can be used to control the heading of the snake robot [50]. In these simulations only $\gamma = 0$ will be considered.

5.1.2 Low-level joint control

In order to control the joint angels (ϕ) to the reference angel a PD controller is used.

$$u_i = \ddot{\phi}_i^* + k_{d,i}(\dot{\phi}_i^* - \dot{\phi}) + k_{p,i}(\phi_i^* - \phi) \qquad i = 1, \cdots, n-1 \tag{5.2}$$

where $K_{p,i} > 0$ and $K_{d,i} > 0$ are the gains of the controller. This controller will exponential stabilize the controller [50].

5.1.3 Simulation parameters

All the initial state values in the simulation are set to zero. The snake robot total center of mass (P_x, P_y) is then placed in origin with the body parallel to the x-axis. The simulation is done with $n = 10$ links where each link have the length $2l = 2 \times 0.07$m. The cross section is assumed to be elliptical with the radius 0.05 and 0.03 m. The density is $\rho = 1000$ kg/m^3. Mass of each link then becomes $m = 0.6597$kg if we assume that the snakes buoyancy is neutral. Note that the weight can be added to the snake robot to fulfill the neutral buoyant assumption.

The fluid parameters are as mention before model with an Morrison equation approach. The added mass coefficients C_A and C_M are both equal to 1. The

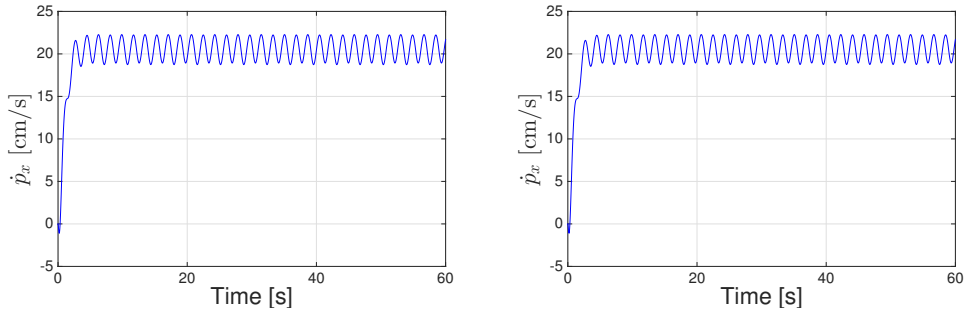

(A) Existing (B) Extended

FIGURE 5.1: The figure shows the velocity of the total mass center in x direction.

friction coefficient are selected as $C_f = 0.03$ and $C_D = 2$. This validation is done without current so the current vector in inertia frame is $[0, 0]$m/s. $K_{p,i} = 200$ and $K_{d,i} = 50$ are used as the gains in the PD controller 5.2. To get and eel like motion the locomotion parameters $\alpha = 30^o$, $\omega = 100^o$, $\beta = 40^o$ and $\gamma = 0^o$ where used. The simulating time is 60 seconds.

5.1.4 Simulation results

In the simulation the snake robot is moving with an eel like motion. The heading is not controlled so the robot is moving freely in a straight line. The simulation result for the velocity for the total center of mass (CM) are shown in figure (5.1)(x direction) and (5.2) (y direction) for both the extended and existing model. In figure 5.3 the angel ϕ_i for the first link ($i = 1$) is plotted together with the desired angel ϕ_i^* calculated from equation (5.1) are shown for both the extended and existing model. To get a better comparison a section of the CM velocity in x direction for both the existing and extended model plotted together in figure 5.4.

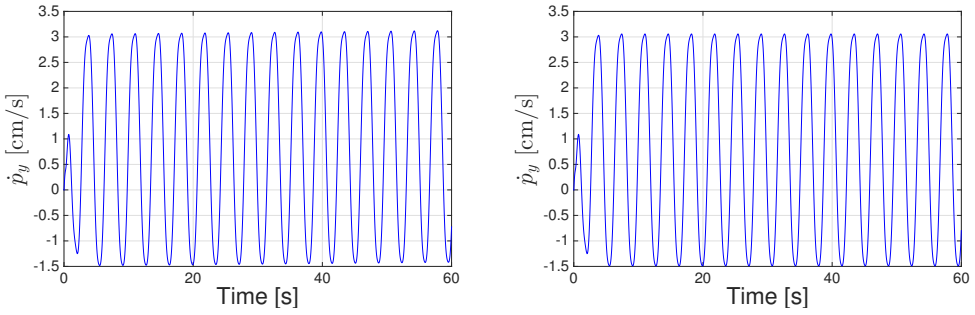

(A) Existing (B) Extended

FIGURE 5.2: The figure shows the velocity of the total mass center in y direction.

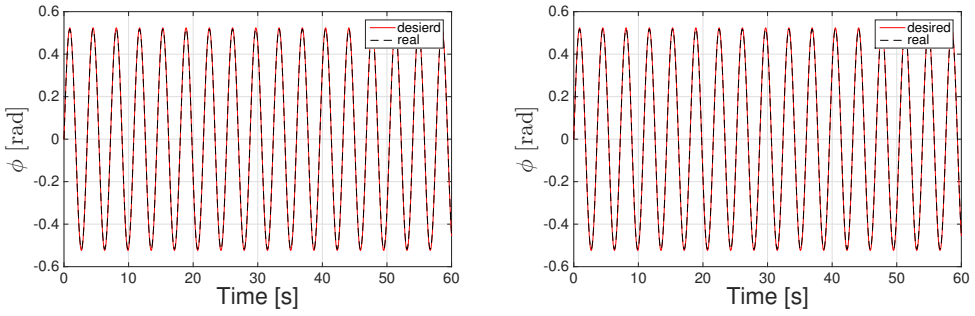

(A) Existing (B) Extended

FIGURE 5.3: The figure shows the angel ϕ of the first joint. Both the desired and the real angel are plotted.

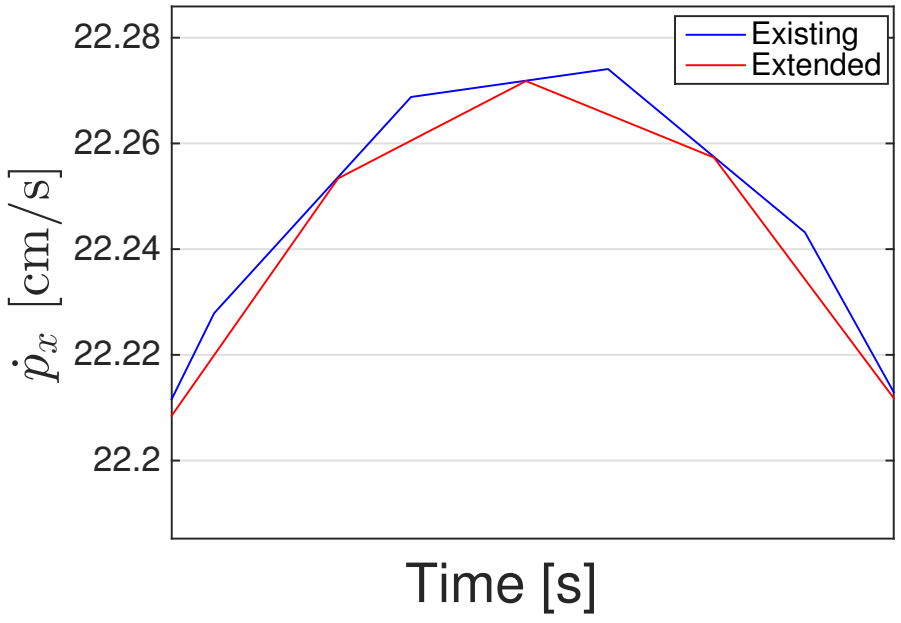

FIGURE 5.4: The figure shows a section of the velocity of CM in x direction for both the extended and the existing model.

As we can see from the figures 5.1, 5.2 and 5.3 the simulation results for the velocity and the first joint angel look exactly the same. The mean speed calculated from the absolute length between the start and ending point divided by the simulation time witch is 60 second gives 0.2023 m/s for both models. Looking at figure 5.4 we se that there actually are a slight difference. As we can see the time step are not synced and not the same length.

5.1.5 Discussion

The results form the to models are almost the same. They give the same mean speed, and the joint angel, and velocity of the mass center have the same frequency and phase. The small difference we see in figure 5.4 is properly due to some small difference in the implementation and that the solver accuracy is 10^{-4}. We see that the time step is not in sync witch will also causes a small difference in the results. The conclusion is therefore that the new equation and implementation is correct.

5.2 Comparison of the model with and without foil and investigation on the foil propulsion

The combined model of the underwater snake robot and a tail presented in chapter 4 are also implemented in *Matlab R2014b*. We will compeer the model with and without a caudal fin or tail. The model gives us the opportunity to place a fin on each link, but we will only place fin on the tail link. The simulation is still done with 10 links and the dynamic equations are solved with ode23tb solver with a relative and absolute error tolerance of 10^{-4}. Sill both the linear, non linear and added mass effects are included in the added mass are included in the underwater snake model and are the parameters are the same for both models. The only difference is that for the simulation with foil the last link has a slight increase in mass, length and inertia force due to the foil. Simulations are done for both snake and eel like motion and with and without tail to see the differences. Then more

simulations are done for the eel motion to cheek the speed en efficiency performance with and without tail and investigate some hydrodynamic parameters.

5.2.1 locomotion

For the eel motion the same locomotion as used in the previously simulations are used. For a snake like locomotion the reference signal is given as

$$\phi_i^* = \alpha sin(\omega t + (i-1)\beta) + \gamma \qquad i = 1, \cdots, n-1 \tag{5.3}$$

where α is the amplitude, ω is the frequency of the motion, β is the phase between the joints and γ is an offset angel that can be used to control the heading of the snake robot [50]. In this validation simulation only $\gamma = 0$ will be considered. The differs between the rreference signal for the eel and the snake is that we for the snake have a constant amplitude while for the eel the amplitude is increasing form head to tail.

5.2.2 Low-level joint control

The same low-level joint control as used in the previously simulation are also used in these simulations.

5.2.3 Tail parameters

We want to test a high aspect ration fin like the ones that tunas and sailfish have. A mean cord (c) of 0.0194 m and span (S) of 0.12 m are used. This gives an aspect ration of 0.62, which is in the range of the lunate tails. Further the tail is placed on the last link with the lift center (c/4 from the leading edge) on the mid point of the link. We have assumed that the yaw axis of the foil then is the joint in front of the foil. The distance a then becomes $a = -0.5 - l/b$ where l is the half the link length and b is the half cord length.

5.2.4 Simulation parameters

The snakes center of mass CM, are placed in the origin with the body parallel to the x-axis and with the head in positive x direction. All the initial values are set to zero, and the simulation is done with $n = 10$ links. The density is $\rho = 1000$ kg/m^3. The length of all links except tail link is $2l_i = 2 \times 0.07$m. The tail link is assumed to be slightly longer so it is possible fit the tail on the link. So for the last link $2l_i = 2 \times 0.075$m. This is only done for the simulations with tail. In the simulation without tail all links have the same length $2l_i = 2 \times 0.07$m. The cross section of the snake is elliptical with the diameters of 0.05m and 0.03m. Assuming that the snake is naturally buoyant the mass of each link is $m_i = 0.6597$. For the tail simulation the last link the mass is assumed to be $m_t = 0.7468$. This is due to the extra length and extra weight of the tail. 20g are added for the foil weight and 20g to balance the link to have the mass center in the mid point of the link. The inertia is calculated to 0.0011 kgm^2 for all the links without tail and 0.0013 kgm^2 for the link with tail.

The added mass coefficients C_A and C_M are both equal to 1. The friction coefficient are selected as $C_f = 0.03$ and $C_D = 2$. This validation is done without current so the current vector in inertia frame is $[0, 0]$m/s. $K_{p,i} = 200$ and $K_{d,i} = 50$ for the simulation without tail and eel motion, $K_{p,i} = 20$ and $K_{d,i} = 5$ for the simulation without tail and snake motion, and $K_{p,i} = 450$ and $K_{d,i} = 100$ for the simulation with tail are used as the gains in the PD controller. The locomotion parameters $\alpha = 30^o$, $\omega = 100^o$, $\beta = 40^o$ and $\gamma = 0^o$ where used in the first comparison simulation, but are later varied. The simulating time is 60 seconds.

5.2.5 Simulation results

The simulation in figure 5.5 and 5.6 shows x velocity of the CM for the snake and eel motion respectively for the model with and without a tail. These two simulations are done with $\alpha = 30^o$, $\omega = 100^o$ and $\beta = 40^o$. We can see that the tail is definitely having a positive effect on the speed performance. We can also

note that snake motion gives a higher velocity. We therefore want to investigate the tail simulations deeper. The eel motion is the chosen motion to study. This is because the shape is closer to the tunniform swimmers that hare known for higher speed and efficiency.

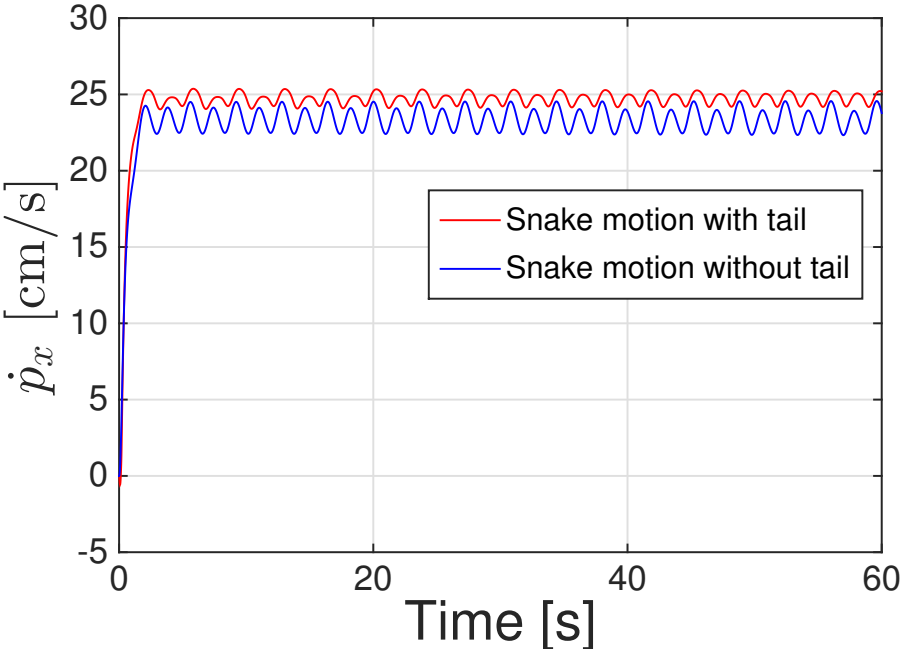

FIGURE 5.5: The figure shows a section of the velocity of CM in x direction for both the extended and the existing model with snake motion.

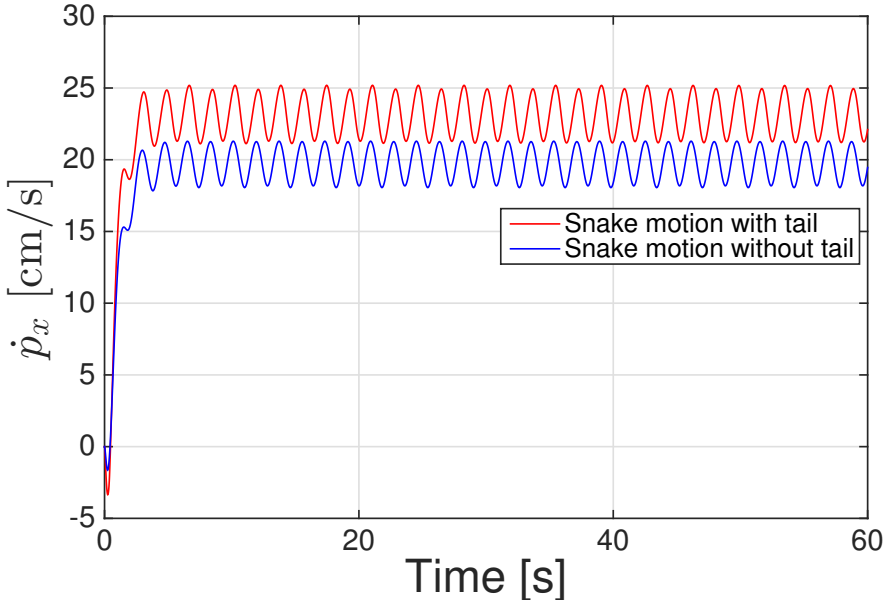

FIGURE 5.6: The figure shows a section of the velocity of CM in x direction for both the extended and the existing model with eel motion.

We then want to compair the eel motion with and without tail for different α, ω and β. This is done by varying on of the parameters and holding two other constant. We have calculated the work the motors have to do per meter the snake are moving (W/m). This is done by integrating the absolute value of the joint torques multiplied with the joint angular velocity with respect to time and divided by the length the robot have moved during the simulation time. Then the W/m are plotted against the mean speed velocity in figure 5.7-5.9 for the different parameters. In figure 5.7 the frequency ω of the reference signal is increased form 80 to 240, while $\alpha = 30^o$ and $\beta = 40^o$. The mean speed is increasing with an increased ω. The model with tail has a higher velocity at the same frequency. If we look at the same velocity for the simulation with and without tail the tail shows a significantly decrease in W/m.

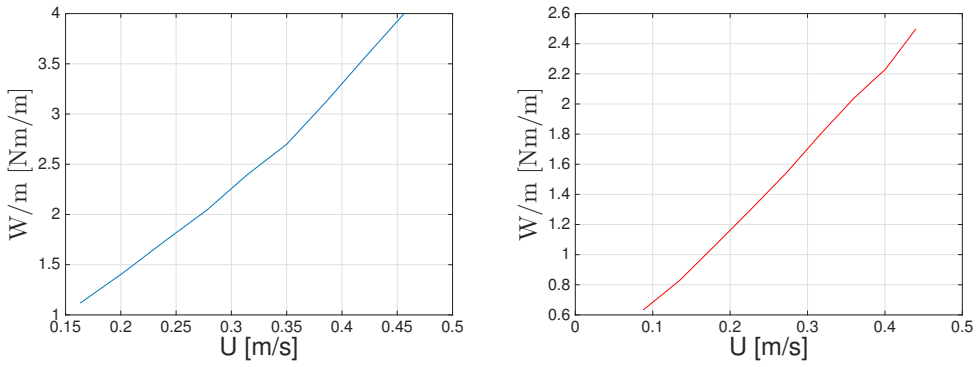

(A) Without tail (B) With tail

FIGURE 5.7: The figure shows the W/m plotted agents the mean velocity U for different ω in the range of 80-240

In figure 5.8 the amplitude α of the reference signal is increased form 15 to 45, while $\omega = 100^o$ and $\beta = 40^o$. The mean speed is increasing with an increased α. The model with tail has a higher velocity at the same amplitude. If we look at the same velocity for the simulation with and without tail the tail shows a significantly decrease in W/m. We should note that at one point the W/m increases drastically and the velocity decreases.

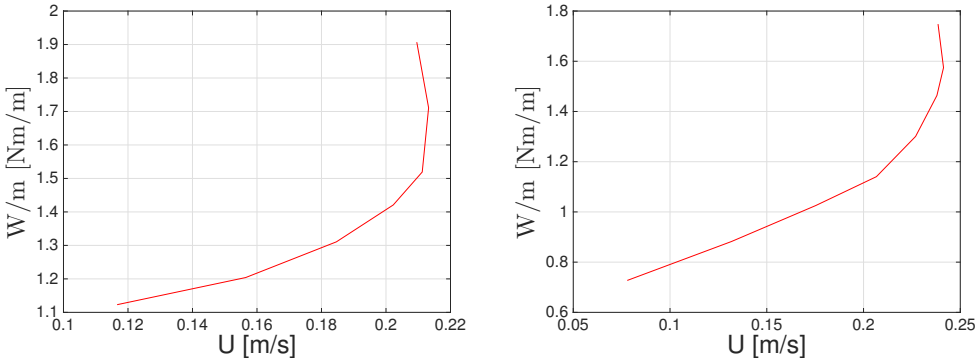

(A) Without tail (B) With tail

FIGURE 5.8: The figure shows the W/m plotted agents the mean velocity U for different α in the range of 15-45

In figure 5.9 the phase δ of the reference signal is increased form 35 to 60, while $\omega = 100^o$ and $\alpha = 30^o$. Here mean speed is decreases with an increase of δ. The model with tail has a higher velocity at the same phase. If we look at the same velocity for the simulation with and without tail the tail shows a significantly decrease in W/m.

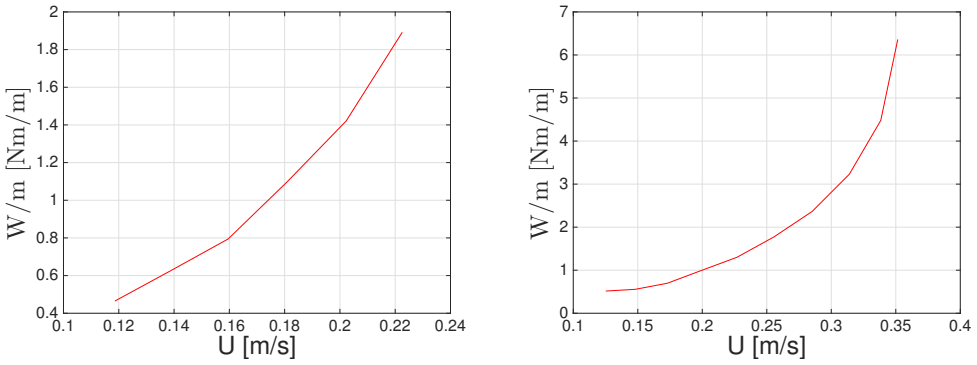

(A) Without tail (B) With tail

FIGURE 5.9: The figure shows the W/m plotted agents the mean velocity U for different δ in the range of 35-60

The tail performance seems to be promising, showing both an increase in efficiency and speed. We therefore wan to cheek and investigate the some hydrodynamic parameters closer. In figure 5.10-5.12 the transvers velocity of the link or cross flow plotted as a function of velocity for three different links. Link 1 is the tail and so on. The increase in velocity is also here archived by changing ether α, ω or

β and holding the to other parameters constant. The KC number is also plotted for the same links.

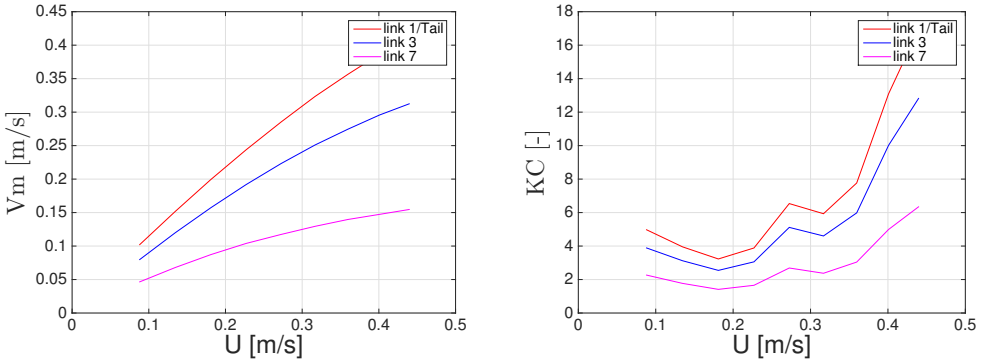

(A) Transvers velocity (B) Keulegan-Carpenter number

FIGURE 5.10: The figure shows the transvers velocity Vm and Keulegan-Carpenter number $\alpha = 30$, $\delta = 40$, ω in the range of 80-240.

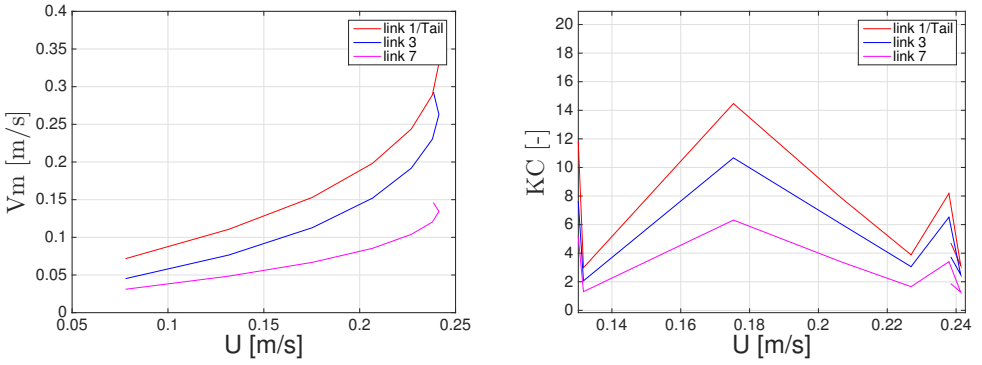

(A) Transvers velocity (B) Keulegan-Carpenter number

FIGURE 5.11: The figure shows the transvers velocity Vm and Keulegan-Carpenter number $\omega = 100$, $\delta = 40$, α in the range of 15-45.

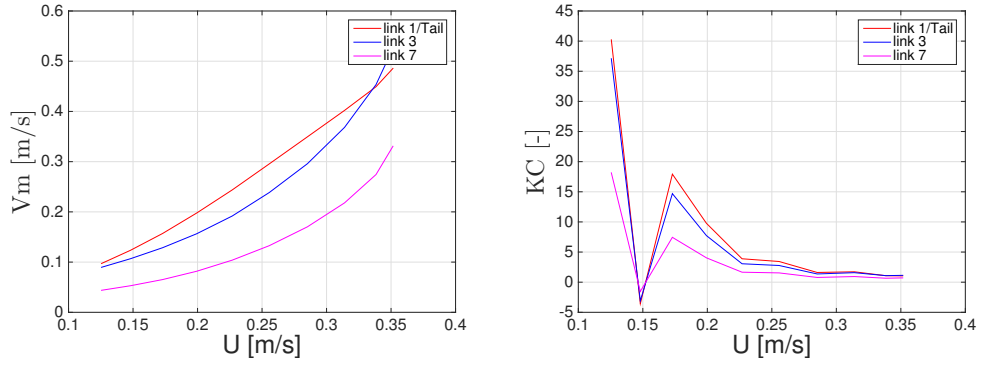

(A) Transvers velocity (B) Keulegan-Carpenter number

FIGURE 5.12: The figure shows the transvers velocity Vm and Keulegan-Carpenter number $\alpha = 30$, $\omega = 100$, δ in the range of 35-60.

In figure 5.13-5.15 the reduced frequency of the link are plotted as a function of velocity for three different links. Link 1 is the tail and so on. The increase in velocity is also hear archived by changing ether α, ω or β and holding the to other parameters constant. The St number is also plotted for the same links.

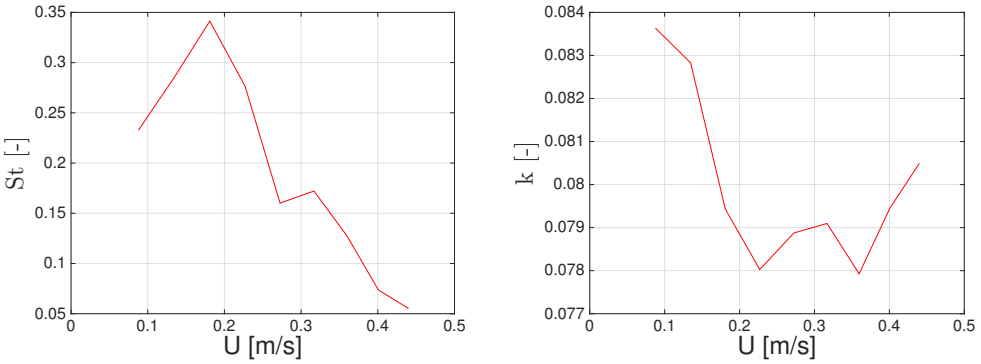

(A) Strouhals number (B) Reduced frequency

FIGURE 5.13: The figure shows the Reduced frequency and Strouhals number $\alpha = 30$, $\delta = 40$, ω in the range of 80-240.

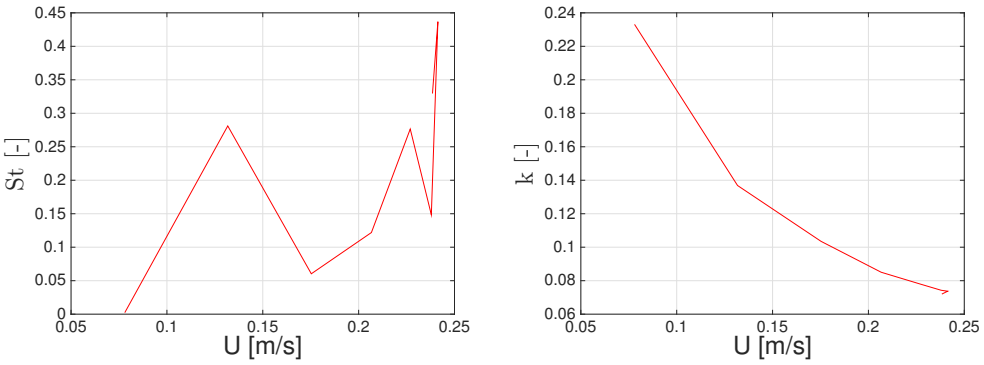

(A) Strouhals number (B) Reduced frequency

FIGURE 5.14: The figure shows the Reduced frequency and Strouhals number $\delta = 40$, $\omega = 100$, α in the range of 14-45.

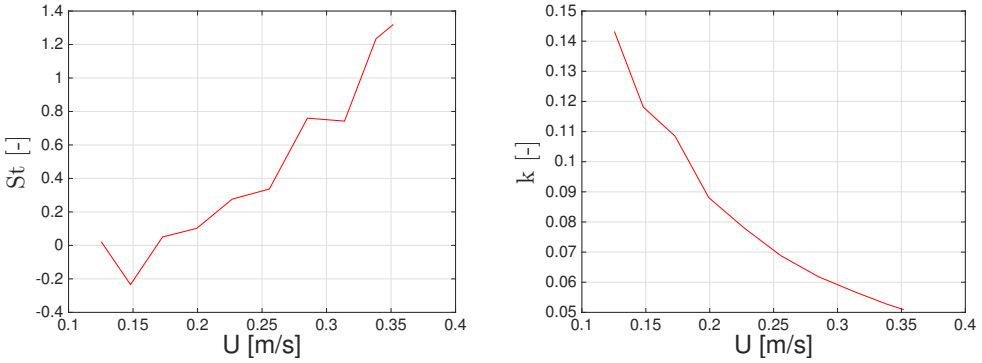

(A) Strouhals number (B) Reduced frequency

FIGURE 5.15: The figure shows the Reduced frequency and Strouhals number $\alpha = 30$, $\omega = 100$, δ in the range of 35-60.

The angel of attack is also interesting to check. A too large angel of attack can cause stalling, which reduces the lift of the foil significantly. The quasi-steady model does not take this into account and we therefore overestimate the lift force if the angel of attack is too large. The angel of attack is plotted for $\alpha = 30^o$, $\omega = 100^o$ and $\beta = 40^o$ in figure 5.16.

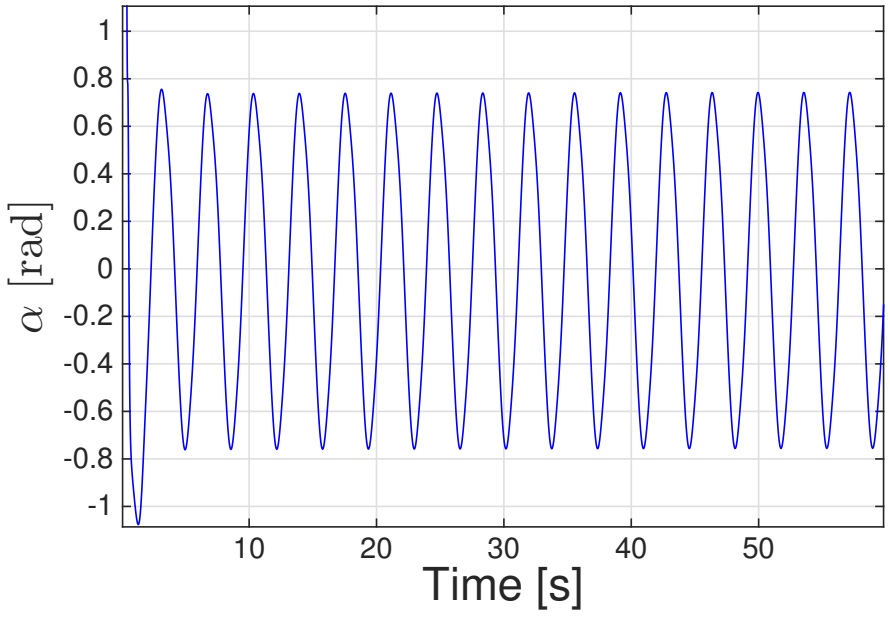

FIGURE 5.16: The figure showes the angel of attack for the foil with $\alpha = 30^o$, $\omega = 100^o$ and $\beta = 40^o$.

5.2.6 Discussion

We have seen that the foil increases the velocity for both snake and eel motion. This also fits well with the literature on fish propulsion and what we were expecting. The comparison of the eel motion with an without tail shows that with that tail is faster and more efficient. If the amplitude α of reference signal gets to large the velocity is decreasing and in general an increase in the phase δ gives a decrees in the speed. For the efficiency plots in figure 5.7-5.9 we can se that the model with and without tail follows the same shape but the on with tail is more efficient at the same velocity.

From the angel of attack plotted in 5.16 we can see that the maximum angel of attack is approximately 0.7 rad or 40^o. This is quit much and the foil will properly stall at this angel. But experiments have shown angel off attack up to 30^o without stalling [58].

Looking at the plots in figure 5.10-5.15 we see that the cross flow increases with an increased amplitude and frequency and decreases with an increased phase. Some of the St number in the simulations with different phases is negative this is du to a calculation error in the calculation and should be neglected.

Looking at the St number in figure 5.13, the St number is decreasing with an increased velocity. One reason for this is that for the fastest frequencies the tail was not able to follow the reference signal so the amplitude gets smaller. So the PD controller should have ben tuned differently for the different frequencies.

From the theory we know that the foil is highly unsteady for $k > 0.2$. Looking at the plots in figure 5.13-5.15 we cans see that using the quasi-steady theory can be defend for most of the simulations.

If we look at the plots of the KC number in figure 5.10-5.12 we can se that the KC number varies significantly not only with the speed U but also with the link number. This motivates for using different drag coefficients for the different links to make the model more accurate.

5.3 Effect of a dorsal fin

The tunnioform swimmers often have a quite distinguish dorsal fin. It is therefore interesting to see what affect this have on the snake robot. We will therefore compair the underwater snake robot with a caudal fin with and without a dorsal fin. This simulation have been done with the combined under water snake robot and tail model. *Matlab R2014b* and the *ode23tb* solver with a relative and absolute error tolerance of 10^{-4} are sill used. The same caudal fin is used in both models and the simulations are done with n=10 links.

5.3.1 Locomotion

In this simulations we will only considering the eel motion. The referees signal is the set same as given in the first simulation.

5.3.2 Low-level joint control

The same low-level joint control as used in the two previously simulations are also used in this simulations.

5.3.3 Tail parameters

The simulations are done with the same caudal fin as in the previously simulation. The cord was 0.0194 m and a span of 0.12 m. It is also placed at the last link with the lift center on the mid point of the link, so a is still $-0.5 - l/b$. The dorsal finn is pleased at linke number 5 from the tail. The dorsal fin has the same cord length as the caudal finn $c = 0.0194$ m but the span is the half, $S = 0.06$ m.

5.3.4 Simulation parameters

The snakes center of mass CM, are placed in the origin with the body parallel to the x-axis and with the head in positive x direction. All the initial values are sett to zero, and the simulation is done with $n = 10$ links. The density is $\rho = 1000$ kg/m^3. The length of all links without foils are $2l_i = 2 \times 0.07$m. The links with foils is assumed to be slightly longer so it is possible fit the foil on the link. So for the links with foil $2l_i = 2 \times 0.075$m. The cross section of the snake is elliptical with the diameters of 0.05m and 0.03m. Assuming that the snake is naturally buoyant the mass of each link whiteout foil is $m = 0.6597$. For the links with mass is assumed to be $m_t = 0.7468$. This is due to the extra length and extra weight of the foil. 20g are added for the foil weight and 20g to balance the link to have the mass center in the mid point of the link. The inertia is calculated to 0.0011 kgm^2 for all the links without tail and 0.0013 kgm^2 for the link with tail. The dorsal fin has only the half span length, but for simplicity we have assume that the weight and inertia is the same.

The added mass coefficients C_A and C_M are both equal to 1. The friction coefficient are selected as $C_f = 0.03$ and $C_D = 2$. This validation is done without current so the current vector in inertia frame is $[0, 0]$m/s. $K_{p,i} = 450$ and $K_{d,i} = 100$ are used as the gains in the PD controller. The locomotion parameters $\alpha = 30^o$, $\omega = 100^o$, $\beta = 40^o$ and $\gamma = 0^o$ where used for both simulations. The simulating time is 60 seconds.

5.3.5 Simulation results

In this simulation study we want to investigate the effect of a dorsal fin. The snake is moving freely in a straight line and the model has a caudal fin in both cases. A simulation with and without a dorsal fin is done. The velocity of the CM is plotted together for the simulation with and without the dorsal fin for the x and y direction in figure 5.17 and 5.18 respectively. The mean speed calculated by the length that robot have moved divided by the simulation time. The mean speed

for the simulation with dorsal fin was found to be 0.2329 m/s and for simulation without dorsal fin 0.2264 m/s. So the dorsal fin gives a higher mean speed. The work the joint motors have to do per meter (W/m) is calculated by integrating the absolute value of the joint torques multiplied with the joint angular velocity and divided by the length the robot have moved during the simulation time. The W/m for the simulation with dorsal fin was fond to be 1.2880 Nm/m and for the simulation without dorsal fin 1.3325 Nm/m. So the simulation with dorsal fin is also more efficient.

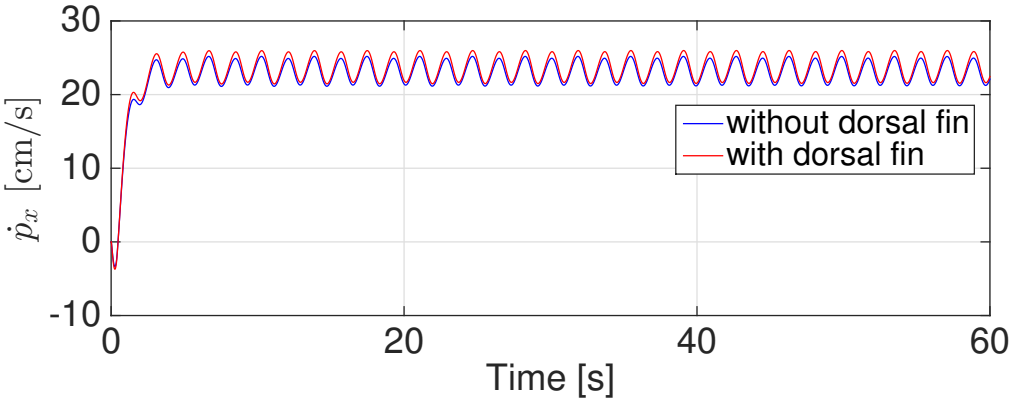

FIGURE 5.17: The figure a comparison of the x velocity of the CM for the combined snake and tail model with and without a dorsal fin.

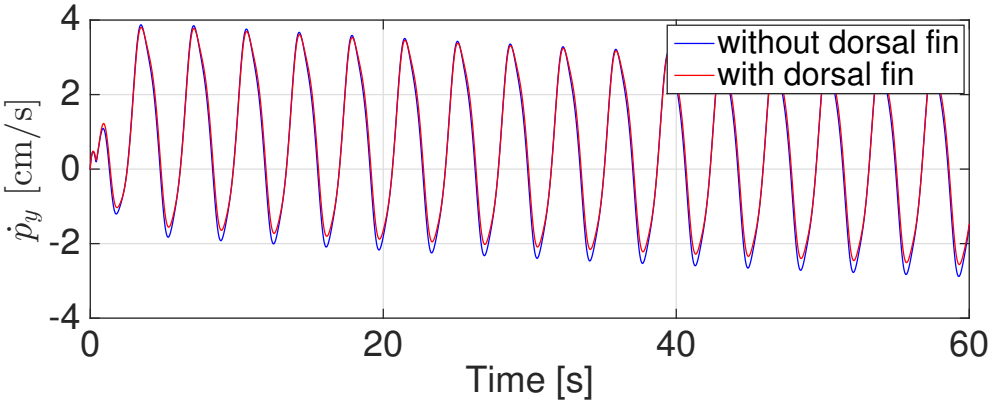

FIGURE 5.18: The figure a comparison of the y velocity of the CM for the combined snake and tail model with and without a dorsal fin.

5.3.6 Discussion

From the figure 5.17, we can see that the simulation which have included a dorsal fin have a higher velocity in x direction. From and figure 5.18, we see that simulation with dorsal fin have a smaller amplitude in the velocity. The dorsal fin is damping out some of the sideways motion of the CM. The simulation with dorsal fin also seems to be more efficient since the work the joint motors have to do per meter is lower. Remark:
In the simulation with foil et first 0.2 seconds the span was set to 0. Tis was because else it took the model time to start the simulations because of the high accelerations in the beginning. The Matlab code for the model presented in [1] is made by Eleni Kelasidi and for the other to simulation this code is modified with the new equations.

Chapter 6

Conclusion and future work

6.1 Conclusion

An extended model of the one presented in [1] of an underwater snake robot is derived and implemented in *Matlab R2014b*. Simulation shows that the extended model gives the as good as the same results. There is a slight difference but this is properly due to numerical calculation differences. The solver used has and accuracy of 10^{-4} and the differences is in this order. The time steps are not synced either. So, we conclusion is that the model is accurate.

Future a quasi-steady model for a foil is combined with the underwater snake robot model. The speed performance for both snake and eel motion are compered with and without tail. The results show significant improvements. Deeper analyses are done for the eel motion. Efficiency study was done by calculating the work per meter the joint motors had to do. Different parameters of the motion was varied to see how the performance is effected. General we can say that higher velocities gives higher work per meter. Also the snake simulation with tail gives a lover work per meter for the same forward velocity. This was what we had hoped for. The reduced frequency k was calculated for the eel motion with tail. For a reduced frequency over 2 the problem is sad to be highly unsteady. A reduced frequency is for the most under this, but still a bit high. Anyway unsteady theories have a

fluid memory effect that requires numerical schemes to calculate. To be able to get the equations on closed form without numerical schemes we thought this was the most accurate way to do it.

The cross flow velocity was plotted for three different links. The results show a significant difference in the cross flow and KC number. Sinse the drag coefficient will be dependent on the KC number one should look deeper into the possibility of modeling the links with different drag coefficients. Also the forward velocity will effect the cross flow and the drag coefficient.

The St number was also calculated. For some parameter we can se that we are in the optimal St number range. But for the simulation where δ were varied something seems to gone wrong due to that the St number becomes negative. This is properly due to the algorithm that calculates the amplitude of the tail motion.

Simulations for eel motion with and without a dorsal fin are done. We see the dorsal fin was improving the speed while the work per meter was decreased. Form the results we can se who it slightly damps the sideways motion of the CM. This is something also hoped for.

When we check the angel of attack, we found that it probably was too large to avoided stalling. The model then over predicts the thrust force.

6.2 Future work

There are a lot of interesting ideas that could be investigated in the future. We think that we only have seen the beginning of the snake robots. The hydrodynamics should be investigated more deeper maybe with experiments. It is not possible to model all the effects in a closed form equation. The interaction between a dorsal fin, caudal fin and the snake robot it self could give a higher efficiency.

A controller for the caudal fin should be made so it is possible to control it to an optimized angel of attack.

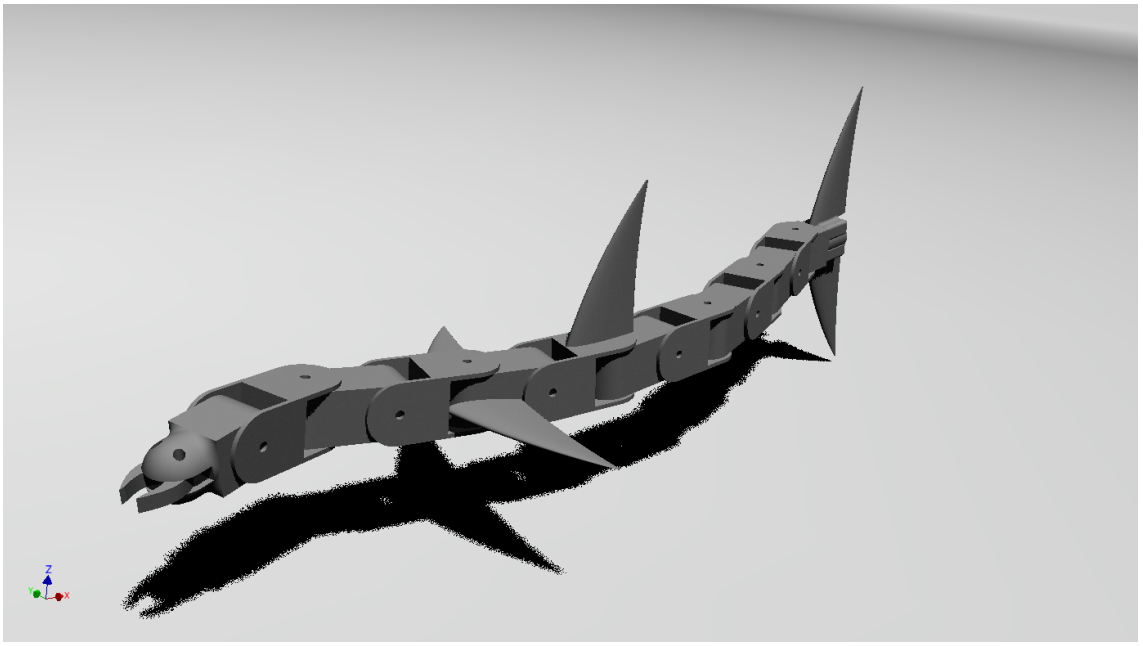

FIGURE 6.1: Future snake robot with fins.

Future a controller for maneuvering and transit should be derived and stability should be investigated.

We think that fins on the snake could improve the efficiency and speed performance which also the model and simulations showed. A future thought about how the snake robot my look like in the future can be seen in figure 6.1.

Appendix A

Coefficients for dynamic tail model

$$
\begin{aligned}
M_\theta = {} & \boldsymbol{J} + \boldsymbol{L}\boldsymbol{S}_{\boldsymbol{\theta}}\boldsymbol{V}\boldsymbol{S}_{\boldsymbol{\theta}} + \boldsymbol{L}\boldsymbol{C}_{\boldsymbol{\theta}}\boldsymbol{V}\boldsymbol{C}_{\boldsymbol{\theta}} + \boldsymbol{\Lambda_1} + \boldsymbol{S}_{\boldsymbol{\theta}}\boldsymbol{A_1}(\boldsymbol{S}_{\boldsymbol{\theta}}^{\boldsymbol{2}}\boldsymbol{K}\boldsymbol{S}_{\boldsymbol{\theta}} + \boldsymbol{S}_{\boldsymbol{\theta}}\boldsymbol{C}_{\boldsymbol{\theta}}\boldsymbol{K}\boldsymbol{C}_{\boldsymbol{\theta}}) \\
& - \boldsymbol{C}_{\boldsymbol{\theta}}\boldsymbol{A_1}(-\boldsymbol{S}_{\boldsymbol{\theta}}\boldsymbol{C}_{\boldsymbol{\theta}}\boldsymbol{K}\boldsymbol{S}_{\boldsymbol{\theta}} - \boldsymbol{C}_{\boldsymbol{\theta}}^{\boldsymbol{2}}\boldsymbol{K}\boldsymbol{C}_{\boldsymbol{\theta}}) \\
& + (K_{S_\theta x} + K_{C_\theta x} + \boldsymbol{S}\pi\rho\boldsymbol{B}^3 a\boldsymbol{S}_{\boldsymbol{\psi}}e + (-\boldsymbol{K}_{\boldsymbol{t},\boldsymbol{x}} - \boldsymbol{K}_{\boldsymbol{t},\boldsymbol{y}})\boldsymbol{B}^{\boldsymbol{2}}\boldsymbol{S}_{\boldsymbol{\psi}}e) \\
& (-m_{11}e^T((\boldsymbol{\mu}_{\boldsymbol{n}}\boldsymbol{S}_{\boldsymbol{\theta}}^{\boldsymbol{2}} - \boldsymbol{S}_{\boldsymbol{\beta}+\boldsymbol{\psi}}\pi\rho\boldsymbol{S}\boldsymbol{B}^2\boldsymbol{S}_{\boldsymbol{\psi}})\boldsymbol{K}\boldsymbol{S}_{\boldsymbol{\theta}} \\
& + (\boldsymbol{\mu}_{\boldsymbol{n}}\boldsymbol{S}_{\boldsymbol{\theta}}\boldsymbol{C}_{\boldsymbol{\theta}} + \boldsymbol{S}_{\boldsymbol{\beta}+\boldsymbol{\psi}}\pi\rho\boldsymbol{S}\boldsymbol{B}^2\boldsymbol{C}_{\boldsymbol{\psi}})\boldsymbol{K}\boldsymbol{C}_{\boldsymbol{\theta}} + \boldsymbol{S}_{\boldsymbol{\beta}+\boldsymbol{\psi}}\boldsymbol{S}\rho\pi\boldsymbol{B}^3 a) \\
& - m_{12}e^T((-\boldsymbol{\mu}_{\boldsymbol{n}}\boldsymbol{S}_{\boldsymbol{\theta}}\boldsymbol{C}_{\boldsymbol{\theta}} - \boldsymbol{C}_{\boldsymbol{\beta}+\boldsymbol{\psi}}\pi\rho\boldsymbol{S}\boldsymbol{B}^2\boldsymbol{S}_{\boldsymbol{\psi}})\boldsymbol{K}\boldsymbol{S}_{\boldsymbol{\theta}} \\
& - (\boldsymbol{\mu}_{\boldsymbol{n}}\boldsymbol{C}_{\boldsymbol{\theta}}^{\boldsymbol{2}} - \boldsymbol{C}_{\boldsymbol{\beta}+\boldsymbol{\psi}}\pi\rho\boldsymbol{S}\boldsymbol{B}^2\boldsymbol{C}_{\boldsymbol{\psi}})\boldsymbol{K}\boldsymbol{C}_{\boldsymbol{\theta}}) + \boldsymbol{C}_{\boldsymbol{\beta}+\boldsymbol{\psi}}\boldsymbol{S}\rho\pi\boldsymbol{B}^3 a) \\
& + (K_{S_\theta y} + K_{C_\theta y} + \boldsymbol{S}\pi\rho\boldsymbol{B}^3 a\boldsymbol{C}_{\boldsymbol{\psi}}e + (-\boldsymbol{K}_{\boldsymbol{t},\boldsymbol{x}} - \boldsymbol{K}_{\boldsymbol{t},\boldsymbol{y}})\boldsymbol{B}^{\boldsymbol{2}}\boldsymbol{C}_{\boldsymbol{\psi}}e) \\
& (-m_{21}e^T((\boldsymbol{\mu}_{\boldsymbol{n}}\boldsymbol{S}_{\boldsymbol{\theta}}^{\boldsymbol{2}} - \boldsymbol{S}_{\boldsymbol{\beta}+\boldsymbol{\psi}}\pi\rho\boldsymbol{S}\boldsymbol{B}^2\boldsymbol{S}_{\boldsymbol{\psi}})\boldsymbol{K}\boldsymbol{S}_{\boldsymbol{\theta}} \\
& + (\boldsymbol{\mu}_{\boldsymbol{n}}\boldsymbol{S}_{\boldsymbol{\theta}}\boldsymbol{C}_{\boldsymbol{\theta}} + \boldsymbol{S}_{\boldsymbol{\beta}+\boldsymbol{\psi}}\pi\rho\boldsymbol{S}\boldsymbol{B}^2\boldsymbol{C}_{\boldsymbol{\psi}})\boldsymbol{K}\boldsymbol{C}_{\boldsymbol{\theta}} + \boldsymbol{S}_{\boldsymbol{\beta}+\boldsymbol{\psi}}\boldsymbol{S}\rho\pi\boldsymbol{B}^3 a) \\
& - m_{22}e^T((-\boldsymbol{\mu}_{\boldsymbol{n}}\boldsymbol{S}_{\boldsymbol{\theta}}\boldsymbol{C}_{\boldsymbol{\theta}} - \boldsymbol{C}_{\boldsymbol{\beta}+\boldsymbol{\psi}}\pi\rho\boldsymbol{S}\boldsymbol{B}^2\boldsymbol{S}_{\boldsymbol{\psi}})\boldsymbol{K}\boldsymbol{S}_{\boldsymbol{\theta}} \\
& - (\boldsymbol{\mu}_{\boldsymbol{n}}\boldsymbol{C}_{\boldsymbol{\theta}}^{\boldsymbol{2}} - \boldsymbol{C}_{\boldsymbol{\beta}+\boldsymbol{\psi}}\pi\rho\boldsymbol{S}\boldsymbol{B}^2\boldsymbol{C}_{\boldsymbol{\psi}})\boldsymbol{K}\boldsymbol{C}_{\boldsymbol{\theta}}) + \boldsymbol{C}_{\boldsymbol{\beta}+\boldsymbol{\psi}}\boldsymbol{S}\rho\pi\boldsymbol{B}^3 a) \\
& (\boldsymbol{K}_{\boldsymbol{t},\boldsymbol{x}} + \boldsymbol{K}_{\boldsymbol{t},\boldsymbol{y}})(-\boldsymbol{B}^2(\boldsymbol{S}_{\boldsymbol{\psi}}\boldsymbol{K}\boldsymbol{S}_{\boldsymbol{\theta}} - \boldsymbol{C}_{\boldsymbol{\psi}}\boldsymbol{K}\boldsymbol{C}_{\boldsymbol{\theta}}) - \boldsymbol{B}^3 a) \\
& + \boldsymbol{S}\rho\pi(\boldsymbol{B}^4(1/8 + a^2) - \boldsymbol{B}^3 a(\boldsymbol{S}_{\boldsymbol{\psi}}\boldsymbol{K}\boldsymbol{S}_{\boldsymbol{\theta}} - \boldsymbol{C}_{\boldsymbol{\psi}}\boldsymbol{K}\boldsymbol{C}_{\boldsymbol{\theta}})) \qquad \text{(A.1a)}
\end{aligned}
$$

$$
\begin{aligned}
W_\theta = {} & \boldsymbol{LS_\theta VC_\theta} - \boldsymbol{LC_\theta VS_\theta} + \boldsymbol{S_\theta A_1}(\boldsymbol{S_\theta^2 KC_\theta} - \boldsymbol{S_\theta C_\theta KS_\theta}) - \boldsymbol{C_\theta A_1}(\boldsymbol{C_\theta^2 KS_\theta} - \boldsymbol{S_\theta C_\theta KC_\theta}) \\
& + (K_{S_\theta x} + K_{C_\theta x} + \boldsymbol{S}\pi\rho\boldsymbol{B}^3 a\boldsymbol{S_\psi} e + (-\boldsymbol{K_{t,x}} - \boldsymbol{K_{t,y}})\boldsymbol{B^2 S_\psi} e) \\
& (-m_{11}e^T((\boldsymbol{\mu_n S_\theta^2} - \boldsymbol{S_{\beta+\psi}}\pi\rho\boldsymbol{SB^2 S_\psi}))\boldsymbol{KC_\theta} - (\boldsymbol{\mu_n S_\theta C_\theta} + \boldsymbol{S_{\beta+\psi}}\pi\rho\boldsymbol{SB^2 C_\psi})\boldsymbol{KS_\theta}) \\
& - m_{12}e^T((-\boldsymbol{\mu_n S_\theta C_\theta} - \boldsymbol{C_{\beta+\psi}}\pi\rho\boldsymbol{SB^2 S_\psi})\boldsymbol{KC_\theta} + (\boldsymbol{\mu_n C_\theta^2} - \boldsymbol{C_{\beta+\psi}}\pi\rho\boldsymbol{SB^2 C_\psi})\boldsymbol{KS_\theta})) \\
& + (K_{S_\theta y} + K_{C_\theta y} + \boldsymbol{S}\pi\rho\boldsymbol{B}^3 a\boldsymbol{C_\psi} e + (-\boldsymbol{K_{t,x}} - \boldsymbol{K_{t,y}})\boldsymbol{B^2 C_\psi} e) \\
& (-m_{21}e^T((\boldsymbol{\mu_n S_\theta^2} - \boldsymbol{S_{\beta+\psi}}\pi\rho\boldsymbol{SB^2 S_\psi}))\boldsymbol{KC_\theta} - (\boldsymbol{\mu_n S_\theta C_\theta} + \boldsymbol{S_{\beta+\psi}}\pi\rho\boldsymbol{SB^2 C_\psi})KS_\theta) \\
& - m_{22}e^T((-\boldsymbol{\mu_n S_\theta C_\theta} - \boldsymbol{C_{\beta+\psi}}\pi\rho\boldsymbol{SB^2 S_\psi})\boldsymbol{KC_\theta} + (\boldsymbol{\mu_n C_\theta^2} - \boldsymbol{C_{\beta+\psi}}\pi\rho\boldsymbol{SB^2 C_\psi})\boldsymbol{KS_\theta})) \\
& (\boldsymbol{K_{t,x}} + \boldsymbol{K_{t,y}})(-\boldsymbol{B}^2(\boldsymbol{S_\psi KC_\theta} + \boldsymbol{C_\psi KS_\theta})) \\
& - \boldsymbol{S}\rho\pi\boldsymbol{B}^3 a(\boldsymbol{S_\psi KC_\theta} + \boldsymbol{C_\psi KS_\theta})
\end{aligned} \tag{A.2a}
$$

$$
\begin{aligned}
V_\theta = {} & \boldsymbol{\Lambda_2} - \boldsymbol{S_\theta A_1}(\boldsymbol{S_\theta C_\theta} V_x^a + \boldsymbol{S_\theta^2} V_y^a) - \boldsymbol{C_\theta A_1}(\boldsymbol{C_\theta^2} V_x^a + \boldsymbol{S_\theta C_\theta} V_y^a) \\
& + (K_{S_\theta x} + K_{C_\theta x} + \boldsymbol{S}\pi\rho\boldsymbol{B}^3 a\boldsymbol{S_\psi} e + (-\boldsymbol{K_{t,x}} - \boldsymbol{K_{t,y}})\boldsymbol{B^2 S_\psi} e) \\
& (-m_{11}e^T\boldsymbol{\mu_n}(-\boldsymbol{S_\theta C_\theta} V_x^a - \boldsymbol{S_\theta^2 V}_y^a) - m_{12}e^T\boldsymbol{\mu_n}(\boldsymbol{C_\theta^2} V_x^a + \boldsymbol{S_\theta C_\theta} V_y^a)) \\
& + (K_{S_\theta y} + K_{C_\theta y} + \boldsymbol{S}\pi\rho\boldsymbol{B}^3 a\boldsymbol{C_\psi} e + (-\boldsymbol{K_{t,x}} - \boldsymbol{K_{t,y}})\boldsymbol{B^2 C_\psi} e) \\
& (-m_{21}e^T\boldsymbol{\mu_n}(-\boldsymbol{S_\theta C_\theta} V_x^a - \boldsymbol{S_\theta^2} V_y^a) - m_{22}e^T\boldsymbol{\mu_n}(\boldsymbol{C_\theta^2} V_x^a + \boldsymbol{S_\theta C_\theta} V_y^a))
\end{aligned} \tag{A.3a}
$$

$$
\begin{aligned}
K_x = {} & -LS_\theta A^T(DD^T)^{-1}D \\
& + (K_{S_\theta x} + K_{C_\theta x} + \boldsymbol{S}\pi\rho\boldsymbol{B}^3 a\boldsymbol{S_\psi} e + (-\boldsymbol{K_{t,x}} - \boldsymbol{K_{t,y}})\boldsymbol{B^2 S_\psi} e)m_{11}e^T \\
& + (K_{S_\theta y} + K_{C_\theta y} + \boldsymbol{S}\pi\rho\boldsymbol{B}^3 a\boldsymbol{C_\psi} e + (-\boldsymbol{K_{t,x}} - \boldsymbol{K_{t,y}})\boldsymbol{B^2 C_\psi} e)m_{21}e^T
\end{aligned} \tag{A.4a}
$$

$$
\begin{aligned}
K_y = {} & LC_\theta A^T(DD^T)^{-1}D \\
& + (K_{S_\theta x} + K_{C_\theta x} + \boldsymbol{S}\pi\rho\boldsymbol{B}^3 a\boldsymbol{S_\psi} e + (-\boldsymbol{K_{t,x}} - \boldsymbol{K_{t,y}})\boldsymbol{B^2 S_\psi} e)m_{12}e^T \\
& + (K_{S_\theta y} + K_{C_\theta y} + \boldsymbol{S}\pi\rho\boldsymbol{B}^3 a\boldsymbol{C_\psi} e + (-\boldsymbol{K_{t,x}} - \boldsymbol{K_{t,y}})\boldsymbol{B^2 C_\psi} e)m_{22}e^T
\end{aligned} \tag{A.4b}
$$

where

$$K_{S_\theta x} = \boldsymbol{L S_\theta A^T (D D^T)^{-1} D (M + \mu_n S_\theta}^2) e \tag{A.5a}$$

$$K_{S_\theta y} = \boldsymbol{L S_\theta A^T (D D^T)^{-1} D (-\mu_n S_\theta C_\theta)} e \tag{A.5b}$$

$$K_{C_\theta y} = \boldsymbol{L C_\theta A^T (D D^T)^{-1} D (-M - \mu_n C_\theta}^2) e \tag{A.5c}$$

$$K_{C_\theta x} = \boldsymbol{L C_\theta A^T (D D^T)^{-1} D (\mu_n S_\theta C_\theta)} e \tag{A.5d}$$

$$V = \boldsymbol{A^T (D D^T)^{-1} D M K} \tag{A.5e}$$

$$A_1 = \boldsymbol{L A^T (D D^T)^{-1} D \mu_n} \tag{A.5f}$$

$$K_{t,x} = \boldsymbol{L S_\theta A^T (D D^T)^{-1} D S_{\beta+\psi}} \pi \rho \boldsymbol{S} \tag{A.5g}$$

$$K_{t,y} = \boldsymbol{L C_\theta A^T (D D^T)^{-1} D C_{\beta+\psi}} \pi \rho \boldsymbol{S} \tag{A.5h}$$

Bibliography

[1] Kelasidi E. Pettersen K. Y. Liljeback P. Gravdahl J. T. Integral line-of-sight for path following of underwater snake robots. *IEEE MSC 2014*, 2014.

[2] Alastair Pollock Photography. URL http://www.alastairpollock.com.

[3] Biosphoto/Christopher Swann, 2013. URL http://www.dailymail.co.uk/news/article-2377154/Eight-ton-orca-leaps-15ft-air-finally-capture-dolphin-hour-chase.html.

[4] R.E. Fish and J. J. Rohr. Review of dolphin hydrodynamics and swimming performance, August 1999.

[5] 2014. URL https://www.ethz.ch/en/news-and-events/eth-news/news/2014/04/looking-at-the-fins-of-the-tuna-fish.html.

[6] Taavi a.eel Salumäe. A flow sensing bioispired robot. *IEEE ROBOTICS AND AUTOMATION MAGAZINE*, September 2014.

[7] 2005. URL http://cswww.essex.ac.uk/staff/hhu/jliua/picgallery.htm.

[8] 2013. URL http://biorob.epfl.ch/amphibot.

[9] Pål Liljeback. *Modelling, Development, and Control of Snake Robots*. PhD thesis, Norwegian University of Sience and Technology, 2011.

[10] D. M. Lane M. Sfakiotakis and J. B. C. Davies. Review of fish swimming modes for aquatic locomotion. *JOURNAL OF OCEANIC ENGINEERING*, 24(237-252), 1999.

[11] Bjørnar Pettersen. *Marin teknikk 3 hydrodynamikk*. Department of marine technology, 2007.

[12] Sverre Steen. *Foil and propeller theory*. Department of marine technology, 2014.

[13] Mr. Michael Rufo. *GhostSwimmer™: Tactically Relevant, Biomimetically Inspired, Silent, Highly Efficient and Maneuverable Autonomous Underwater Vehicle*. Boston Engineering Corporation, 411 Waverley Oaks Road, Suite 114, Waltham, MA, 2452.

[14] URL http://www.amplicon.com/marine/rov-systems.cfm.

[15] URL http://www.mbari.org/auv/MappingAUV/sonars.htm.

[16] M. S. Triantafyllou and G. S. Triantafyllou. An efficient swimming machine. *Scientific American*, 272(3):40–48, 1995.

[17] Sir James Lighthill. *Mathematical Biofluiddynamics*. University of Cambridge, 1975.

[18] R. Bonfil, M. Meÿer, M.C. Scholl, R. Johnson, S. O'Brien, H. Oosthuizen, S. Swanson, D. Kotze, and M. Paterson. Transoceanic migration, spatial dynamics, and population linkages of white sharks. *Science*, 310(5745):100–103, 2005.

[19] Terje Bongard and Eivin Røskaft. *Det biologiske mennesket*. Tapir akademiske forlag, 2010.

[20] J. GRAY. Studies in animal locomotion: Vi. the propulsive powers of the dolphin. *Journal of Experimental Biology*, 13(2):192–199, 1936.

[21] T. Yao-Tsu Wu. Hydromechanics of swimming propulsion. part 1. swimming of a two-dimensional flexible plate at variable forward speeds in an inviscid fluid. *Journal of Fluid Mechanics*, 46(02):337–355, 1971.

[22] T. Yao-Tsu Wu. Hydromechanics of swimming propulsion. part 2. some optimum shape problems. *Journal of Fluid Mechanics*, 46(03):521–544, 1971.

[23] T. Yao-Tsu Wu. Hydromechanics of swimming propulsion. part 3. swimming and optimum movements of slender fish with side fins. *Journal of Fluid Mechanics*, 46(03):545–568, 1971. ISSN 1469-7645.

[24] Frank E. Fish, Paul Legac, Terrie M. Williams, and Timothy Wei. Measurement of hydrodynamic force generation by swimming dolphins using bubble dpiv. *The Journal of Experimental Biology*, 217(2):252–260, 2014.

[25] Minoru Nagai. *Thinking Fluid Dynamics with Dolphins*. NLD: IOS Press, 2002.

[26] Fredrik Dukan. *ROV Motion Control Systems*. PhD thesis, Norwegian University of Sience and Technology, 2014.

[27] The Universety of Texas, 05 2015. URL http://wpressutexas.net/cs378h/index.php?title=AUV_Background.

[28] Damian Isla. Robotuna project to model real fish. URL http://tech.mit.edu/V115/N49/robotuna.49n.html.

[29] D. S. Barrett J. M. Anderson, K. Streitlien and M. S. Triantafyllou. Oscillating foils of high propulsive efficiency. *Fluid Mech.*, 360:41–72, 1998.

[30] M.J. Wolfgang, J.M. Anderson, M.A. Grosenbaugh, D.K. Yue, and M.S. Triantafyllou. Near-body flow dynamics in swimming fish. *The Journal of Experimental Biology*, 202(17):2303–2327, 1999.

[31] G. S. Triantafyllou, M. S. Triantafyllou, and M. A. Grosenbaugh. Optimal thrust development in oscillating foils with application to fish propulsion. *Journal of Fluids and Structures*, 7(2):205–224, 1993.

[32] M. S. Triantafyllou, G. S. Triantafyllou, and R. Gopalkrishnan. Wake mechanics for thrust generation in oscillating foils. *Physics of Fluids A: Fluid Dynamics (1989-1993)*, 3(12):2835–2837, 1991.

[33] M. S. Triantafyllou, G. S. Triantafyllou, and D. K. P. Yue. Hydrodynamics of fishlike swimming. *Annual Review of Fluid Mechanics*, 32(1):33–53, 2000.

[34] A. H. Techet, F. S. Hover, and M. S. Triantafyllou. Separation and turbulence control in biomimetic flows. *Flow, Turbulence and Combustion*, 71(1-4):105–118, 2003.

[35] D.S. Barrett, M.S. Triantafyllou, D.K.P. Yue, M.A. Grosenbaugh, and M.J. Wolfgang. Drag reduction in fish-like locomotion. *Journal of Fluid Mechanics*, 392:183–212, 1999.

[36] S. C. Licht, M. S. Wibawa, F. S. Hover, and M. S. Triantafyllou. In-line motion causes high thrust and efficiency in flapping foils that use power downstroke. *The Journal of Experimental Biology*, 213(1):63–71, 2010.

[37] A. P. Maertens, M. S. Triantafyllou, and D. K. P. Yue. Efficiency of Fish Propulsion. *ArXiv e-prints*, September 2014.

[38] S. Licht, F. Hover, and M. S. Triantafyllou. Design of a flapping foil underwater vehicle. In *Underwater Technology, 2004. UT '04. 2004 International Symposium on*, pages 311–316, 2004.

[39] J. Liu and H. Hu. Biological inspiration: From carangiform fish to multijoint robotic fish. *Journal of Bionic Engineering*, 7(1):35–48, 2010. URL http://www.scopus.com/inward/record.url?eid=2-s2.0-77950191838&partnerID=40&md5=7f741db60667de5c0d45e33ebb7b8fe1. cited By 53.

[40] J. Yu, S. Wang, and M. Tan. A simplified propulsive model of bio-mimetic robot fish and its realization. *Robotica*, 23(1):101–107, 2005.

[41] Taavi Salumäe and Maarja Kruusmaa. Flow-relative control of an underwater robot. *Proceedings of the Royal Society A: Mathematical, Physical and Engineering Science*, 469(2153), 2013.

[42] H. El Daou, T. Salumae, A. Ristolainen, G. Toming, M. Listak, and M. Krusmaa. A bio-mimetic design and control of a fish-like robot using compliant structures. In *Advanced Robotics (ICAR), 2011 15th International Conference on*, pages 563–568, 2011. doi: 10.1109/ICAR.2011.6088645.

[43] Mathieu Porez, Frédéric Boyer, and Auke Jan Ijspeert. Improved lighthill fish swimming model for bio-inspired robots: Modeling, computational aspects and experimental comparisons. *The International Journal of Robotics Research*, 33(10):1322–1341, 2014.

[44] A.J. Ijspeert and A. Crespi. Online trajectory generation in an amphibious snake robot using a lamprey-like central pattern generator model. pages 262–268, 2007.

[45] A. Crespi, A. Badertscher, A. Guignard, and A.J. Ijspeert. Amphibot i an amphibious snake-like robot. *Robotics and Autonomous Systems*, 50(4):163–175, 2005.

[46] A.J. Ijspeert, J. Hallam, and D. Willshaw. Evolving swimming controllers for a simulated lamprey with inspiration from neurobiology. *Adaptive Behavior*, 7(2):151–172, 1999.

[47] A.J. Ijspeert and J. Kodjabachian. Evolution and development of a central pattern generator for the swimming of a lamprey. *Artificial Life*, 5(3):247–269, 1999.

[48] S. Hirose and H. Yamada. Snake-like robots. *Robotics and Automation Magazine, IEEE*, 16(1):88–98, 2009.

[49] E. Kelasidi, K. Y. Pettersen, J. T. Gravdahl, and P. Liljeback. Modeling of underwater snake robots. In *IEEE International Conference on Robotics and Automation (ICRA)*, pages 4540–4547, 2014.

[50] K. Y. Pettersen E. Kelasidi and J. T. Gravdahl. *A waypoint guidance strategy for underwater snake robots.* Mediterranean Conference on Control and Automation (MED), 2014.

[51] Auke Jan Ijspeert. *AmphiBot II: An Amphibious Snake Robot that Crawls and Swims using a Central Pattern Generator*. Climbing and Walking Robots, 2006.

[52] Auke Jan Ijspeert. *Central pattern generators for locomotion control in animals and robots: A review*, volume 21. Neural Networks, 2008.

[53] O. M. Faltinsen. *Sea loads on shipes and offshore structurea*. Camebridge university press, 1993.

[54] Fredsøe Jørgen Sumer B. Mutlu. *Hydrodynamics around Cylindrical Structures*. World Scientific, 2006.

[55] Odd M. Faltinsen. *Hydrodynamics of High-speed Marine Vehicles*. Camebridge university press, 2005.

[56] J. Gordon Leishman. *Principles of Helicopter Aerodynamics*. Camebridge university press, second edition edition, 2006.

[57] J.N.Newman. *Marine Hydrodynamics*. Camebridge, 1977.

[58] Eirik Bøckmann. *Wave Propultion of Ships*. PhD thesis, Norwegian University of Sience and Technology, 2015.

[59] M Sato. *Serpentine locomotion with robotic snakes*, volume 22. Control Systems, IEEE, 2002.